

*From Chromatin Readers to Heart Failure:
BET Protein Family Members in Cardiac Remodeling*

Dissertation

for the award of the degree

“Doctor rerum naturalium”

of the Georg-August-Universität Göttingen

within the doctoral program Molecular Medicine

at the Georg-August University School of Science (GAUSS)

submitted by

Dawid Lbik

born in Lublin, Poland

Göttingen, January 2019

Thesis Committee Members

Prof. Dr. André Fischer (first reviewer)

Epigenetics and Systems medicine in Neurodegenerative Diseases
German Center for Neurodegenerative Diseases

Prof. Dr. Steven Johnsen (second reviewer)

Translational Cancer Research
University Medical Center Göttingen

PD. Dr. Roland Dosch

Developmental Biochemistry
Georg-August University Göttingen

Additional Members of the Examination Board

Prof. Dr. Sigrid Hoyer-Fender

Developmental Biology
Zoology and Anthropology, Georg-August University Göttingen

Prof. Dr. Bernd Wollnik

Human Genetics
Georg-August-University Göttingen

PD. Dr. Karl Toischer

Cardiology and Pneumology
University Medical Center Göttingen

Date of oral examination:

Affidavit

I hereby declare that I have written the dissertation

“From Chromatin Readers to Heart Failure:
BET Protein Family Members in Cardiac Remodeling”

independently with no other aids or sources than quoted.

Dawid Lbik

Göttingen, 08.01.2019

List of Publications

Peer Review Publications

- **Mohamed BA, Schnelle M, Khadjeh S, Lbik D, Herwig M, Linke WA, Hasenfuss G, Toischer K** (2016a). Molecular and structural transition mechanisms in long-term volume overload: Chronic volume overload. **European Journal of Heart Failure** 18, 362–371
- **Mohamed BA, Asif AR, Schnelle M, Qasim M, Khadjeh S, Lbik D, Schott P, Hasenfuss G, Toischer K** (2016b). Proteomic analysis of short-term preload-induced eccentric cardiac hypertrophy. **Journal of Translational Medicine** 14

Conference Abstracts

- **Lbik D, Khadjeh S, Mohamed BA, Fischer A, Hasenfuß G, Toischer K.** (2018) The Absence of the Chromatin Reader Brd2 Decreases Heart Function and Increases Mortality After Pressure Overload. **Circulation.** 2018;136:A20724

Für meine Kinder

Noah Jakob

Emma Matilda

Oskar Janusz

Table of Contents

Affidavit	4
List of Publications	5
Table of Contents	I
List of Figures	IV
List of Tables	V
List of Abbreviations	VI
Abstract	VII
1 Introduction	1
1.1 Heart failure	1
1.1.1 Cardiac remodeling	2
1.1.2 Molecular mechanisms of cardiac remodeling	3
1.1.3 Pharmacotherapies	5
1.2 Epigenetics and gene regulation	6
1.2.1 Histone code: of writers, erasers and readers	9
1.2.2 BET protein family members	9
1.2.3 The role of BET proteins in the heart	11
1.3 Objectives	13
2 Materials and Methods	15
2.1 Animals	15
2.1.1 Animal welfare	15
2.1.2 Generation of mouse strains	15
2.1.3 JQ1 treatment	15
2.1.4 Tamoxifen application	16
2.1.5 Echocardiography	16
2.1.6 Transverse aortic constriction (TAC)	16
2.1.7 Heart dissections	17
2.2 Molecular analysis	18
2.2.1 In-silico oligonucleotide design	18
2.2.2 Genotyping	18
2.2.3 RNA isolation	19
2.2.4 cDNA synthesis	20
2.2.5 Molecular cloning	20
2.2.6 Quantitative real time PCR	20
2.2.7 Total protein extraction	21
2.2.8 Subcellular fractionation	22

2.2.9 Immunoblotting	22
2.3 Histological and immunocytochemical analyses	23
2.3.1 Langendorff CM isolation	23
2.3.2 Immunocytochemistry	24
2.3.3 Confocal microscopy.....	25
2.3.4 Paraffin embedding, dewaxing and rehydration.....	25
2.3.5 Masson's trichrome staining.....	25
2.3.6 Picro Sirius Red staining	26
2.3.7 Wheat germ Agglutinin staining.....	26
2.3.8 Quantification of histological stainings.....	26
2.4 Next Generation Sequencing.....	27
2.4.1 mRNA library preparation.....	27
2.4.2 Raw read and Quality check	27
2.4.3 Mapping and Normalization.....	27
2.4.4 Differential expression analysis	27
2.4.5 Analysis of differentially expressed genes.....	28
2.4.6 Gene set enrichment analysis	28
2.4.7 Microarray analysis	28
3 Results.....	29
3.1 BET protein family members in the mouse heart.....	29
3.1.1 BETs are expressed in the heart and localized in nuclei	29
3.1.2 Particular BETs are differently regulated after pressure overload.....	30
3.2 Effects of JQ1-mediated BET inhibition after pressure overload	32
3.2.1 JQ1 administration does not improve survival after TAC	32
3.2.2 TAC-induced cardiac remodeling is unaffected by JQ1	33
3.2.3 JQ1-treated animals show less wall thickening but reduced contractility	36
3.2.4 JQ1 modulates the immune response, cell cycle, and muscle contraction	37
3.2.5 JQ1 does not reverse stress-induced gene expression	40
3.3 The role of Brd2 in the healthy and diseased mouse heart	42
3.3.1 Generation and validation of Brd2 knockout mice	42
3.3.2 Characterization of Brd2 Δ BDI mutant mice	45
3.3.3 The survival of Brd2 Δ BDI mice is slightly reduced after TAC.....	47
3.3.4 Brd2 Δ BDI and control mice show comparable cardiac remodeling.....	48
3.4 The role of <i>Brd4</i> in the healthy and diseased mouse heart	50
3.4.1 Generation and validation of Brd4 knockout mice	50
3.4.2 Brd4 knockout mice show basal concentric hypertrophy	54
3.4.3 Brd4 KO mice show thicker ventricular walls but normal cardiac function.....	56
3.4.4 Brd4 KO mice show higher mortality after TAC	57

3.4.5	Brd4 KO attenuates cardiac remodeling after TAC.....	58
3.4.6	Brd4 KO hearts show basal fibrosis that increases after TAC	60
3.4.7	Brd4 KO mice show partially preserved heart function after TAC	61
3.4.8	Brd4 KO induces differential expression of genes involved in ECM organization, energy metabolism, and cardiac muscle contraction	63
3.4.9	BRD4 depletion blunts the response to TAC-induced cardiac stress.....	66
4	Discussion.....	70
4.1	Expression of BET members in the healthy and diseased heart	70
4.2	Cardio protective effects of JQ1 could not be reproduced.....	72
4.3	Functional analysis of Brd2 and Brd4 in the murine heart	75
4.3.1	Generation of mice with cardiomyocyte-specific deletion of the first bromodomain of BRD2	75
4.3.2	Heart development, function and remodeling are independent from the first bromodomain of BRD2.....	77
4.3.3	Successful generation of cardiomyocyte-specific Brd4 knockout mice	79
4.3.4	BRD4 is necessary to suppress hypertrophic genes in the healthy heart	81
4.3.5	Brd4 is necessary for the PO-induced remodeling and hypertrophy	83
4.4	Conclusions	86
5	Appendix.....	89
6	Bibliography	96
	Acknowledgements	107
	Curriculum Vitae	108

List of Figures

Figure 1.1: Projected total costs of all cardiovascular diseases by age.	1
Figure 1.2: Overview of pathological hypertrophy.	3
Figure 1.3: Molecular mechanisms in cardiac remodeling.	4
Figure 1.4: Organization of chromatin and gene regulatory mechanisms.	8
Figure 1.5: Phylogenetic tree of bromodomain-containing proteins and structure of BET proteins.	11
Figure 3.1: BRD2 and BRD4 are expressed in the heart and localized in the nucleus.	30
Figure 3.2: BET genes are differently regulated after pressure overload.	31
Figure 3.3: Experimental design for BET inhibition with JQ1 after TAC.	32
Figure 3.4: The survival after TAC showed no difference between vehicle and JQ1 treated animals.	33
Figure 3.5: JQ1 and vehicle treated mice show comparable cardiac remodeling and cardiac stress marker expression 4 and 8 weeks after TAC.	34
Figure 3.6: Hearts from JQ1 and vehicle treated animals show comparable cardiomyocyte hypertrophy after TAC.	35
Figure 3.7: Echocardiographic phenotyping showed an overall comparable systolic dysfunction, left ventricular dilation and wall thickening in both groups after TAC.	36
Figure 3.8: Four weeks after TAC hearts show wide gene expression changes and mild reaction to JQ1-dependent BET inhibition.	38
Figure 3.9: JQ1 modulates multiple biological pathways such as immune response, cell cycle, and muscle contraction.	39
Figure 3.10: JQ1 does not reverse TAC-induced genes.	41
Figure 3.11: Generation of cardiomyocyte-specific <i>Brd2</i> knockout mice.	43
Figure 3.12: The Cre-mediated recombination in the <i>Brd2</i> locus leads to the expression of a <i>Brd2</i> mRNA with a deletion of the target exons 3 and 4.	44
Figure 3.13: The deletion of <i>Brd2</i> exons 3 to 4 results in the expression of a truncated protein.	45
Figure 3.14: Morphometric characterization and echocardiographic analysis of <i>Brd2</i> Δ BDI mice showed no differences to cre control mice.	47
Figure 3.15: <i>Brd2</i> Δ BDI mating scheme and experimental design.	47
Figure 3.16: The survival after TAC is reduced in <i>Brd2</i> Δ BDI mutant mice compared to control but not to cre control.	48
Figure 3.17: <i>Brd2</i> Δ BDI and controls show comparable cardiac remodeling and cardiac stress marker expression 5 weeks after TAC.	49
Figure 3.18: Echocardiographic phenotyping shows no significant differences between <i>Brd2</i> Δ BDI, control and cre control mice 5 weeks after TAC.	50
Figure 3.19: Generation of cardiomyocyte-specific <i>Brd4</i> knockout mice.	51
Figure 3.20: Generation of inducible cardiomyocyte-specific <i>Brd4</i> knockout mice.	52
Figure 3.21: Tamoxifen-induced deletion of exons 6 and 7 in the <i>Brd4</i> locus via MerCreMer leads to decreased <i>Brd4</i> expression in the heart.	53
Figure 3.22: Successful <i>Brd4</i> knockout could not be clearly validated by immunoblotting.	54
Figure 3.23: Morphometric characterization of <i>Brd4</i> knockout mice showed concentric hypertrophy in comparison to control mice.	55
Figure 3.24: Basal echocardiographic phenotyping showed increased left ventricular wall thickness in <i>Brd4</i> KO mice.	56
Figure 3.25: <i>Brd4</i> KO mating scheme and experimental design.	57

Figure 3.26: The survival after TAC is reduced in Brd4 KO mice compared to control with the strongest mortality in the early phase after TAC.	58
Figure 3.27: Brd4 KO and control mice show increased cardiac stress marker expression 5 weeks after TAC, but Brd4 KO mice do not develop cardiomegaly.	59
Figure 3.28: The basal cardiomyocyte hypertrophy in Brd4 KO animals does not change after TAC.	60
Figure 3.29: Brd4 KO hearts showed mild fibrosis after Sham that increased after TAC.	61
Figure 3.30: Brd4 KO animals show limited remodeling capacity after TAC and slightly preserved ejection fraction.	63
Figure 3.31: Depletion of Brd4 from cardiomyocytes induces cardiac remodeling, alters ECM organization, energy metabolism, and cardiac muscle contraction.	64
Figure 3.32: Brd4 KO animals show gene expression changes associated with HCM.	65
Figure 3.33: Brd4 KO hearts show marginal transcriptional changes after TAC, but a wide range of genes associated with metabolism and human diseases is differentially expressed between TAC Brd4 KO and TAC control.	67
Figure 3.34: Deletion of Brd4 mostly affects energy metabolism and membrane repolarization.	69
Figure 4.1: A model of BRD4 function in cardiomyocytes including relevant literature.	88
Figure 5.1: Power calculation to determine sample size for animal experiments.	90
Figure 5.2: Knockdown validation of the BRD2 and BRD4 antibodies used in this thesis.	90
Figure 5.3: Gene set enrichment analysis reveals BET-mediated regulation of RNA processing, translation initiation, biosynthesis, and transport.	91
Figure 5.4: Brd4 KO-specific DEGs regulate metabolic processes, cellular response to stimuli and cardiac muscle contraction.	95

List of Tables

Table 2.1: Genotyping primer.	18
Table 2.2: Standard genotyping reaction.	19
Table 2.3: Standard genotyping protocol.	19
Table 2.4: qPCR primer.	21
Table 2.5: qPCR reaction.	21
Table 2.6: qPCR protocol.	21
Table 2.7: Antibodies used for immunoblotting.	23
Table 2.8: Tyrode solution.	24
Table 2.9: Digestion buffer.	24
Table 2.10: Stop solution.	24
Table 2.11: Antibodies used for immunocytochemistry.	25
Table 5.1: LV M-Mode – Calculation Definitions.	89
Table 5.2: ImageJ script - Minimal Fiber diameter.	89
Table 5.3: ImageJ script – Fibrotic area.	89
Table 5.4: Sequence alignment of truncated <i>Brd2</i> mRNA.	92

List of Abbreviations

ACE	angiotensin-converting enzyme	LV-EDD	left ventricular end-diastolic diameter
ACTN1	actinin alpha 1	LV-ESD	left ventricular endsystolic diameter
ANP	atrial natriuretic peptide	LV-W/BW	LV-weight-to-body-weight
ARB	angiotensin receptor blocker	MAPKKK	MAP kinase kinase kinases
ATR	angiotensin II receptor	MEF2	myocyte-specific enhancer factor 2
AWThd/s	anterior wall thickness	MEK	mitogen-activated protein kinase kinase
Bcl2	B-cell lymphoma 2	MerCreMer	fusion protein of cre recombinase and modified estrogen receptor
BDI/II	bromodomain 1 or 2	MFD	minimal fiber diameter
BET	bromodomain and extraterminal domain	miRNAs	micro RNAs
BNP	brain natriuretic peptide	mRNA	messenger RNA
bp	base pairs	Myc	Myc proto-oncogene
BRD2	Bromodomain-containing protein 2	NFAT	nuclear factor of activated T-cells
BRD4	Bromodomain-containing protein 4	Nppa	gene encoding ANP
CaMKII	calcium/calmodulin-dependent protein kinase type II	Nppb	gene encoding BNP
cAMP	cyclic AMP	NPR	natriuretic peptide receptor
cDNA	complementary DNA	p38	p38 kinases
cGMP	cyclic GMP	PBS	phosphate buffered saline
CM	cardiomyocytes	PCR	polymerase chain reaction
CTD	c-terminal domain	PFA	paraformaldehyde
DAPI	4',6-diamidino-2-phenylindole	PKA	protein kinase A
DMSO	dimethyl sulfoxide	PKA/Ca/G	protein kinase A/Ca/G
DNMTs	DNA methyl-transferases	PKCα	protein kinase Ca
EDTA	ethylenediaminetetraacetic acid	PKG	protein kinase G
EF	ejection fraction	PLC	phospholipase C
ERK1/2	extracellular regulated kinases 1/2,	PLN	phospholamban
ET	extra-terminal domain	PO	pressure overload
FS	fractional shortening	PTMs	post-translational modifications
GATA4	GATA binding protein 4	PWThd/s	posterior wall thickness
GC	guanylate cyclase	RGB	red-green-blue
gDNA	genomic DNA	ROS	reactive oxygen species
GO	gene ontology	RPKM	reads per kilobase million
GPCRs	G protein coupled receptors	RT-qPCR	quantitative real-time PCR
HAT	histone acetyl transferase	RYR2	ryanodine receptor 2
HBSS	Hank's balanced salt solution	SD	standard deviation
HDAC	histone deacetylase	SEM	standard error of the mean
HF	heart failure	SERCA	sarcoplasmic reticulum Ca ²⁺ ATPase
HP-β-CD	2-Hydroxypropyl- β -cyclodextrin	Sham	placebo surgery
JNK	JUN N-terminal kinase	TAC	transverse aortic constriction
JNKs	JUN N-terminal kinases	TBS-T	tris buffered saline with Tween-20
JQ1	BET inhibitor developed by Jun Qui	Tcf	transcription factor
KO	knockout	WGA	wheat germ agglutinin
LV	left ventricle	β-AR	β -adrenergic receptor

Abstract

Heart failure (HF) is the pathologic inability of the heart to supply the body with sufficient amounts of oxygen-rich blood. This increasingly common, life-threatening condition occurs in the final stage of various cardiac pathologies that reduce heart function. Common pharmacotherapies of HF aim to inhibit the renin-angiotensin system and adrenergic receptors that are activated in response to the reduced pumping function and have been available for over 20 years. However, the morbidity and mortality rates of affected patients remain high. To this day the development of new, more effective therapies poses a major challenge in medical research.

The new therapeutic strategy investigated in this work is based on increasing evidence that epigenetics play an important role in the pathogenesis of HF. The rationale behind targeting epigenetic processes to treat the development of HF is that they modulate multiple transcriptional networks simultaneously. For instance, the small molecule JQ1 was shown to displace the bromodomain and extraterminal domain (BET) reader proteins BRD2, BRD3, and BRD4 from chromatin, preventing re-expression of the fetal gene program, pathologic hypertrophy, and fibrosis after pressure overload (PO). To allow effective and safe application of BET inhibition as treatment for HF, it is necessary to assess if targeting BET proteins has added benefits in comparison to current pharmacotherapies such as improved survival and to elucidate functions of individual BET members specifically in cardiac cells. However, previous studies miss to report mortality rates for JQ1 treated animals and do not consider that JQ1 acts systemically and inhibits all four BET family members alike. Thus, the mechanisms underlying BET-mediated cardio protection remain elusive.

First, to characterize and validate cardiac BET expression at baseline and in response to PO I performed gene expression analysis and immunoblotting using hearts of adult wildtype mice. I identified *Brd2* as the highest expressed BET family member in the heart with four times higher mRNA levels compared to *Brd3/Brd4* and revealed TAC-induced expression of the long BRD4 isoform.

Second, to describe the effect of BET inhibition on life expectancy after PO induction I monitored the survival of JQ1-treated wildtype mice for up to 2 months after TAC and analyzed the hearts using echocardiography as well as histological and molecular methods. I found PO-dependent mortality unchanged with JQ1-mediated BET inhibition and observed pathologic changes such as expression of cardiac stress markers, cardiomegaly, cardiomyocyte hypertrophy, interstitial fibrosis, and systolic dysfunction, which were comparable to vehicle-treated animals after TAC. This contradicts previous reports on cardio-protective features of JQ1 in a mouse PO model (Anand et al. 2013). As experimental differences such as sex, age, mouse strain, TAC-performance, and JQ1-batch cannot be excluded as explanations for the discrepant results, future studies should take these possible confounding factors into account.

Moreover, a reliable cardiac-specific biomarker of BET-inhibition should be explored to allow successful therapy monitoring.

Third, using conditional alleles I generated mice expressing a truncated BRD2 protein lacking the first bromodomain, *Brd2 Δ BDI*, and mice with a cardiomyocyte-specific *Brd4* knockout, *Brd4* KO, to investigate whether these gene deletions alter the response to PO. Homozygous *Brd2 Δ BDI* mice were viable and their hearts and cardiac functions were not significantly different from Cre-positive control mice at baseline and after PO induction. In contrast, cardiomyocyte-specific homozygous deletion of *Brd4* during early embryonic development was lethal suggesting that BRD4 is essential during cardiogenesis. For further examination *Brd4* KO was induced at postnatal week five and resulted in animals that were viable for over 12 months. Adult *Brd4* KO mice showed basal concentric hypertrophy, preserved ejection fraction, mild interstitial fibrosis, and cardiac stress marker expression. These features are characteristic for hypertrophic cardiomyopathy (HCM) and were further supported by transcriptome analysis that revealed differential expression of genes involved in extracellular matrix remodeling, energy metabolism, sarcomere composition, and cardiac muscle contraction. Moreover, *Brd4* KO mice subjected to TAC showed significantly higher mortality within the first month after surgery, which might be attributed to diastolic dysfunction or arrhythmias. Nevertheless, no significant wall thickening or left ventricular mass increase, despite the basal hypertrophy was observed in *Brd4* KO mice after TAC. This lack of stress response was confirmed by mRNA sequencing as no relevant changes were detected in *Brd4* KO animals after TAC compared to Sham. However, *Brd4* KO mice that survived the acute phase of PO showed better heart function in comparison to TAC control.

My findings suggest that the function of BRD2 in cardiomyocytes is either independent from its first bromodomain, substituted by another protein upon disruption, or not essential and therefore needs further investigation. Furthermore, beside the established function of BRD4 as co-activator of cardiac stress response, my findings lead to the conclusion that BRD4 has a second function as co-repressor of e.g. pro-hypertrophic genes in the healthy heart. I further propose that the shift between both cardiac functions might be mediated by a stress-induced switch from the short to the long *Brd4* isoform and a respective interaction with e.g. an inactive or active P-TEFb complex (Schröder et al. 2012).

My thesis provides the first functional insight into cardiomyocyte-specific loss of *Brd4 in vivo*, links it to the development of HCM, establishes basal BRD4-mediated negative regulation of transcription, and provides evidence for its depletion to blunt stress-response. These findings could contribute to the development of more selective therapeutic approaches for HF as compared to inhibition of all BET members and to our understanding of HCM development and manifestation.

1 Introduction

1.1 Heart failure

Cardiovascular diseases are the major cause of death worldwide, accounting for over 17 million deaths per year (WHO 2018). This number is expected to rise by 35% to 23 million deaths by 2030 due to increased life expectancies (Heidenreich et al. 2013). The subclass of cardiovascular diseases with the strongest increase in incidents is heart failure (HF). Prevalence of HF is estimated between 2 and 3% of the population with a strong increase in elders with a prevalence between 10 and 20% in 70- to 80-year-old people (Dickstein et al. 2008). Projections estimate an increase of 46% in HF prevalence from 2012 to 2030 (Benjamin et al. 2018). The prognosis for chronic heart failure is poor, with a 5-year mortality rate of about 50% after initial diagnosis (Dickstein et al. 2008; Heidenreich et al. 2013). Furthermore, HF as the leading cause of hospitalization and healthcare expenditures poses a socioeconomic challenge for the ageing population (Hill and Olson 2008). In the United States, the total costs of all cardiovascular diseases are expected to double by 2030 to about 1 000 billion US dollars (Figure 1.1) (Heidenreich et al. 2011).

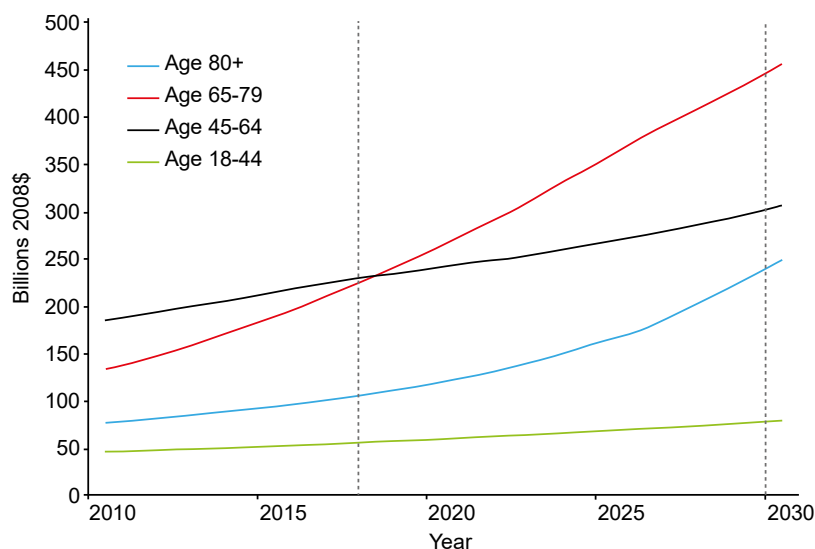


Figure 1.1: Projected total costs of all cardiovascular diseases by age.

In the US, the total (direct and indirect) costs p.a. for cardiovascular diseases are estimated to double by the year 2030 with highest increase for elderly patients at the age of 65-79 years (red) and over 80 years (blue). Adapted from Heidenreich and colleagues (Heidenreich et al. 2011).

Various pathological conditions such as ischemic heart disease, mitral regurgitation, aortic stenosis, congenital cardiomyopathy or alcohol excess have been described to cause HF. They all have in common to reduce ventricular function. As a consequence, the heart is not able to adequately supply tissues with oxygenated blood. This results in shortness of breath,

excessive tiredness, multi-organ dysfunction, and premature death (Benjamin et al. 2018). The underlying molecular, cellular, and interstitial changes that lead to changed morphology and function after heart injury are referred to as cardiac remodeling (Hill and Olson 2008; Azevedo et al. 2016).

1.1.1 Cardiac remodeling

During the progression to HF, the heart is subject to hemodynamic stress. The ventricular wall can either be stretched during diastole by increased blood volume (volume overload) or must contract against an increased pressure during systole (pressure overload) (Toischer et al. 2010; Mohamed et al. 2016). A prominent trigger of pressure overload (PO) is aortic stenosis (Rockman et al. 1991; Burchfield et al. 2013; Merino et al. 2018), which is mainly caused by calcification of the aortic valve and leads to the narrowing of the ventricle's outflow tract (Rogers 2013). In order to adapt to such altered workload and normalize the reduced ventricular function, the heart undergoes cardiac remodeling (Hill and Olson 2008; Azevedo et al. 2016; Nakamura and Sadoshima 2018).

Activation of neuroendocrine stimulation normalizes the output by vasoconstriction and increased contractility, whereas cardiomyocyte hypertrophy increases the number of contractile units. Initially, this leads to reduction in ventricular chamber dimensions and increased wall thickness (concentric hypertrophy), where cardiomyocytes incorporate additional sarcomeres, resulting in increased cellular diameters. At this compensated state the contractile function is largely preserved. However, persistent stress and prolonged activation of those compensatory processes become maladaptive and lead to decompensation with contractile dysfunction and finally HF (**Figure 1.2**). The involved pathological changes include dilatation of the ventricular chamber, increased apoptosis, interstitial fibrosis, impaired Ca^{2+} handling, mitochondrial dysfunction, reactivation of the fetal gene program, and altered sarcomere structure (Hill and Olson 2008; Toischer et al. 2010; van Berlo et al. 2013; Nakamura and Sadoshima 2018). This small set of cellular responses is activated by a complex network of signal transduction cascades.

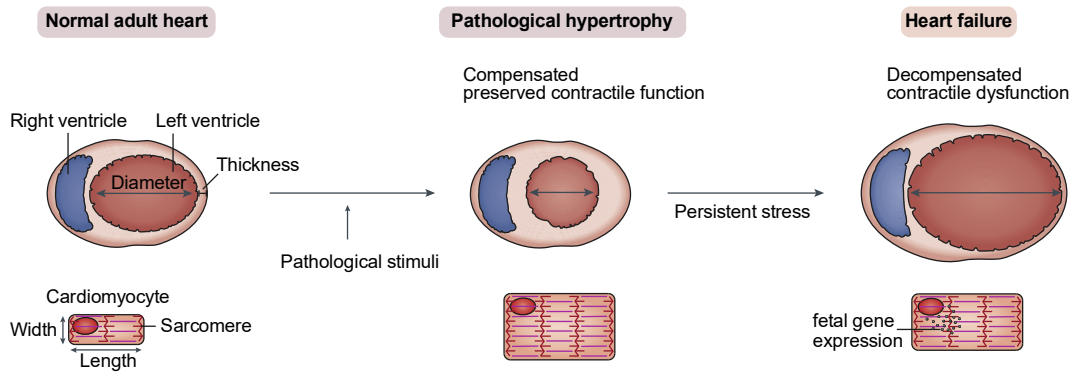


Figure 1.2: Overview of pathological hypertrophy.

The heart undergoes remodeling in order to preserve contractility and reduce wall stress in response to pathological stimuli. Adaptive changes include the reduction of ventricular diameter and ventricular wall thickening (concentric hypertrophy) through increased thickness of individual cardiomyocytes. Thus, the heart compensates higher workload and preserves contractility. With persistent stress these changes become maladaptive and lead to ventricular dilatation and loss of wall thickness (eccentric hypertrophy) with lengthening of cardiomyocytes. This decompensation is accompanied by increased apoptosis, interstitial fibrosis, and impaired contractility, finally leading to heart failure. Adapted from Nakamura and Sadoshima (Nakamura and Sadoshima 2018).

1.1.2 Molecular mechanisms of cardiac remodeling

Stress induced proximal signals such as neuroendocrine hormones and mechanical forces trigger various signaling pathways (Figure 1.3) that drive cardiac remodeling and progression to HF (Hill and Olson 2008; van Berlo et al. 2013). The neuroendocrine hormones angiotensin II, endothelin 1, and catecholamines are secreted upon cardiac stress. They bind the G protein coupled receptors (GPCRs) angiotensin II receptor, endothelin 1 receptor, and β -adrenergic receptors, respectively. These GPCRs indirectly activate second messengers which in turn activate effector kinases and phosphatases that influence contractility and gene expression of the cardiomyocytes. Catecholamines activate protein kinase A (PKA) via cyclic AMP (cAMP). Angiotensin II and endothelin 1 lead to the induction of protein kinase α (PKC α), calcium/calmodulin-dependent protein kinase type II (CaMKII), and Calcineurin via the Ca²⁺ calmodulin complex. PKA, PKC α , and CaMKII increase contractility by regulating the Ca²⁺ handling proteins ryanodine receptor 2 (RYR2), sarcoplasmic reticulum Ca²⁺ ATPase (SERCA), and phospholamban (PLN) (Zhang 2003; van Berlo et al. 2013; Zhang et al. 2013; Newton et al. 2016; Nakamura and Sadoshima 2018).

Further, CaMKII induces the nuclear export of class II histone deacetylase 4 (HDAC4). Class II HDACs 4, 5, and 9 were shown to repress cardiac hypertrophy, whereas class I HDACs 1, 2, and 3 induce hypertrophy (Bucks and Olson 2006; Bucks et al. 2009). The Ca²⁺-activated serine/threonine protein phosphatase Calcineurin dephosphorylates nuclear factor of activated T-cells (NFAT) and leads to its translocation into the nucleus (Molkentin et al. 1998; Nakamura and Sadoshima 2018). The MAPK signaling cascade is induced by activated G proteins in cardiomyocytes upon binding of the neuroendocrine hormones. JUN N-terminal kinases

(JNKs), p38 kinases, and extracellular regulated kinases 1/2 (ERK1/2) comprise the MAPK cascade and are activated by the mitogen-activated protein kinase kinases MEK3/6, MEK4/7, and MEK1/2, respectively. JNK and p38 kinases phosphorylate and activate myocyte-specific enhancer factor 2 (MEF2) and GATA binding protein 4 (GATA4) (ROSE et al. 2010; Nakamura and Sadoshima 2018). In the nucleus, the transcription factors NFAT, MEF2, and GATA4 induce the expression of pro-hypertrophic genes (van Berlo et al. 2013; Nakamura and Sadoshima 2018).

Furthermore, angiotensin II, endothelin 1, and catecholamines induce mitochondrial dysfunction, fibrosis and cell death by increasing levels of reactive oxygen species (ROS) and metabolic intermediates. Additionally, the peptide hormones atrial natriuretic peptide (ANP, gene *Nppa*) and brain natriuretic peptide (BNP, gene *Nppb*) are secreted by cardiomyocytes in response to stretching. These hormones act in an autocrine or paracrine manner, lead to increased levels of cyclic GMP (cGMP), and thus activate protein kinase G (PKG). PKG inhibits cell growth, but the natriuretic peptide receptor (NPR) is desensitized during cardiac remodeling and HF (Nakamura and Sadoshima 2018). Existing and experimental pharmaceuticals target single components of this complex signaling network to treat pathologic remodeling and HF.

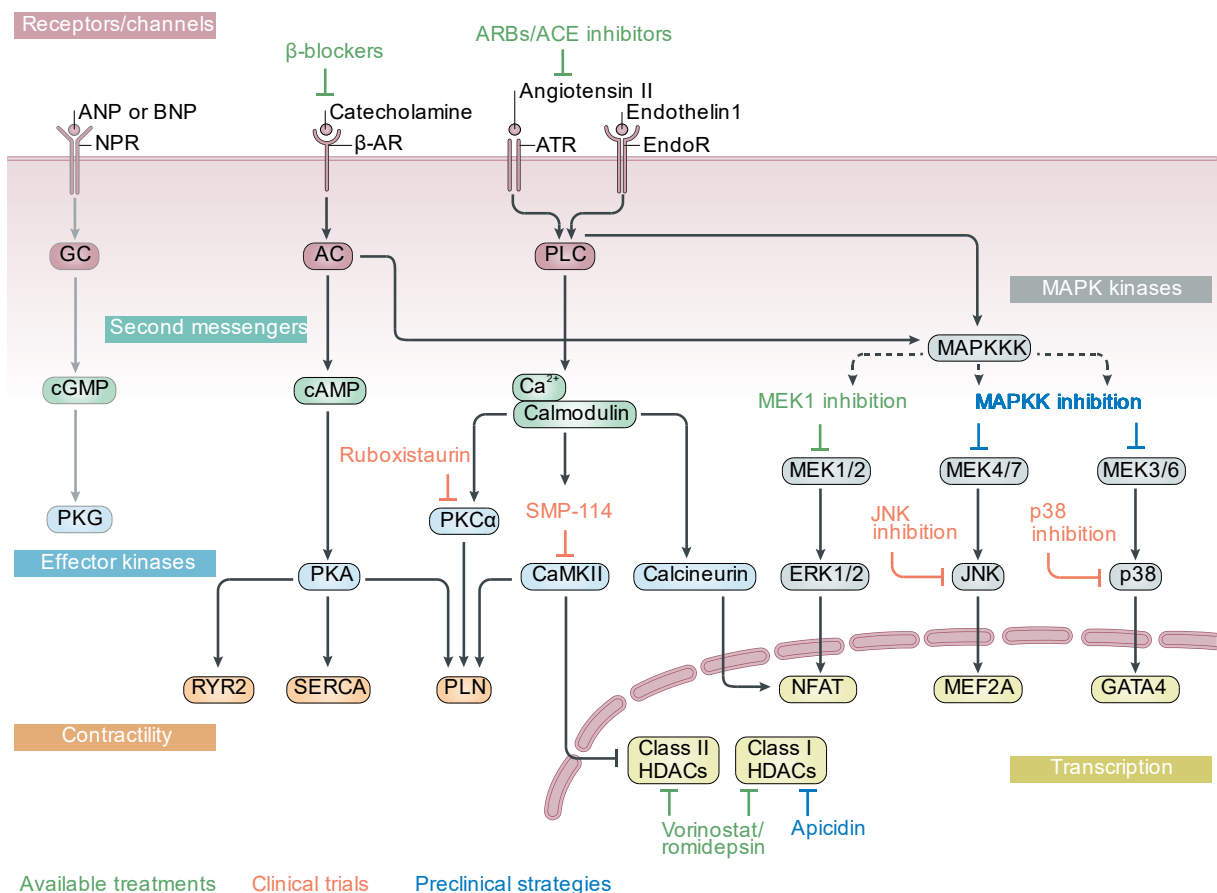


Figure 1.3: Molecular mechanisms in cardiac remodeling.

Simplified scheme of signaling pathways activated during cardiac remodeling. Furthermore, current treatments (red), FDA-approved drugs that could potentially be used for cardiovascular indications (orange), and druggable targets identified in preclinical animal models (blue) are depicted. AC= adenylyl cyclase, ACE= angiotensin-converting enzyme, ANP= atrial natriuretic peptide, β -AR= β -adrenergic receptor, ARB= angiotensin receptor blocker, ATR= angiotensin II receptor, BNP= brain natriuretic peptide, CaMKII= calcium/calmodulin-dependent protein kinase type II, ERK1/2= extracellular regulated kinases 1/2, GATA4= GATA binding protein 4, GC= guanylate cyclase, HDAC= histone deacetylase, JNK= JUN N-terminal kinase, MAPKKK= MAP kinase kinase kinases, MEF2= myocyte-specific enhancer factor 2, MEK= mitogen-activated protein kinase kinase, NFAT= nuclear factor of activated T-cells, NPR= natriuretic peptide receptor, p38= p38 kinases, PKA/Ca/G= protein kinase A/Ca/G, PLC= phospholipase C, PLN= phospholamban, RYR2= ryanodine receptor 2, SERCA= sarcoplasmic reticulum Ca²⁺ ATPase. (adapted from (Nakamura and Sadoshima 2018), (van Berlo et al. 2013)).

1.1.3 Pharmacotherapies

Available pharmacotherapies of HF patients target neurohormonal signaling pathways by inhibiting the renin-angiotensin system (angiotensin-converting enzyme inhibitors, angiotensin receptor blockers) or antagonizing beta-adrenergic receptors (β -blockers) (Figure 1.3) and have been shown to improve survival in HF patients. However, the therapeutic efficacy of this approach is limited, as morbidity and mortality remain high (Benjamin et al. 2018). Therefore, it is necessary to identify new therapies for this common, costly, and potentially fatal condition. Various preclinical and clinical studies pursuing this goal focus on the inhibition of single targets such as different MAPK kinases, PKC α , or CaMKII (Figure 1.3) (van Berlo et al. 2013). Some of these strategies seem promising but they have in common to target only single components of the complex signaling network activated during cardiac remodeling. This might be disadvantageous, especially because of the redundancy of different signaling cascades in activation of few transcription factors (e.g. NFAT, MEF2, GATA4), which induce pathologic gene expression (Hill and Olson 2008; van Berlo et al. 2013).

Nevertheless, cellular responses do not result from the activation of transcription factors alone. It is rather the interplay of DNA-binding regulators with the chromatin structure and the epigenetic landscape in general that drive changes in cell state (Anand et al. 2013). In the heart, chromatin remodeling mechanisms such as post-transcriptional histone modifications and DNA methylation were shown to associate with stress-induced pathways of pathological hypertrophy and HF (McKinsey and Olson 2005; Gilsbach et al. 2014). As changes in chromatin structure modulate multiple transcriptional networks simultaneously, chromatin-dependent gene regulatory mechanisms constitute potent therapeutic targets to suppress pathologic gene expression associated with cardiac remodeling and development of HF (Haldar and McKinsey 2014).

1.2 Epigenetics and gene regulation

Epigenetic mechanisms not only organize genetic information but enable the implementation of external input into genomic instructions. This allows dynamic and contextual regulation of the transcriptome (McKinsey and Olson 2005; Duygu et al. 2013). Genetic information is packaged as a complex between DNA, histone and nuclear non-histone proteins. The smallest organizational units that are used to package DNA are nucleosomes. A nucleosome consists of 147 base pairs (bp) of DNA wrapped around a histone octamer that consists of two copies of the four core histones (H2A, H2B, H3, and H4) (Tonna et al. 2010; Duygu et al. 2013; Mahmoud and Poizat 2013; Khalil 2014). The resulting “bead on a string”-like DNA fiber is further condensed to chromatin (**Figure 1.4**) (Tonna et al. 2010). Based on the DNA-accessibility, chromatin is further classified into the highly condensed and mostly inactive heterochromatin or the more accessible and transcriptionally active euchromatin. To allow transcription, packaged DNA is dynamically modified by ATP-dependent nucleosome remodelers (Tonna et al. 2010; Bell et al. 2011; Blakey and Litt 2015a).

The three major epigenetic mechanisms are expression of non-coding RNA species, DNA methylation, and post-translational modifications (PTMs) of the unstructured amino-terminal tail of histones (“histone tail”). Non-coding RNAs represent the largest part of the transcriptome and are divided into subgroups of long non-coding RNAs, small interfering RNAs and micro RNAs (miRNAs) (Duygu et al. 2013; Mahmoud and Poizat 2013; Khalil 2014). The best studied non-coding RNAs are miRNAs. They are about 22 nucleotides long and were shown to catalyze gene silencing by binding to messenger RNA (mRNA) (Ambros 2004). DNA methylation is a process by which a methyl group is transferred to a cytosine that precedes a guanine nucleotide (CpG) catalyzed by DNA methyl-transferases (DNMTs). DNA methylation is an essential process during development and is typically associated with transcriptional repression (Gilsbach et al. 2014). Common PTMs of histone tails include acetylation, methylation, phosphorylation, and ubiquitination. These modifications are enzymatically added or removed, alter chromatin structure, thus, modulate DNA accessibility, and regulate gene expression (Mahmoud and Poizat 2013; Blakey and Litt 2015a; Blakey and Litt 2015a).

The various cellular mechanisms controlling expression or repression of specific gene products (RNA or protein) can be summarized by the term “gene regulation”. There are three levels of gene regulation: transcriptional, post-transcriptional, and post-translational gene regulation (Harrison and Shanahan 2014). **Figure 1.4** shows a schematic overview of gene regulatory mechanisms. On a global scale, chromatin structure and remodeling play an important role in transcriptional regulation by maintaining the overall accessibility to the DNA (Bell et al. 2011; Keung et al. 2015). Chromatin structure can be changed by DNA modifications, such as methylation or hydroxy-methylation of cytosine residues, and by post translational modifications of “histone tails” such as methylation and acetylation of lysine residues

(Mahmoud and Poizat 2013). On a single gene scale, transcription factors regulate gene expression by binding regulatory DNA elements (enhancers) and recruiting transcriptional complexes to the promoter close to the transcriptional start sites of target genes (Spitz and Furlong 2012). Beside classical DNA-binding transcription factors, proteins recognizing specific histone tail modifications, so called chromatin readers, were shown to regulate gene expression by several interactions with the general transcriptional machinery (Jiang et al. 1998; Jang et al. 2005; Yang et al. 2005).

Post-transcriptional regulation occurs on the mRNA level during transcription, transcript processing, or translation. Processing of mRNA (e.g. alternative splicing, poly-adenylation, and capping) regulates the exon-composition, translation rate, and transcript stability. RNA methylation by specific methyl-transferases has been shown to reduce mRNA half-life (Wang et al. 2014) but increase translation efficacy (Wang et al. 2015). Non-coding RNAs were shown to directly regulate transcription (Holoch and Moazed 2015; Catalanotto et al. 2016), to catalyze mRNA degradation, or inhibit translation via various mechanisms (Fabian et al. 2010). Post-translational mechanisms involve proteolytic processing or degradation, translocation, and diverse modifications of proteins (e.g. methylation, acetylation or phosphorylation) (Karve and Cheema 2011). Histone acetyl transferases, for example, acetylate histone tails which are then recognized by specialized reader proteins that, in turn, recruit co-activators to regulate the transcription of target genes (Gillette and Hill 2015). This example shows the complexity of gene regulation, with its various mechanisms that allow multi-level, spatiotemporal, and dose-dependent regulation.

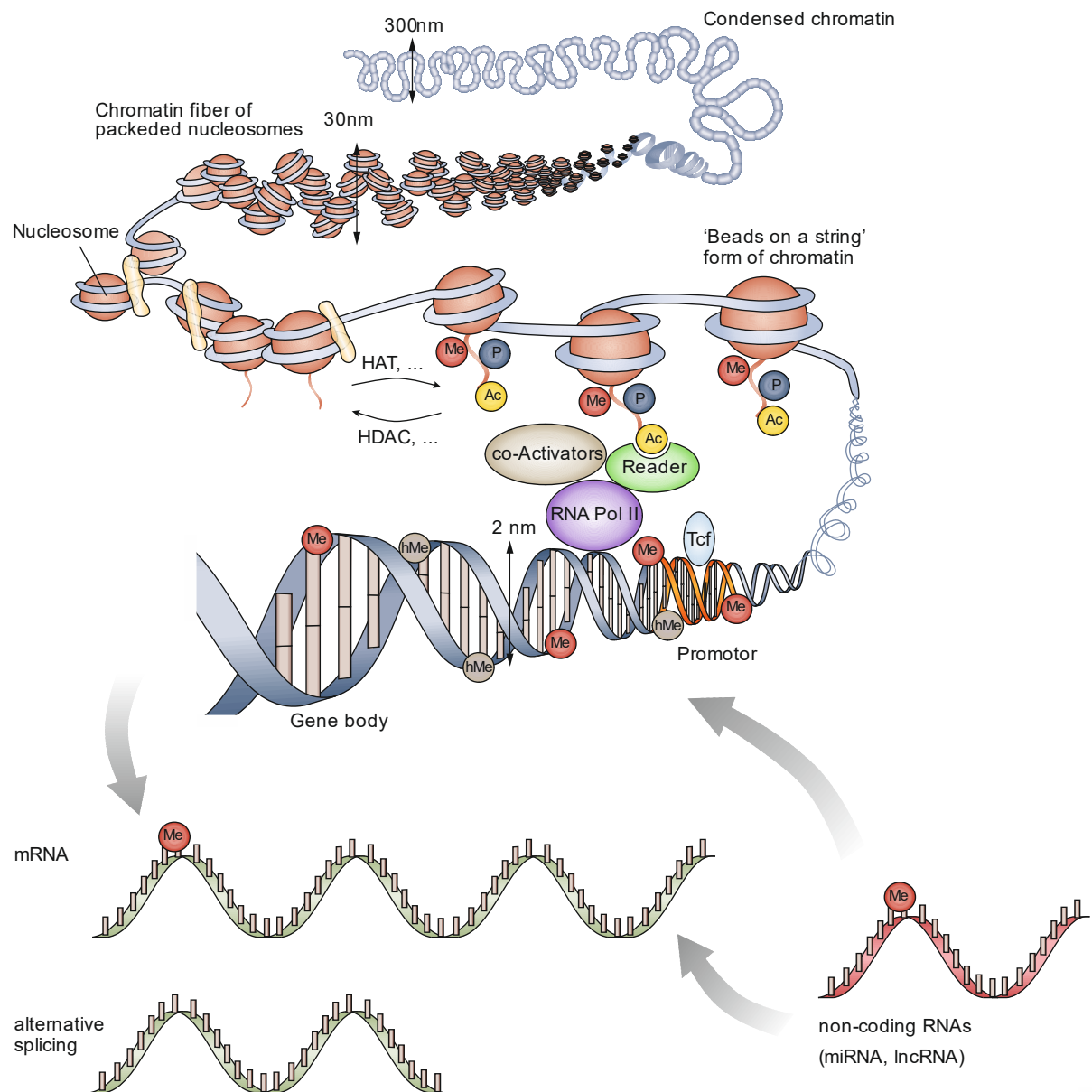


Figure 1.4: Organization of chromatin and gene regulatory mechanisms.

Genetic information is organized as chromatin which is a highly condensed form of a complex between DNA and histone proteins. The smallest organizational units of chromatin are nucleosomes that are used to package DNA. A nucleosome consists of 147 bp of DNA wrapped around dimers of the four core histones, the histone octamer. Various cellular mechanisms regulate gene expression. Both, DNA modifications (methylation or hydroxy-methylation) and post-translational modifications of histone tails can change chromatin structure to be more accessible (active) or condensed (repressed). Transcription can be activated or blocked at a specific position by either DNA-binding proteins (transcription factors) that recognize specific promoters, or by specialized “readers” of chromatin modifications. Post-transcriptional mechanisms include alternative splicing, RNA methylation or silencing by non-coding RNAs. Non-coding RNAs can directly regulate transcription or inhibit translation via various mechanisms. Post-translational mechanisms involve proteolytic processing or degradation, translocation, and diverse modifications (e.g. methylation, acetylation or phosphorylation) of proteins. HAT= histone acetyl transferase, HDAC= histone deacetylase, Tcf= transcription factor, Ac= acetyl group, Me= methyl group, P= phosphoryl group, nm= nanometer. Adapted from Tonna and colleagues (Tonna et al. 2010).

1.2.1 Histone code: of writers, erasers and readers

The possible combinations of methyl, acetyl, and phosphoryl groups on different histone residues are referred to as the histone code (Jenuwein 2001). Three protein classes, writers, erasers and readers, are involved in the establishment and translation of the histone code (Jenuwein 2001; Gillette and Hill 2015). Writers like histone methyl transferases add modifications to histone tails. Erasers like histone demethylases remove those modifications. Chromatin readers recognize various modification patterns on histone tails and for example recruit transcriptional regulators (Gillette and Hill 2015). The histone code with its dynamic PTMs, together with the combinatorial pattern recognition of chromatin readers enables a high level of chromatin plasticity and, thus, selective spatiotemporal transcriptional regulation (Jenuwein 2001; Blakey and Litt 2015a; Blakey and Litt 2015b).

N- ϵ -acetylation of lysine residues is the most frequent PTM of histones and is regulated by histone acetyl transferases (HATs) and histone deacetylases (HDACs). HATs are writers and add acetyl groups, whereas, HDACs act as erasers and remove acetyl marks. Histone acetylation is an important process in general development and various diseases. For instance, aberrant expression of HDACs and altered histone acetylation patterns deregulate transcription and contribute to the development of cardiomyopathies (Backs and Olson 2006; Mahmoud and Poizat 2013). Generally, acetylated chromatin is associated with open chromatin and transcriptional activation but also DNA repair (Bell et al. 2011). Chromatin readers with one or more bromodomains selectively recognize acetylated lysine residues and recruit chromatin remodelers and other effector complexes to target sites in the chromatin (Filippakopoulos et al. 2012), thus, promoting gene transcription (Jiang et al. 1998; Jang et al. 2005; Yang et al. 2005). The bromodomain is an evolutionary conserved protein domain comprised of about 110 amino acids. There are 61 bromodomain-containing proteins in human, which can be classified in eight families by structure similarity. These include various nuclear proteins like HATs (PCAF), transcriptional co-activators (TAFs, TRIM/TIF1), and the bromodomain and extra-terminal domain (BET) proteins (Filippakopoulos et al. 2010; Filippakopoulos et al. 2012).

1.2.2 BET protein family members

Members of the BET protein family (**Figure 1.5A**) include the ubiquitously expressed BRD2, BRD3, BRD4, and the testis specific BRDT, all of which have two tandem N-terminal bromodomains (BDI and BDII) and an extra-terminal (ET) domain (**Figure 1.5B**) (Houzelstein et al. 2002; Shang et al. 2007; Shang et al. 2009; Filippakopoulos et al. 2010). BET chromatin readers were shown to specifically bind acetylated lysine residues of histone tails (Filippakopoulos et al. 2010; Filippakopoulos et al. 2012) to promote transcription by recruiting

transcriptional complexes like mediator (Jiang et al. 1998) and the positive transcription elongation factor b (P-TEFb) (Jang et al. 2005; Yang et al. 2005) to acetylated chromatin.

BET proteins have been shown to be essential for embryonic development and differentiation in the mouse model. Both, Brd2 (Shang et al. 2007; Gyuris et al. 2009; Shang et al. 2009; WANG et al. 2009) and Brd4 (Houzelstein et al. 2002) homozygous for the respective null allele are embryonic lethal.

Brd4^{-/-} embryos die shortly after implantation at about embryonic day 5.5 (E5.5) and explanted blastocyst are not able to maintain the inner cell mass. Brd4^{+/-} animals display pre- and postnatal growth defects, significant mortality in the first two weeks of postnatal life, and various anatomical abnormalities like abnormal head shape, abnormally thick epidermis, reduced subcutaneous fat, abnormal liver cells, and cataracts. Isolated Brd4^{+/-} fibroblasts show reduced proliferation rates and increased sensitivity to the DNA-damaging agent methyl methane sulfate (Houzelstein et al. 2002).

In comparison, Brd2^{-/-} embryos survive until E12.5 and show reduced growth, defects in neural tube closure, and an increase in cell death, before they get resorbed. Isolated fibroblasts from these embryos do also proliferate more slowly than fibroblasts from wildtype embryos (Shang et al. 2007; Gyuris et al. 2009; Shang et al. 2009; WANG et al. 2009).

Consistent with these findings, BET proteins have been shown to play an important role in the cell cycle (Dey et al. 2009; Zhao et al. 2011). For instance, BRD4 stays at H4K5ac during mitosis, marks the start sites of many M/G1 genes, accelerates the expression of G1 genes, and promotes the progression to S phase (Dey et al. 2009; Filippakopoulos et al. 2010). Due to their involvement in cell cycle and gene regulation, BET proteins have been proposed as promising therapeutic targets in cancer (Filippakopoulos et al. 2010; Helin and Dhanak 2013), which led to the development of various small molecules like I-BET, I-BET-151, RVX-208, PFI-1 and JQ1 that specifically block the BET bromodomains (Filippakopoulos et al. 2010; Fu et al. 2015; Pérez-Salvia and Esteller 2017).

JQ1 was the first-in-class potent and highly selective BET inhibitor available and was shown to displace BET bromodomains from acetylated chromatin by competitive binding and, thus to suppress transcription of downstream targets (Filippakopoulos et al. 2010; Delmore et al. 2011). BET inhibition by JQ1 was used to investigate BET function in pathologic conditions such as cancer (Filippakopoulos et al. 2010; Delmore et al. 2011), HIV infection (Banerjee et al. 2012), and heart failure (Anand et al. 2013; Spiltoir et al. 2013).

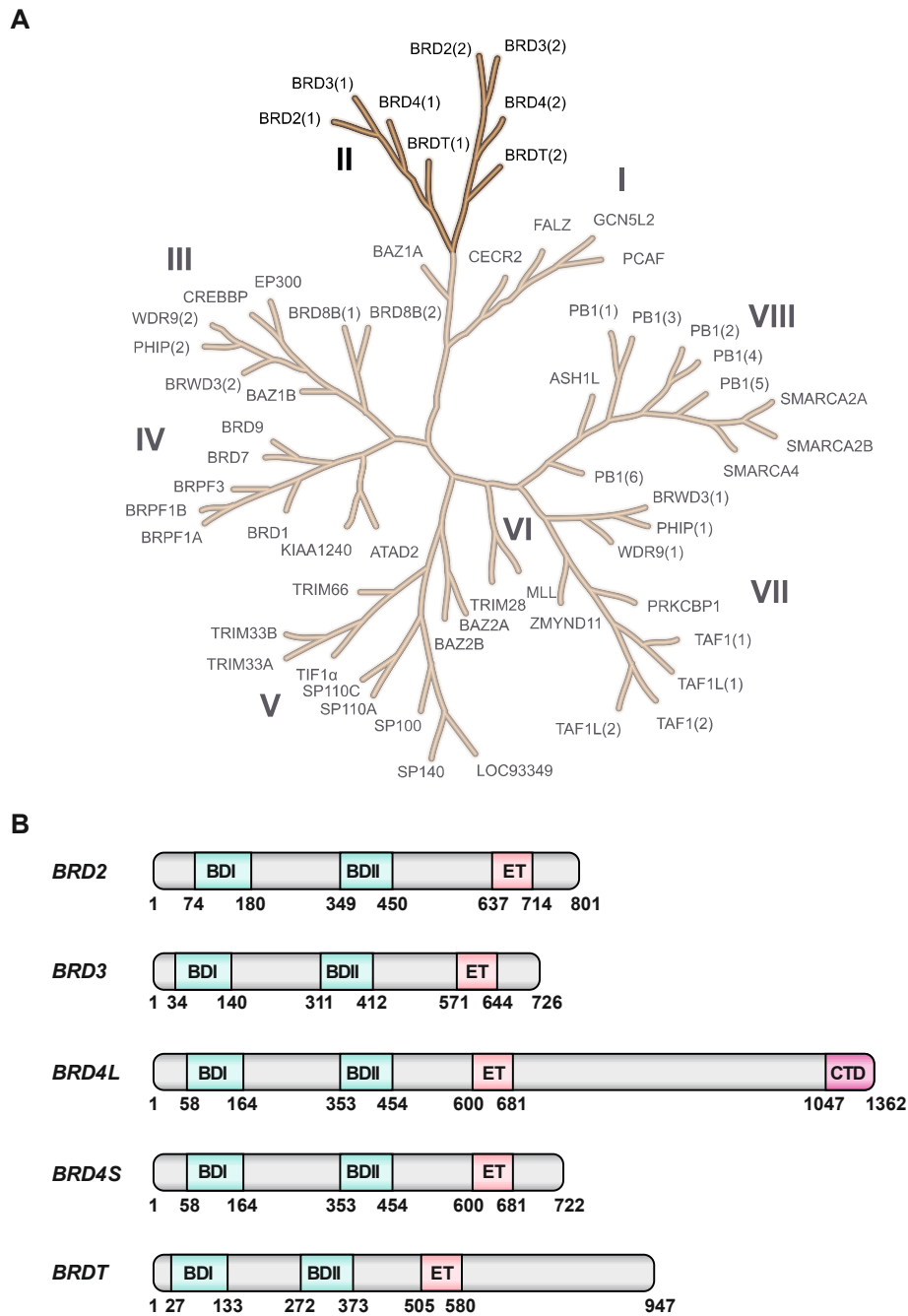


Figure 1.5: Phylogenetic tree of bromodomain-containing proteins and structure of BET proteins. Phylogenetic tree showing the eight families (I-VIII) of human bromodomain-containing proteins (adapted from (Filippakopoulos et al. 2012)) (A). Main features of BET proteins (adapted from (Fu et al. 2015)) (B). BDI/II= bromodomain 1/2, BET= bromodomain and extraterminal domain proteins, CTD= C-terminal domain, ET= extraterminal domain.

1.2.3 The role of BET proteins in the heart

The potential of BET inhibition in the heart has first been discovered in a high throughput assay of cardiomyocyte hypertrophy. Using phenylephrine-stimulated primary neonatal rat ventricular myocytes (NRVMs), an *in vitro* model for adrenergic activation, JQ1 was found to block hypertrophy and suppress expression of ANP, BNP, and SERCA2 mRNA (Anand et al. 2013;

Spiltoir et al. 2013). BET inhibition by JQ1 was further investigated *in vivo* in mice that were subjected to transverse aortic constriction (TAC), a murine pressure overload model. TAC induces cardiac remodeling, hypertrophy and left ventricular systolic dysfunction (Rockman et al. 1991). Daily administration of JQ1 for 4 weeks, however, was shown to block pathologic cardiac hypertrophy, to preserve cardiac function, and to attenuate cardinal histopathologic features of HF in mice subjected to TAC (Anand et al. 2013; Spiltoir et al. 2013).

In particular, morphometric and echocardiographic analyses revealed that JQ1 protects the heart from left ventricular wall thickening and dilatation, preserves the left ventricular mass, and protects the animals from systolic dysfunction after TAC. Furthermore, JQ1 was shown to normalize cardiomyocyte size, attenuate apoptosis, and reduce interstitial fibrosis after TAC, as demonstrated by histologic staining. As shown by quantitative real time PCR, JQ1 inhibits the expression of hypertrophic marker genes like *Nppa* and *Nppb* (Anand et al. 2013; Spiltoir et al. 2013). Moreover, global gene expression analysis revealed that JQ1-treatment reverses the expression of TAC-induced genes to levels of Sham-treated hearts, and that these genes show an enrichment for biological processes described for cardiac remodeling and development of HF like cell cycle regulation, cytoskeleton assembly, response to wounding, growth, and extracellular matrix organization. Gene set enrichment analysis (GSEA) of the TAC-induced genes showed a positive enrichment for HF gene sets that result from Calcineurin, NF κ B and GATA4 activation, which were negatively enriched with JQ1-treatment after TAC (Anand et al. 2013).

These cardio protective effects of BET inhibition have mostly been brought into context of BRD4, which was shown to be the highest expressed BET protein in the heart that gets further activated by hypertrophy (Anand et al. 2013; Spiltoir et al. 2013). Chromatin immunoprecipitation (ChIP) sequencing showed strong enrichment of BRD4 at active transcriptional start sites and at the majority of active enhancers in the murine heart (Anand et al. 2013). Thus, BRD4 was shown to promote the expression of the pro-hypertrophic ANP, and the connective tissue growth factor (CTGF) after TAC. Mechanistically BET proteins have been proposed to mediate transcriptional pause release through activation of the P-TEFb complex, which phosphorylates the C-terminal domain of RNA polymerase II (Anand et al. 2013).

These data show that BRD4 is induced in response to hypertrophic stimuli, enriches at transcriptional start sites and enhancers of a specific gene set, and plays a crucial role in the integration of pro-hypertrophic transcription factors like NFAT and GATA4. Therefore, BRD4 was proposed as co-activator of hypertrophic gene expression (Haldar and McKinsey 2014).

These studies demonstrate that BET proteins are promising therapeutic targets for HF. Indeed, BET inhibition is being established in human in the clinical trials with RVX-208 as therapeutic approach to reduce major adverse cardiac events in high-risk cardiovascular disease patients (Tsujiyama et al. 2018). Nevertheless, nothing is known about the specific roles of BRD2 and

BRD3 although they were detected in the heart as well (Anand et al. 2013; Spiltoir et al. 2013; Duan et al. 2017) and are also affected by BET inhibitors like JQ1 (Filippakopoulos et al. 2010).

1.3 Objectives

To ensure safety and efficacy of BET inhibitors as treatment of HF and to support the development of novel compounds, it is important to first identify the exact functions of individual BET members in cardiac cells: This would help to understand how BET inhibition directly affects the heart and could potentially help to refine this therapeutic approach. Therefore, further investigation on the roles of BET proteins in the heart are necessary and should answer the following questions: (i) what are the functions of the individual BET proteins in the heart? (ii) do the cardio protective effects of BET inhibition improve the prognosis of established pressure overload? and (iii) can the depletion of individual BET proteins in cardiac cells replicate the cardio protective properties of BET inhibition by JQ1?

Haldar and McKinsey suggested that the generation of conditional BET alleles is essential to allow the detailed examination of particular BET proteins and their individual functions in cardiac cells (Haldar and McKinsey 2014). In order to elucidate the cardio protective properties of BET inhibition and the contribution of BET chromatin readers to cardiac remodeling and the development of heart failure, the aims of my thesis are to:

1. *Measure BET mRNA and protein levels in the healthy and diseased murine heart*

I will describe cardiac BET expression by mRNA sequencing, quantitative PCR, immunoblotting, and immunocytochemistry in healthy adult mice and in mice with TAC-induced PO.

2. *Analyze the impact of JQ1-mediated BET inhibition on the survival of mice in the first two months after TAC*

To investigate if BET inhibition influences PO-mediated mortality, I will monitor the survival of JQ1-treated mice for eight weeks after TAC. Further, I will compare the effects of JQ1 and vehicle on pathogenesis four and eight weeks after PO-induction using histological, molecular, and echocardiographic methods.

3. *Generate and validate mice with a cardiomyocyte-specific disruption of Brd2 and Brd4*

To enable *in vivo* analysis of loss-of-function for particular BET members in specific tissues, conditional *Brd2* and *Brd4* alleles were previously generated in our group. My aim is to generate mice with a cardiomyocyte-specific disruption of *Brd2* and *Brd4*, respectively, by using our conditional alleles. To validate the Cre-mediated gene disruption, I will analyze cardiac DNA, mRNA, and protein levels in the resulting mice via PCR and immunoblotting.

4. *Examine the influence of Brd2 and Brd4 disruption on heart morphology and function in the newly generated mice*

My aim is to phenotype the hearts of the newly generated mice with a cardiomyocyte-specific disruption of *Brd2* or *Brd4* by histological, morphometric, and echocardiographic measurements.

5. *Investigate if loss of Brd2 or loss of Brd4 function in cardiomyocytes can protect the heart from TAC-mediated pathologic changes*

Data from BET inhibition by JQ1 suggest that BET proteins activate pro-hypertrophic genes upon induction of cardiac stress. In the final part of my thesis I investigate *in vivo* if and how the disruption of *Brd2* and *Brd4* in cardiomyocytes affects the heart's response to pressure overload. To identify changes in mortality, morphology, histopathology, stress signaling, and heart function I monitor the survival of the animals for over 4 months after PO-induction and perform morphometric, histological, molecular, and echocardiographic analyses 5 weeks after TAC.

2 Materials and Methods

2.1 Animals

2.1.1 Animal welfare

All animal experiments were approved and conducted in accordance with institutional and governmental guidelines. All animals in context of this thesis were maintained under standard laboratory conditions with 12 hours light/dark cycling and access to food and water ad libitum. C57BL/6N mice were delivered from Charles River, all other animals were bred in-house. Animals were kept in groups of 5 and were allowed to habituate for 1-2 weeks prior to interventions.

2.1.2 Generation of mouse strains

Two conditional knockout (KO) mouse lines were used in this study. In the *Brd2* conditional KO mouse line (*Brd2^{fl/fl}*, C57BL/6N and C57BL/6J mixed background), the coding exons 3 and 4 of *Brd2* gene were flanked by loxP sites (Benito et al. unpublished). The *Brd2* alleles were genotyped using primers Brd2-KO-F and Brd2-KO-R. PCR amplified 210 bp from the wildtype and 320 bp from the floxed allele. Male *Brd2^{fl/fl}* mice were crossed with *α MHC-Cre* females (Jackson no. 011038, C57BL/6N and C57BL/6J mixed background) (Agah et al. 1997) to generate *α MHC-Cre;Brd2^{fl/fl}* mice.

In the *Brd4* conditional KO mouse line (*Brd4^{fl/fl}*, C57BL/6N and C57BL/6J mixed background), the exons 6 and 7 of the *Brd4* gene were flanked by loxP sites (Benito et al. unpublished). The *Brd4* alleles were genotyped using primers Brd4-GT-F and Brd4-GT-R. PCR amplified 251 bp from the wildtype and 362 bp from the floxed allele. Male *Brd4^{fl/fl}* mice were crossed with *α MHC-Cre* (Jackson no. 011038, C57BL/6N and C57BL/6J mixed background) or *α MHC-MerCreMer* (C57BL/6J background) females to generate *α MHC-Cre;Brd4^{fl/fl}* or *α MHC-MerCreMer;Brd4^{fl/fl}* mice. *α MHC-MerCreMer* mice were a gift from Dr. Laura Zelerayan and originally generated by Dr. Jeffrey Molkentin (Sohal et al. 2001).

2.1.3 JQ1 treatment

JQ1 was a kind gift from Dr. Jun Qi and James Bradner, MD, from the Dana-Farber Cancer Institute (Boston, Massachusetts). The compound was dissolved in dimethyl sulfoxide (DMSO) (Sigma, #D2650-5X10ML) to produce a concentrated stock at a concentration of 50 mg/ml and stored in aliquots at -20°C. Before application, appropriate amounts of the JQ1 stock were thawed and diluted in 9 parts of 10% 2-Hydroxypropyl- β -cyclodextrin (10% HP- β -CD) (Sigma, C0926-5G) to obtain a JQ1 working solution. The JQ1 working solution was delivered daily for 28 consecutive days by intraperitoneal injection at concentration of 50 mg/kg/day starting one day after surgery. As control, half of the animals received DMSO in 10% HP- β -CD (vehicle).

The experiments were conducted in C57BL/6N female mice, which were randomly assigned to either the JQ1- or the vehicle treatment group.

2.1.4 Tamoxifen application

In order to activate Cre-recombinase in *α MHC-MerCreMer* positive mice Tamoxifen was applied. To prepare Tamoxifen working solution at a concentration of 10 mg/ml, 50 mg Tamoxifen (Sigma, T5648) were suspended in 100% ethanol and subsequently dissolved in 4.5 ml Miglyol (Caelo, #3274) by vigorous shaking. The Tamoxifen solution was delivered to 5-week-old animals by intraperitoneal injection at a dosage of 30 mg/kg/day for three consecutive days (Bersell et al. 2013).

2.1.5 Echocardiography

The heart function and dimensions of untreated, Sham, and TAC operated mice were examined by transthoracic echocardiography using a Vevo 2100 system equipped with a MS-400 30 MHz transducer (Visualsonics) as previously described (Pistner et al. 2010). Fractional flow reserve was calculated from pressure gradients across the transverse aorta, which were measured by Doppler echocardiography with a 20 MHz transducer (MS-250). Therefore, the animals were first anesthetized with isoflurane (1-2 %) using a respiratory mask and their thorax depilated with hair removal cream. Short sequences of the beating hearts were recorded in B-mode in the long axis or the short axis view and M-Mode in mid papillary view, respectively. During the recordings vital parameters were monitored to stay in the defined range (body temperature, heart rate, respiration).

Using the LV-trace function of the VevoLab software (version 3.1.0), echocardiographic M-Mode images were analyzed to determine heart dimensions: anterior wall thickness (AWThd/s), posterior wall thickness (PWThd/s), left ventricular enddiastolic diameter (LV-EDD), left ventricular endsystolic diameter (LV-ESD), and heart rate. These parameters were used to calculate characteristic variables (**Appendix Table 5.1**) such as ejection fraction (EF), fractional shortening (FS), left ventricular mass, and left ventricular weight to body weight ratio. Echocardiography was performed by the SFB1002 service team Marcel Zoremba and Roland Blume (Cardiology and Pneumology, University Medical Center Göttingen). The data was analyzed in a blind test with respect to genotype and treatment. GraphPad Prism (v. 7.03) was used to plot and analyze data. Two-way ANOVA with Tukey post-hoc test ($p < 0.05$), if not stated otherwise, was used to determine statistical significance among groups.

2.1.6 Transverse aortic constriction (TAC)

Transverse aortic constriction has been previously described (Rockman et al. 1991; Hu et al. 2003; deAlmeida et al. 2010). The aim of this surgical procedure is to reduce the diameter of the transverse aorta. Mice aged 8-10 weeks were randomized into Sham or TAC groups. Right

before surgery, mice were anesthetized by intraperitoneal injection of 50 μ l 0.9% sodium chloride solution containing Medetomidin (0.5 mg/kg), Midazolam (5 mg/kg) and Fentanyl (0.05 mg/kg).

A 1-1,5 cm long suprasternal incision was made, and the aortic arch was visualized using a binocular operating stereoscope. The thymus and fat tissue were gently separated from the aortic arch. After identification of the transverse aorta, a 6-0 polyviolene suture was placed between the first and second trunk of the aortic arch and two loose knots were tied. To standardize the constriction, a 27 gauge blunt needle was placed parallel to the transverse aorta, the knots fastened and the needle removed. For the Sham control surgery, the procedure is identical except for the constriction of the aorta. The mouse is closed using a 6-0 prolene suture.

After surgery the anesthesia was antagonized by subcutaneous injection of 50 μ l 0.9% sodium chloride solution containing Atipamezol (2.5 mg/kg) and Flumazenil (0.1 mg/kg). Subcutaneous injection of Buprenorphin in the common dose of 0.05-0.1 mg/kg was used for analgesia. The mouse was allowed to recover on a heating pad.

3 days later, Doppler velocity was measured using a 20 MHz probe to quantify the pressure gradient across the TAC/Sham region by transthoracic echocardiography. During 3 days after surgery, mice received analgesic therapy with carprofen (subcutaneous) and animal health status was checked every day. 1, 4 and 8 weeks after surgery, mice were analyzed by echocardiography and hearts were harvested for molecular characterization or histology. Surgeries were performed by Sarah Zafar (AG Zimmermann, Pharmacology and Toxicology, University Medical Center Göttingen), Sabrina Koszewa and Alessya Kretzschmar (AG Toischer, Cardiology and Pneumology, University Medical Center Göttingen). Power calculation using G*Power (v.3.1.9.2) (Faul et al. 2007) was performed to determine sample sizes based on mean ejection fractions of animals subjected to Sham and TAC in previous studies from our group (**Appendix Figure 5.1**).

2.1.7 Heart dissections

Mice were anesthetized with isoflurane and sacrificed by cervical dislocation. The body weight was determined before dissection. Next, the thorax was cut open and the heart excised at the aorta and transferred into a petri dish filled with sterile saline. A 21 gauge blunt needle was carefully placed into the aorta and fixed with fine forceps allowing a retrograde perfusion with sterile saline to remove residual blood. The heart was weighted, atria and the right ventricle removed, and the left ventricle weighted again before it was snap frozen in liquid nitrogen. The tibia was dissected and measured using an electronic gauge.

2.2 Molecular analysis

2.2.1 *In-silico oligonucleotide design*

Oligonucleotides for legacy PCRs were designed with DNADynamo (BluetractorSoftware), whereas RT-qPCR primers were designed using Primer-BLAST (<https://www.ncbi.nlm.nih.gov/tools/primer-blast/>). Primer-BLAST was operated with the following settings, product size: 100-200 bp; exon junction span: may not span exon-exon junction; intron inclusion: yes (if possible); organism: *Mus musculus* (taxid:10090); allow splice variants: yes. Melting temperatures were calculated using the Thermo Fisher Tm Calculator (<https://www.thermofisher.com/de/de/home/brands/thermo-scientific/molecular-biology/molecular-biology-learning-center/molecular-biology-resource-library/thermo-scientific-web-tools/tm-calculator.html>). All oligonucleotides were synthesized by Eurofins Genomics.

2.2.2 *Genotyping*

The genotypes of genetically modified mice were analyzed by legacy PCR using primers depicted in **Table 2.1** and MangoTaq™ Polymerase (Bioline, BIO-21078). To isolate genomic DNA (gDNA), tail biopsies were digested overnight in 200 µl DirectPCR-Tail lysis buffer (Viagen Biotech, #102-T) including 200 µg/ml Proteinase K at 55°C and 400 rpm on a heating block. Proteinase K was heat inactivated for 45 min at 85°C prior to the assembly (**Table 2.2**) and run (**Table 2.3**) of the PCR reaction.

Table 2.1: Genotyping primer

Primer	Sequence (5' – 3')
Brd2-KO-F	CCATGGCAACCATTAAGTCC
Brd2-KO-R	GTGAAGTGAATTGCAACCAGC
Brd2-recomb-F	GGGCTGGAAAGTGCTATCC
Brd2-recomb-R	CACATCCCCACAAGAATTCC
Brd4-GT-F	GTTACCTGCTCACGTTTGG
Brd4-GT-R	TGCCCTCACTTCCTTCCG
Brd4-recomb-F	GTGTGATTGGCAAGAAAGGC
Brd4-recomb-R	AGTCTAAAGGGAAACTGAACGC
Cre-ctrl-F	CAAATGTTGCTTGTCTGGTG
Cre-ctrl-R	GTCAGTCGAGTGCACAGTTT
Cre-F	ATGACAGACAGATCCCTCCTATCTCC
Cre-R	CTCATCACTCGTTGCATCATCGAC
MerCreMer-F	TCTATTGCACACAGCAATCCA
MerCreMer-Tg-R	CCAGCATTGTGAGAACAAGG
MerCreMer-wt-R	CCAACTCTTGTGAGAGGAGCA

Table 2.2: Standard genotyping reaction

Reagents	Volume (μ l)
5x reaction buffer (colored)	4.0
MgCl ₂ (50 mM)	1.5
dNTPs (100 mM)	0.5
Forward primer (10 pmol/ μ l)	1.0
Reverse primer (10 pmol/ μ l)	1.0
gDNA	1.5
H ₂ O (to 20 μ l)	10.3
Mango-Taq polymerase	0.2

Table 2.3: Standard genotyping protocol

Step	Temp. ($^{\circ}$ C)	Time
Denaturation	95	3 min
Amplification (x30)	95	30 sec
	58-60	30 sec
	72	30 sec
Elongation	72	5 min

The PCR reactions, together with a 100 bp DNA ladder (Thermo Fischer, SM1153), were separated by gel electrophoresis for 45 min at 120 V in a TBE (45 mM Tris-borate, 1 mM EDTA) buffered 2 % agarose gel. The ethidium bromide (0.2-0.5 μ g/ ml gel) stained DNA was imaged using the Alpha Imager gel documentation system (Protein Simple).

2.2.3 RNA isolation

In order to reproducibly obtain high quality RNA from heart samples or isolated cardiomyocytes the RNeasy Fibrous tissue Mini kit (Qiagen, 74704) was used according to the manufacturer's manual.

In short, up to 30 mg of snap frozen heart tissue or 10-25 μ l pellet of isolated cardiomyocytes was placed into a 2ml tube containing a 7 mm stainless steel bead (Qiagen, 69990) and 300 μ l RLT buffer with 40 mM DTT and homogenized for 5 min and 50 Hz using a Tissue Lyser LT (Qiagen, 85600). After addition of 590 μ l RNase-free water and 10 μ l Proteinase K, the lysate was incubated for 10 min at 55 $^{\circ}$ C and spun for 3 min at 10,000 x g. The clear supernatant was transferred into a fresh 1.5 ml tube and mixed with 0.5 vol of 100% ethanol. The precipitated RNA was transferred to a spin column and bound to the silica membrane spinning for 15 sec at 10,000 x g. After washing with 350 μ l buffer RW1 and spinning for 15 sec at 10,000 x g the membrane was incubated for 15 min at room temperature with 10 μ l DNase I in 70 μ l RDD buffer followed by a second wash with buffer RW1. Next, the membrane was washed twice with 500 μ l buffer RPM (supplemented with 100% ethanol) and first spun for 15 sec at 10,000 x g and second for 1 min at 10,000 x g. After incubating with 30 μ l elution buffer for 1 min at room temperature, the RNA was eluted into a fresh RNase-free 1.5 ml tube by spinning for 1 min at 10,000 x g and immediately placed on ice. All isolation steps were carried out at room

temperature. Based on the absorbance at 260nm, the RNA concentrations were photometrically determined using a Nanodrop 2000 (Thermo Fisher). The RNA was subsequently used for reverse transcription (RT) or stored at -80°C.

2.2.4 cDNA synthesis

For gene expression studies, total RNA was reverse transcribed into complementary DNA (cDNA) using the iScript™ cDNA Synthesis Kit (Bio-Rad, 1708891).

To allow for cloning of the complete coding region of a gene of interest, total RNA was reverse transcribed using the Superscript IV reverse transcriptase (Thermo Fischer, 18090010) together with Oligo (dT) primers (Thermo Fischer, 18418012) according to the manufacturer's instructions.

2.2.5 Molecular cloning

To analyze the *Brd2* mRNA sequence of *Brd2*ΔBDI mice, total left ventricular RNA (2.2.3) was reverse transcribed using Superscript IV reverse transcriptase and Oligo (dT) primers (2.2.4). *Brd2* was amplified from cDNA using custom made primers annealing upstream of the start codon (5'-GCTGAGCGGCGGCGGTTCC-3') and downstream of the stop codon (5'-GAGCCTTCTGCCCATCTGGCC-3'), respectively, using Phusion® High Fidelity DNA Polymerase (New England Biolabs, M0530S) according to the manufacturer's protocol. The PCR product was purified by 1% agar (PeqLab) gel-electrophoresis in TAE-buffer (40 mM Tris, 20 mM acetic acid, 1 mM EDTA), extracted with Monarch® DNA Gel Extraction Kit (New England Biolabs, T1020S), and ligated into pMiniT™ 2.0 vector with NEB® PCR Cloning Kit (New England Biolabs, E1202S). The resulting plasmid was transformed into NEB® 10-beta Competent *E. coli* (New England Biolabs, C3019H), amplified, purified with Nucleospin Plasmid EasyPure (Macherey-Nagel, #740727.50), and validated by Sanger sequencing with *Sp6-20* (5'-CTATTTAGGTGACACTATAG-3') and *T7prom* (5'-TAATACGACTCACTATAGGG-3') standard primers (LGC Genomics, FlexiRun). The sequencing results were aligned to *Brd2* cDNA sequence (CCDS28641.1) and analyzed using DNADynamo (BluetractorSoftware).

2.2.6 Quantitative real time PCR

To analyze gene expression levels reverse transcription quantitative real-time PCR (RT-qPCR) was performed. Primers (Table 2.4) were designed using Primer-BLAST (<https://www.ncbi.nlm.nih.gov/tools/primer-blast/>) as described in "nucleotide design". The SsoAdvanced Universal SYBR Green Supermix (Bio-Rad, #1725272) was diluted with nuclease-free water, supplemented with primers according to Table 2.5 and transferred into ice-cooled 96 well plates (Bio-Rad, #2239441) where cDNA or nuclease-free water (no template control) were added. The reaction plates were covered with adhesive sealing film

(Bio-Rad, #MSB1001), spun at 1000xg for 1 min and measured using settings according to **Table 2.6** with the IQ5 Real Time PCR System (Bio-Rad).

Table 2.4: qPCR primer

Primer	Sequence (5' – 3')
MmBrd2_e2_e3_F	ATGCTGCAAAACGTGACTCC
MmBrd2_e2_e3_R	TACAGAAGCCATTGTGGGGC
MmBrd2_e7_e8_F	GTTAAAGCACTGCAACGGCA
MmBrd2_e7_e8_R	CATCCCGGTAGTCACGGTTC
MmBrd2_e11_e12_F	CCTTCGAAAGAAACCCCGGA
MmBrd2_e11_e12_R	TCCACTGACATCCTGCAACC
MmBrd3_e5_e6_F	CCCCTGTACCAACCATCACT
MmBrd3_e5_e6_R	GTGTCTGCTTTCCGCTTAC
MmBrd3_e9_e10_F	AAAGGCTCCCACCAAGAAGG
MmBrd3_e9_e10_R	ATCATAGCTCATGGGCAGGC
MmBrd4_e3_e4_F	GGAAACACCAGTTTGCGTGG
MmBrd4_e3_e4_R	AGTTGTTTTCCAAGCGCTTCTT
MmBrd4_e5_e6_F	TCGTCTTAATGGCAGAAGCTC
MmBrd4_e5_e6_R	GATACACCAGGCTTTGCTGC
MmBrd4_e15_e16_F	CAAGTCAGACCCCTACTCAGC
MmBrd4_e15_e16_R	CTGCCCTTTACCTGCTTCTT
MmNppa_new_F	CTGCTTCGGGGGTAGGATTG
MmNppa_new_R	GCTCAAGCAGAATCGACTGC
MmNppb_new_F	AAGGACCAAGGCCTCACAAA
MmNppb_new_R	GCCAGGAGGTCTTCCTACAAC
MmRn18s-F	CATGCATGTCTAAGTACGCAC
MmRn18s-R	GTCGGCATGTATTAGCTCTAG

Table 2.5: qPCR reaction

Reagents	Volume (µl)
Nuclease-free H ₂ O	7.8
Forward primer (10 pmol/µl)	0.6
Reverse primer (10 pmol/µl)	0.6
SsoAdvanced SYBR Green Mix	10
cDNA (2.5 ng)	1

Table 2.6: qPCR protocol

Step	Temp. (°C)	Time
Denaturation	95	3 min
Amplification (x45)	95	10 sec
	60	30 sec
Meltcurve (x81)	55-95	6 sec/step

2.2.7 Total protein extraction

For downstream applications like western blotting or mass spectrometry heart tissue or cells were mechanically homogenized and lysed using RIPA buffer. In short, about 30 mg of snap

frozen heart tissue was placed in RNase-free 2 ml tubes containing a 5 mm stainless steel bead (Qiagen, 69989) that were precooled on dry ice for at least 15 min and incubated for another 15 min on dry ice. To prevent the lysis buffer from freezing, the samples were incubated on room temperature for 2 min before Pierce RIPA buffer (Thermo Fischer, 89900) supplemented with cOmplete™ protease inhibitors (Sigma, 000000011873580001) was added. The samples were then immediately placed in the Tissue Lyser LT (Qiagen, 85600) and homogenized for 5 min with 50 Hz. The lysates were briefly spun in a precooled centrifuge to remove the foam and placed on an overhead rotor at 4°C for at least 30 min before they were cleared for 15 min at 16,000 x g and transferred into a fresh 1.5 ml tube. Based on the absorbance at 562nm, the protein concentrations were photometrically determined using a Pierce™ BCA Protein Assay Kit (Thermo Fischer, 23225) and a 96-well plate reader (Biotek). For longtime storage the protein was kept at -80°C.

2.2.8 Subcellular fractionation

To examine protein localization and to especially enrich nuclear and chromatin-bound proteins from tissue and cells, the Subcellular Protein Fractionation Kit for tissue (Thermo Fischer, # 87790) was used according to the manufacturer's protocol. When handling cardiomyocytes, the cell strainer was omitted, and lysis buffer volumes adjusted according to the protocol of the Subcellular Protein Fractionation Kit for cultured cells (Thermo Fischer, # 78840).

2.2.9 Immunoblotting

Protein levels were detected after separation by SDS-PAGE, subsequent transfer onto nitrocellulose membrane following immunostaining ("Western blot"). Protein samples (10-30 µg) containing protease inhibitors (Sigma, 000000011873580001) were denatured for 10 min at 95°C in 4x Laemmli buffer (Bio-Rad, #1610747) and 0.2M DTT and separated using stain-free 4-15% TGX Gels (Bio-Rad; #) by applying a constant Voltage of 200 V for 35 min. The polyacrylamide gel was UV-activated (1 min) for subsequent stain-free imaging. Separated proteins were then transferred onto 0.2 µm nitrocellulose membrane (Bio-Rad, #1704270) using the Trans-Blot® Turbo™ System (Bio-Rad, #170-4155) at a constant current of 2.5 A. To check transfer efficiency and for later normalization, the membrane was imaged using the stain-free system with a ChemiDoc XRS+ (Bio-Rad, #1708265). Membranes were then cut as required and blocked in 5% milk (Roth, #T145.3) in TBS-T (20 mM Tris-base, 50 mM NaCl, 0.1% Tween 20, pH=7.5) for one hour at room temperature. After blocking, membranes were incubated with primary antibodies (**Table 2.7**) in 1% milk in TBS-T at 4°C overnight. Next, membranes were washed three times in TBS-T and incubated with horseradish peroxidase conjugated secondary antibodies ECL anti-Rabbit IgG and ECL anti-Mouse IgG (**Table 2.7**) for one hour on room temperature. Afterwards membranes were washed trice in TBS-T before the SuperSignal™ West Femto Maximum Sensitivity Substrate (Thermo Fisher, #34095) was

added. Chemiluminescence signal was detected with a Chemidoc XRS+ imager. Band intensities were quantified with Image Lab using background subtraction, normalized to total protein in Microsoft Excel 2016, plotted and analyzed in GraphPad using two-tailed t-test.

Table 2.7: Antibodies used for immunoblotting

Antibody	Dilution	Source	Antibody ID
Rabbit-anti-BRD2	1:1000	CST, #5848S	AB_10835146
Rabbit-anti-BRD4	1:1000	Abcam, ab128874	AB_11145462
Rabbit-anti-BRD4	1:1000	CST, #13440	AB_2687578
Mouse anti-GAPDH	1:10000	Merck Millipore, MAB374	AB_2107445
Donkey anti-Rabbit IgG HRP-conjugated	1:10000	GE Healthcare, NA934	AB_772206
Sheep anti-Mouse IgG HRP-conjugated	1:10000	GE Healthcare, NA931	AB_772210

2.3 Histological and immunocytochemical analyses

2.3.1 Langendorff CM isolation

Adult ventricular cardiomyocytes were isolated via the Langendorff perfusion as previously described (Toischer et al. 2017). Mice were anesthetized and sacrificed by cervical dislocation. The heart was dissected by cutting the aorta and then quickly transferred into a petri dish filled with ice-cold Ca-free Tyrode (**Table 2.8**). Next, the aorta was connected to a 20G cannula, the heart mounted on a Langendorff apparatus, and retrogradely perfused with Tyrode (flow rate 3.5 ml/min) for 3 min at 37°C. Thereafter, perfusion was continued for 7 min with 20 mL Tyrode supplemented with LiberaseTM TM (Sigma, LIBTM-RO), trypsin, and CaCl₂ (**Table 2.9**) until the heart became soft. Afterwards, the atria were carefully excised and discarded, whereas the digested ventricles were dissected for 30 sec in 2.5 mL digestion buffer. To stop the digestion, 2.5 mL Stop solution (**Table 2.10**) were added to the cell suspension, which was then homogenized using a 1 mL syringe without a needle for 3 min. After 10 min of sedimentation the supernatant was removed, and the cardiomyocyte pellet washed twice with Tyrode. Freshly isolated cardiomyocytes were either directly used for immunocytochemistry or the pellet snap frozen on liquid nitrogen and stored at -80°C for later protein or RNA isolation.

Table 2.8: Tyrode solution

Reagents	concentration (mmol/l)
NaCl	113
KCl	4.7
KH ₂ PO ₄	0.6
Na ₂ HPO ₄ x 2 H ₂ O	0.6
MgSO ₄ x 7 H ₂ O	1.2
NaHCO ₃	12
KHCO ₃	10
HEPES	10
taurine	30
2,3-butanedione monoxime (BDM)	10
glucose	5.5
phenol red	0.032

Table 2.9: Digestion buffer

Reagents	volume
Tyrode	20 ml
Liberase™ TM	300 µl
Trypsin 10-fold, 2.5%	111.2 µl
10 mM CaCl ₂	25 µl

Table 2.10: Stop solution

Reagents	volume
Tyrode	2.25 ml
Bovine calf serum	250 µl
10 mM CaCl ₂	3.125 µl

2.3.2 Immunocytochemistry

Directly after isolation, 200 µl of suspended cardiomyocytes were plated for 30 min on laminin-coated Ø 18 mm coverslips (10 µl laminin [2 mg/ml] 1:10 in Tyrode per coverslip) placed in a 12-well-plate. The buffer was replaced by 4% paraformaldehyde and cells fixed for 10 min. After a quick washing step with blocking buffer (10% bovine calf serum, 0.2% Triton X-100 in PBS), the cells were blocked and permeabilized in blocking buffer for one hour at room temperature. After blocking, cells were incubated with primary antibodies (**Table 2.11**) in blocking buffer at 4°C overnight. Next, the cells were washed trice with blocking buffer and incubated with secondary antibodies (**Table 2.11**) in blocking buffer overnight at 4°C in a dark chamber. Afterwards, the cells were washed three times with PBS and mounted on slides

using ProLong® Gold antifade with DAPI (Thermo Fischer, P36935) which was allowed to harden overnight at room temperature and in the dark.

Table 2.11: Antibodies used for immunocytochemistry

Antibody	Dilution	Source	Antibody ID
Rabbit-anti-BRD2	1:500	Bethyl, A302-583A	AB_2034829
Rabbit-anti-BRD2	1:500	CST, #5848S	AB_10835146
Rabbit-anti-BRD4	1:500	Abcam, ab128874	AB_11145462
Mouse anti-Actinin	1:500	Sigma, A7811	AB_476766
Alexa Fluor® 633 Goat anti-Rabbit IgG (H+L)	1:1000	Thermo, A-21070	AB_2535731
Alexa Fluor® 514 Goat anti-Mouse IgG (H+L)	1:1000	Thermo, A-31555	AB_2536171

2.3.3 Confocal microscopy

Confocal microscopy was performed using Zeiss LSM 710 (Zeiss) microscope equipped with a Plan-Apochromat x63/1.40 oil-immersion objective. Images were acquired for Alexa Fluor 514 (514 nm diode laser excitation) and Alexa Fluor 633 (633 nm diode laser excitation) with a resolution of 2048 x 2048 pixels, at a speed of 31 seconds per frame and 16-fold line averaging. ZEN 2010 software was used for image analysis.

2.3.4 Paraffin embedding, dewaxing and rehydration

Dissected hearts were fixed in 4% paraformaldehyde (PFA) at 4°C overnight. The fixed hearts were dehydrated in an ethanol series, and infiltrated in paraffin for sectioning using a dip and dunk tissue processor (Leica, TP1020) by incubating in 60% ethanol, 2x 75% ethanol, 2x 96% ethanol, 2x 100% ethanol, 2x xylol, and 3x paraffin, each for 90 min. Paraffin blocks were prepared using an embedding station (Leica, EG1150H) and 5 µm thick heart cross sections were generated at a Microtom (Leica RM 2165). For downstream applications, paraffin cross sections were incubated at 65°C for one hour, dewaxed in xylol (5 min twice) and rehydrated in a decreasing ethanol series (2x 100 % - 95% - 70% - 50%- 30 %, 5 min each step) and in distilled water.

2.3.5 Masson's trichrome staining

After dewaxing, the 5 µm paraffin sections were post-fixed with Bouin's solution (Sigma, HT10-1-32) overnight at room temperature and stained using Masson's trichrome staining kit (Sigma, HT15-1KT) according to the manufacturer's instructions. In short, Bouin's solution was removed and slides rinsed with tap water until colorless, incubated with Hematoxylin QS (Vectorlabs) for 40 sec and rinsed with tap water for 5 min. After washing with distilled water, the slides were stained with Biebrich Scarlet-acid Fuchsin solution for 2 min and immediately placed in phosphotungstic/phosphomolybdic acid solution and incubated for 30 min. Next, the slides were immersed in aniline blue solution for 10 min, de-stained for 1 min in 1% acetic acid and washed in distilled water. The slides were then dehydrated in an increasing ethanol series

(30% - 50% - 70% - 95% - 100%) and xylol, each for 1 min. The slides were mounted using Permount medium (Fischer Scientific, SP15-100). Nuclei are stained blue/violet, cytoplasm red, muscle fibers red and collagen blue.

2.3.6 Picro Sirius Red staining

Connective tissue of dewaxed and rehydrated 5 µm paraffin section was stained using the Picro-Sirius Red Stain Kit (Abcam, ab150681) according to the manufacturer's instructions. In short, dewaxed and rehydrated slides were covered with Picro-Sirius Red solution and incubated for 60 min at room temperature. The slides were then quickly rinsed twice in acetic acid solution and once in absolute alcohol. After dehydration in two changes of absolute alcohol, the slides were cleared and mounted with Permount (Fischer Scientific, SP15-100) medium. Cytoplasm and muscle fibers are stained yellow, whereas collagen is stained red.

2.3.7 Wheat germ Agglutinin staining

To visualize cell borders, dewaxed and rehydrated heart sections were washed twice with Hank's balanced salt solution (HBSS) without phenol (life technologies #14025-092) and labeled for 15 min at room temperature with a wheat germ agglutinin (WGA) conjugate (Invitrogen, W11262) in HBSS at a concentration of 10 µg/ml. After two consecutive washes with PBS, the slides were mounted using ProLong® Gold antifade with DAPI (Thermo Fischer, P36935) which was allowed to harden overnight at room temperature and in the dark.

2.3.8 Quantification of histological stainings

Images of histological stainings were analyzed using the ImageJ distribution Fiji (Schindelin et al. 2012; Rueden et al. 2017). To determine the minimal fiber diameters (MFD) of heart cells, 5 images (200x magnification) from one WGA-stained heart section per mouse were captured, digitized and analyzed using semi-automated segmentation (macro: **Appendix Table 5.2**). In brief, grey-scale images underwent smoothing, background subtraction, and contrast adjustments before they were transformed to binary images (black-and-white) using regional gradient thresholding to allow identification and analysis of the particles (cell lumen). MFDs from >1200 cells per mouse were analyzed and plotted with GraphPad using two-way ANOVA. To determine the percentage of fibrous area from Picro-Sirius Red stained heart sections, images of one section per mouse were captured at a 100x magnification and analyzed with a custom-made ImageJ macro (**Appendix Table 5.3**). Therefore, brightfield images were split in the red-green-blue (RGB) channels and the area of the whole section as well as of the fibrotic regions measured using automated thresholds. The amount of fibrosis was calculated in Microsoft Excel 2016 and plotted and analyzed with GraphPad using two-way ANOVA with Tukey correction for multiple comparisons.

2.4 Next Generation Sequencing

2.4.1 mRNA library preparation

Sequencing of RNA-seq samples and basic analysis (2.4.2 – 2.4.4) was conducted at the Microarray and Deep-Sequencing Facility Göttingen (Transcriptome and Genome Analysis Laboratory, TAL, headed by Gabriela Salinas) by Orr Shomroni. RNA-seq libraries were generated using the TruSeq RNA Library Preparation Kit v2, Set A (48 samples, 12 indexes) RS-122-2001 protocol from Illumina starting with 500 ng of total RNA. Quality and integrity of RNA was assessed with the Fragment Analyzer from Advanced Analytical by using the standard sensitivity RNA Analysis Kit (DNF-471). All samples selected for sequencing exhibited an RNA integrity number over 8. The ligation step was optimized by diluting the adapters concentration to increase ligation efficiency (>94%), and finally the number of PCR cycles was reduced to avoid PCR duplication artifacts as well as primer dimers in the final library product. For accurate quantitation of cDNA libraries, a fluorometric based system, the QuantiFluor™ dsDNA System from Promega, was used. The size of final cDNA libraries was determined by using the dsDNA 905 Reagent Kit (Fragment Analyzer from Advanced Bioanalytical) exhibiting a sizing of 300 bp in average. Libraries were pooled and sequenced on an Illumina HiSeq 4000 (Illumina) generating 50 bp single-end reads (30-40 Mio reads/sample).

2.4.2 Raw read and Quality check

Sequence images were transformed with Illumina software BaseCaller to BCL files, which was demultiplexed to fastq files with bcl2fastq v2.17.1.14. The sequencing quality was asserted using FastQC (Andrews 2010).

2.4.3 Mapping and Normalization

Sequences were aligned to the reference genome *Mus musculus* (mm10 version 89, https://www.ensembl.org/Mus_musculus/Info/Index) using the STAR aligner (Dobin et al. 2013) (version 2.5.2a) allowing for 2 mismatches within 50 bases. Subsequently, read counting was performed using featureCounts (Liao et al. 2014).

2.4.4 Differential expression analysis

Read counts were analyzed in the R/Bioconductor environment (version 3.4.2, www.bioconductor.org) using the DESeq2 (Love et al. 2014) package version 1.14.1. Candidate genes were filtered using an absolute log₂ fold-change >0.5 and FDR-corrected p-value <0.05. Gene annotation was performed using *Mus Musculus* entries via biomaRt R package version 2.32.1 (Durinck et al. 2009).

2.4.5 Analysis of differentially expressed genes

InteractiVenn (<http://www.interactivenn.net/>) was used to calculate gene set overlaps (Heberle et al. 2015). Heatmapper (<http://heatmapper.ca/>, (Babicki et al. 2016)) was used to generate heatmaps. WebGestalt (<http://www.webgestalt.org>, (Zhang et al. 2005)) was used for Gene Ontology (GO) functional analysis with categories being significantly enriched with $p < 0.05$ and false discovery rate (FDR) < 0.05 if not otherwise indicated. Cytoscape 3.6.1 plugin ClueGO 2.5.2 (Bindea et al. 2009) (Bonferroni adjusted p -value < 0.05 , κ -score = 0.4) GO term fusion was used for gene network visualization using ontology for molecular function, biological process and cellular compartment if not otherwise indicated.

2.4.6 Gene set enrichment analysis

Gene set enrichment was analyzed using GSEA (Mootha et al. 2003; Subramanian et al. 2005). Mouse gene symbols (uppercase letters) and Reads Per Kilobase Million (RPKM) were converted to a tab delimited text file (.txt) and a categorical class file format (.cls) was generated. Data were not ranked and analyzed with following settings, number of permutations: 1000; permutation type: phenotype, max size: 1000, number of markers: 1000.

2.4.7 Microarray analysis

Quality control and differential expression analysis of the microarray data was performed at the Microarray and Deep-Sequencing Facility Göttingen (Transcriptome and Genome Analysis Laboratory, TAL, headed by Gabriela Salinas) by Orr Shomroni. The data analysed was previously published data GSE48110 (Anand et al. 2013). The complete analysis was done in the R/bioconductor environment (version 3.5.1). Quality control for the data was performed using arrayQualityMetrics (version 3.36.0) (Kauffmann et al. 2009), generating plots for between array comparisons, array intensity distributions, variance mean dependence and individual array quality. Differential expression analysis between the different conditions was performed using R package limma (version 3.36.2) (Ritchie et al. 2015) using annotation package mogene10sttranscriptcluster.db (version 8.7.0) (MacDonald 2017), where samples from the 3 conditions (TAC, TAC_JQ1 and Sham) were tested against each other, while separating the samples based on their day association (day 3, 11 or 28).

3 Results

3.1 BET protein family members in the mouse heart

3.1.1 BETs are expressed in the heart and localized in nuclei

Anand and colleagues previously described that the BET protein family members *Brd2*, *Brd3*, and *Brd4* are expressed in the murine heart, with significantly higher levels of *Brd4*. Furthermore, they showed that BRD4 is localized in cardiomyocyte nuclei (Anand et al. 2013). Transcriptome analysis of adult mice of the FVB/N inbred strain by mRNA sequencing (Khadjeh et al. unpublished) showed *Brd2*, *Brd3*, and *Brd4* expression in the left ventricle. The comparison of the gene length normalized counts (RPKMs) revealed a 4-fold higher expression of *Brd2* in the heart than *Brd3* and *Brd4* ($p < 0.0001$, one-way ANOVA with Tukey post-hoc test, $n=5$). (**Figure 3.1A**). Immunocytochemistry of isolated cardiomyocytes from 3-month-old wildtype mice revealed co-localized fluorescent signals for BRD2 or BRD4 with DAPI indicating nuclear localization (**Figure 3.1B**). In all following experiments I focused on *Brd2* as the highest expressed BET member in the heart, and *Brd4* as the most intensively studied one.

Immunoblotting with left ventricular total protein from 3 months old FVB/N mice detected BRD2 at about 110 kDa (**Figure 1.1C left**), whereas BRD4 showed only very weak signal (data not shown). Therefore, further BRD4 immunoblots were performed using subcellular protein fractions from left ventricle. In a direct comparison, BRD4 was only detectable in the nuclear and chromatin-bound protein but not in the cytosolic and membrane-bound fractions (**Figure 3.1C right**). Interestingly in the BRD4 blot, a protein band at 100 kDa was observed in the nuclear fraction that was replaced by a signal at approximately 125 kDa in the chromatin-bound protein fraction. Additionally, a protein band at 150 kDa was detected in both fractions but was identified as unspecific signal *in vitro* using *siBrd4* (**Appendix Figure 5.2**) (Ana Kutschat and Feda Hamdan, unpublished).

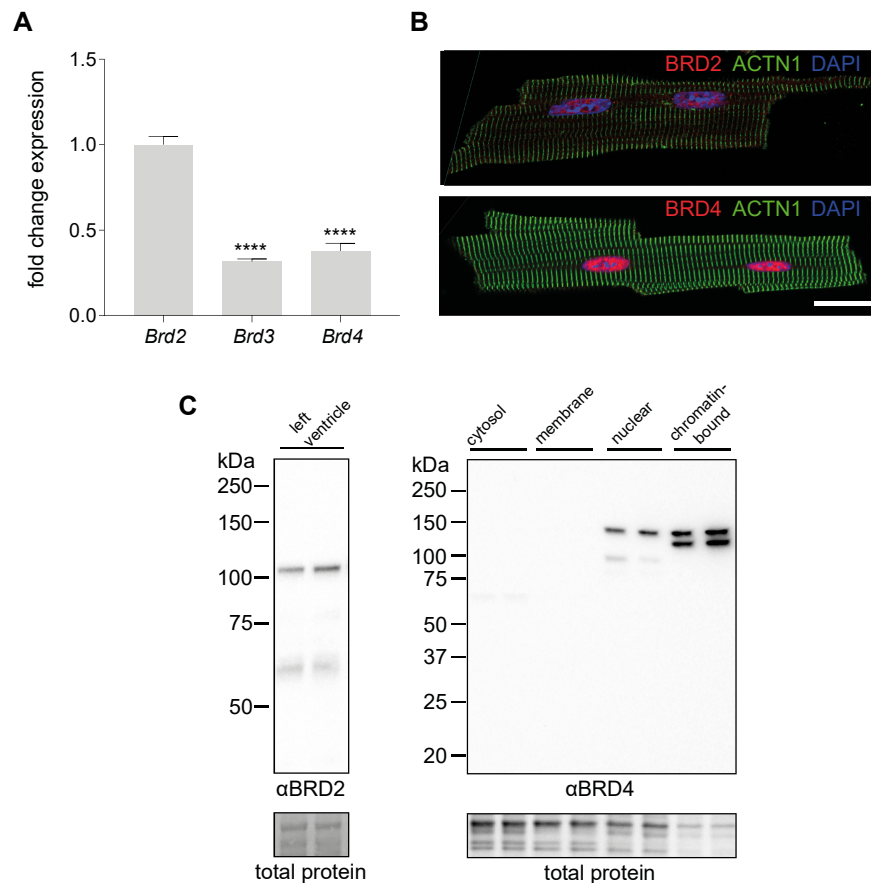


Figure 3.1: BRD2 and BRD4 are expressed in the heart and localized in the nucleus.

Transcriptome analysis showed *Brd2*, *Brd3*, and *Brd4* expression in the left ventricle. Comparison of length normalized read counts (RPKM) revealed significantly higher expression levels for *Brd2* ($p < 0.0001$, one-way ANOVA with Tukey post hoc, $n = 5$). Shown as fold change expression to *Brd2*. Error bars indicate SD (**A**). BRD2 and BRD4 (red) can be detected by immunocytochemistry in isolated cardiomyocytes and co-localizes with DAPI (blue), ACTN1 (green) visualizes the sarcomere structure (bar = 20 μ m) (**B**). Western Blot showed BRD2 and Brd4 are predominantly present in the nuclear and chromatin-bound protein fraction (**C**).

3.1.2 Particular BETs are differently regulated after pressure overload

Spiltoir and colleagues previously suggested that BRD2 protein levels are decreased, BRD3 levels remain unchanged, and BRD4 levels are increased after TAC-induced PO (Spiltoir et al. 2013). After validation of BET expression in the murine heart, I wanted to test whether particular BET proteins are altered after PO under our laboratory conditions. Therefore, the expression of *Brd2*, *Brd3*, and *Brd4* was analyzed using previous mRNA sequencing data from our group (Khadjeh et al. unpublished) obtained from left ventricular RNA of wildtype animals (FVB/N strain) one and eight weeks after TAC or Sham (control) surgery. Regardless of the time point or treatment, all samples showed much higher expression of *Brd2* in the heart than of *Brd3* or *Brd4* ($p < 0.0001$, two-way ANOVA with Tukey post-hoc test, $n = 5$). Adjusted p-values showed no significant difference in BET expression between TAC and Sham operated animals in none of the timepoints. RT-qPCR analysis confirmed that *Brd2* and *Brd4* are not regulated after PO induction as shown for animals 8 weeks after TAC (**Figure 3.2D**). Analysis of BRD2

and BRD4 protein levels in left ventricles of animals 8 weeks after TAC or Sham surgery using immunoblotting showed that BRD2 levels were unchanged, whereas an additional BRD4 protein band at about 200 kDa (arrow) was detectable only after TAC (**Figure 3.2 B-C**). As this suggested a potential change towards the long isoform of *Brd4* after stress induction, an additional RT-qPCR was performed using primers spanning the exons three to four (exon 3-4) and five to six (exon 5-6), which detect both the short and long isoform, as well as primers targeting exons 15 to 16 (exon 15-16) that are exclusive to the long isoform. Relative *Brd4* expression was compared to that of exon 3-4 Sham and overall showed a significantly lower expression of the long isoform ($p < 0.0001$ to exon3-4 Sham and exon5-6 Sham/TAC, $p > 0.01$ to exon3-4 TAC, two-way ANOVA). After TAC, however, decreased expression of the 5' coding region (exon3-4 and exon 5-6) but not the 3' coding region (exon15-16) of *Brd4* was observed (**Figure 3.2E**).

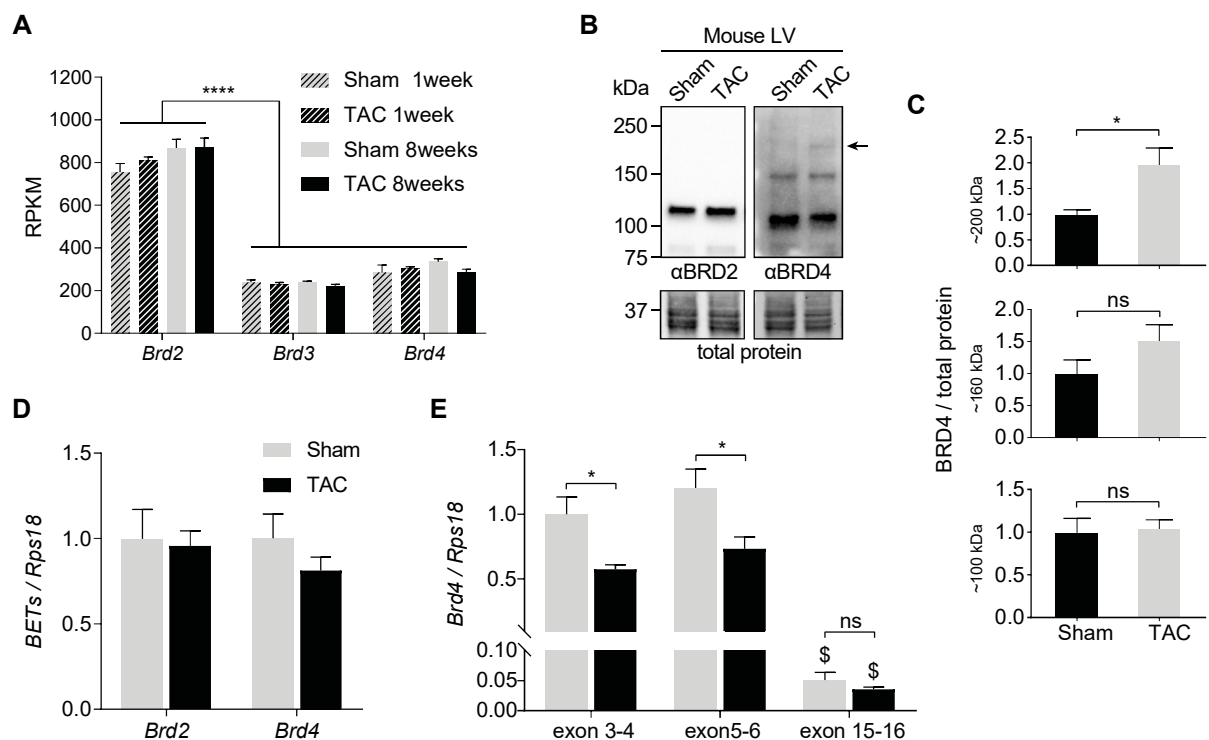


Figure 3.2: BET genes are differently regulated after pressure overload.

Gene length normalized counts (RPKM) from RNA sequencing revealed an overall significantly higher expression of *Brd2* in the heart compared to *Brd3* and *Brd4* ($p < 0.0001$, two-way ANOVA with Tukey post-hoc, $n = 5$). Data shown as mean RPKM \pm SD. **(A)** Western blot with total protein from left ventricle showed BRD2 and BRD4 were present 8 weeks after control (Sham) or TAC surgery **(B)** and that an additional BRD4 band appeared at 200 kDa after TAC when quantified and normalized to total protein ($p < 0.05$, unpaired two-tailed t-test, $n = 4-8$) **(C)**. *Brd2*, *Brd3* and *Brd4* mRNA was not significantly changed 8 weeks after TAC (RT-qPCR, $n = 5-6$) **(D)**. Detailed expression analysis of *Brd4* showed an overall significantly lower expression of the long isoform ($\$ = p < 0.0001$ to exon3-4 Sham) and a significantly decreased expression of the 5' coding region 8 weeks after TAC (RT-qPCR, $n = 5-6$, normalized to exon3-4 Sham) **(E)**. If not stated otherwise unpaired two-tailed t-test was used. Error bars indicate SEM if not stated otherwise, * = $p < 0.05$, **** = $p < 0.0001$, ns = not significant. (A) Normalized counts were kindly provided by Sara Khadjeh, (B-C) is courtesy of Eric Buchholz.

3.2 Effects of JQ1-mediated BET inhibition after pressure overload

3.2.1 JQ1 administration does not improve survival after TAC

BET-inhibition with the small molecule JQ1 has previously been reported to prevent TAC-induced cardiac remodeling and HF (Anand et al. 2013) but no effect on the overall survival after TAC was described. BET-inhibition with JQ1 in PO was performed in order to verify the previous findings and to analyze its impact on TAC-dependent mortality (**Figure 3.3**). Therefore, 8 weeks old female wildtype mice (C57BL/6N) underwent TAC or Sham surgery. Half of TAC-animals were randomly chosen to receive daily intraperitoneal injections of JQ1 in a concentration of 50mg/kg/d for 28 days and starting 24 hours after surgery. The remaining TAC animals and the Sham group received daily intraperitoneal injections of DMSO in the vehicle solution. The animals were analyzed by echocardiography 4 weeks after TAC and sacrificed for molecular testing 3 days later (group1). Animals were treated as in group 1 but additionally 50% of Sham-animals received JQ1. After treatment all animals were analyzed by echocardiography 4 and 8 weeks after surgery before being sacrificed for molecular testing 3 days after the second echo (group2).

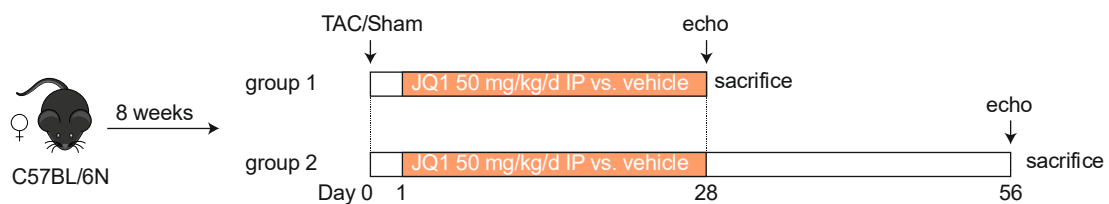


Figure 3.3: Experimental design for BET inhibition with JQ1 after TAC.

8 weeks old female C57BL/6N mice underwent TAC or Sham surgery. 50% of TAC-animals were randomly chosen to receive daily intraperitoneal injections of JQ1 in a concentration of 50mg/kg/d for 28 days and starting 24 hours after surgery. The remaining TAC animals and the Sham group received daily intraperitoneal injections of DMSO in the vehicle solution. The animals were analyzed by echocardiography 4 weeks after TAC and sacrificed for molecular testing 3 days later (**group1**). Animals were treated as in group 1 but additionally 50% of Sham-animals received JQ1. After treatment all animals were analyzed by echocardiography 4 and 8 weeks after surgery before being sacrificed for molecular testing 3 days after the second echo (**group2**).

To ensure consistent constrictions in all animals, the pressure gradients across the transverse aorta were determined after TAC. The average fractional flow reserve values were comparable and showed a more than 14-fold TAC-dependent increase ($p < 0.0001$, Sham $n = 7-17$, TAC $n = 29-39$) from about 4.5 mmHG at baseline (Sham) to 73 mmHG ($\pm 18SD$) in the vehicle group and 70 mmHG ($\pm 25SD$) in JQ1 treated animals (**Figure 3.4A**). Significant and comparable TAC-mediated mortality was observed in vehicle ($p < 0.0001$, Log-rank Mantel-Cox test, $n = 24-29$) and in JQ1 treated animals ($p = 0.0006$, Log-rank Mantel-Cox test, $n = 24-40$), whereas no Sham mouse died within the time frame of the observation (**Figure 3.4B**).

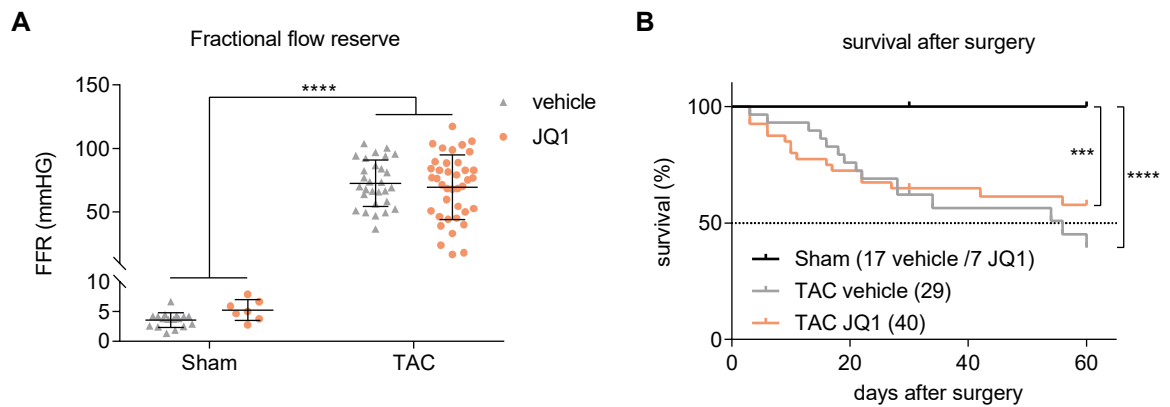


Figure 3.4: The survival after TAC showed no difference between vehicle and JQ1 treated animals.

The successful TAC was ensured by measurement of the fractional flow reserve 24 to 72 hours after surgery which was comparably increased in both groups after TAC (data presented as mean +SD, each point represents the measurement for one animal, ****= $p < 0.0001$, two-way ANOVA with Tukey test) **(A)**. Kaplan-Meier curve showing the percent of living animals for the time after TAC or Sham without the first 48 hours after surgery (Log-rank Mantel-Cox test, numbers in brackets represent animals examined, dotted lines indicate median survival) **(B)**.

3.2.2 TAC-induced cardiac remodeling is unaffected by JQ1

Despite the expected cardio-protective effects of BET inhibition, TAC-dependent mortality was not decreased by JQ1. To confirm the previously reported beneficial effects of JQ1, the collected hearts of vehicle or JQ1 treated animals four and eight weeks after surgeries were examined by histologic staining and gene expression analysis.

As demonstrated by Masson's trichrome stain and the comparison of left ventricle to body weight ratios (**Figure 3.5 A-B**), JQ1 and vehicle treated animals showed equally enlarged left ventricles 4 and 8 weeks after TAC ($p < 0.0001$, two-way ANOVA with Tukey post hoc). Moreover, both treatment groups showed the same significant increase of *Nppa* and *Nppb* mRNA levels after TAC (**Figure 3.5 C-D**).

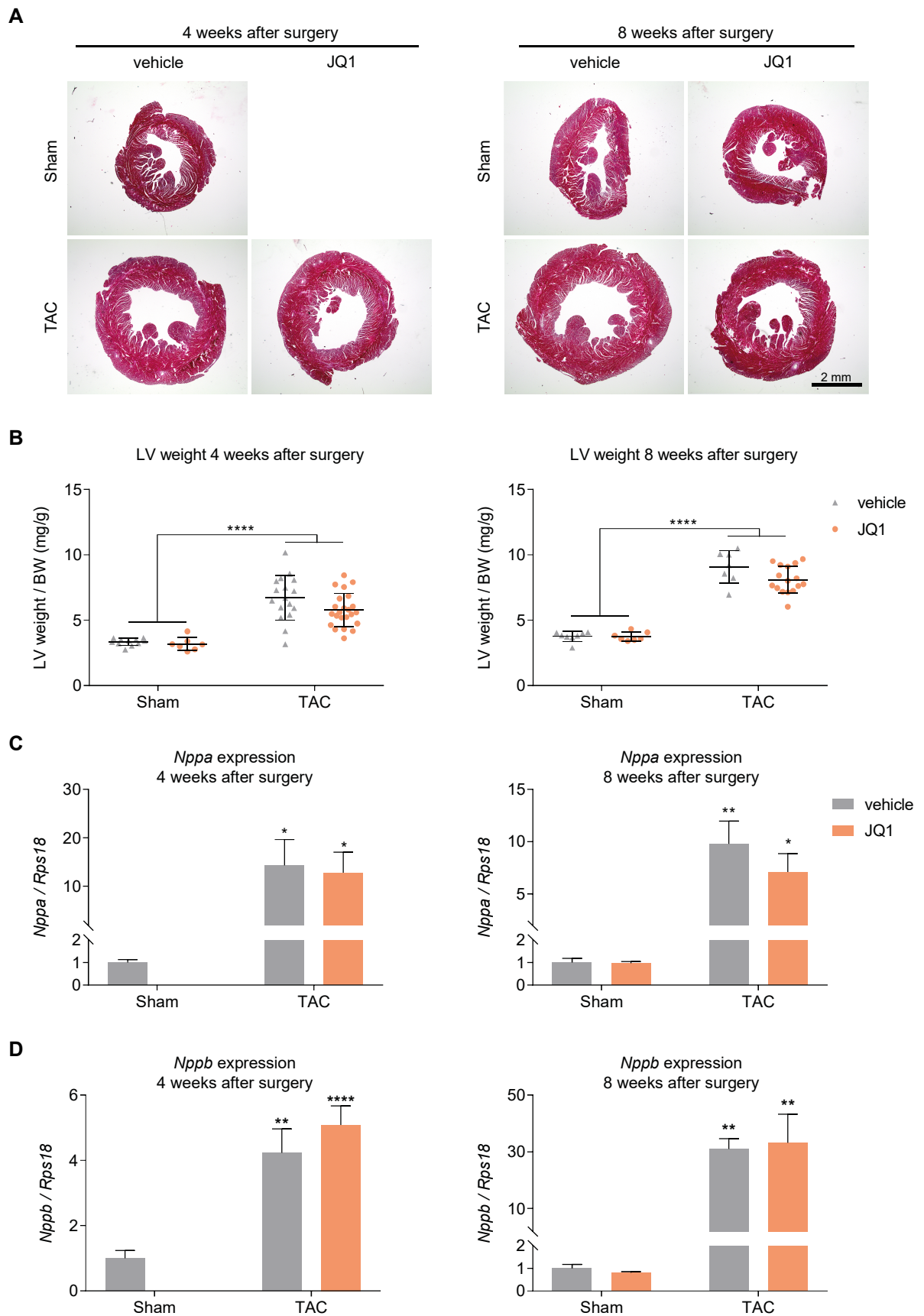


Figure 3.5: JQ1 and vehicle treated mice show comparable cardiac remodeling and cardiac stress marker expression 4 and 8 weeks after TAC.

Masson's trichrome stain showed increase in size of the left ventricle after TAC in the JQ1 and vehicle group, respectively (bar=2 mm) (A). Both treatment groups showed the same extremely significant increase of left ventricular weight 4 and 8 weeks after TAC in comparison to Sham (error bars

indicate SD) (B). Expression levels of *Nppa* mRNA (C), and *Nppb* mRNA were increased in both groups after TAC (RT-qPCR, n=5-6) (D). Two-way ANOVA together with Tukey correction for multiple comparisons was used. Error bars indicate SEM if not stated otherwise, * = $p < 0.05$, ** = $p < 0.01$, *** = $p < 0.001$.

WGA-stained heart cross sections were used to determine the diameter of individual cardiomyocytes (Figure 3.6A). Four and eight weeks after TAC, mean MFDs of vehicle and JQ1 treated animals were significantly higher than in the Sham groups (Figure 3.6B) demonstrating TAC-dependent hypertrophy regardless treatment. The comparison of MFD frequencies in hearts after Sham or TAC surgeries showed a shift to increased cell diameters after TAC in vehicle and JQ1 treated animals alike (Figure 3.6C). JQ1-treated mice showed slightly smaller cell diameters 4 weeks after TAC than 8 weeks after TAC (Figure 3.6C right) but such difference was not observed in vehicle treated animals (data not shown). Thus, in our hands JQ1 had no effect on TAC-induced cardiac remodeling.

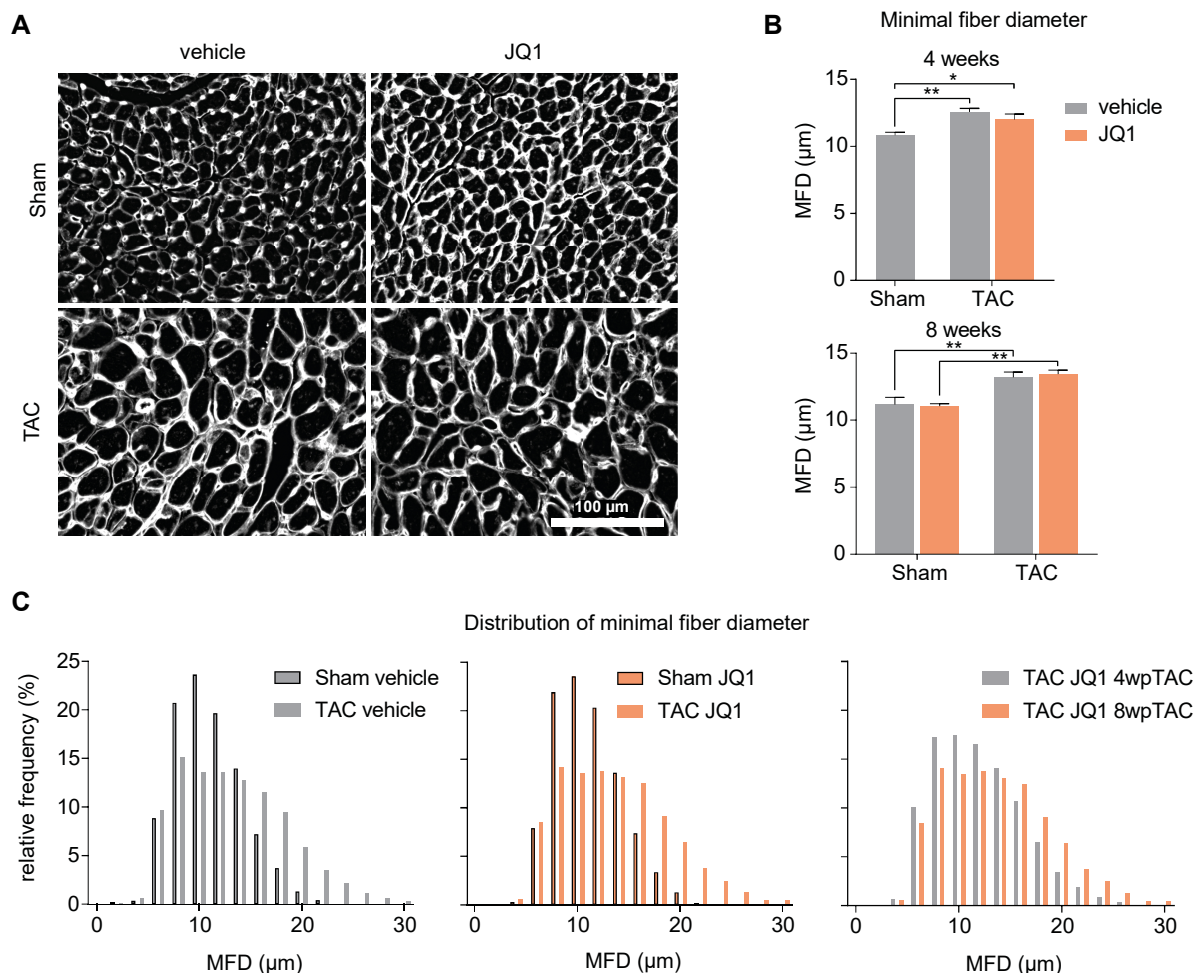


Figure 3.6: Hearts from JQ1 and vehicle treated animals show comparable cardiomyocyte hypertrophy after TAC.

Representative pictures of Wheat Germ Agglutinin staining (bar=100 μ m) (A), analysis of the minimal fiber diameter (MFD) 4 weeks after TAC (one-way ANOVA with Fischer's LSD test, n=3) (B, top) and 8 weeks after TAC (two-way ANOVA with Fischer's LSD test, n=3) (B, bottom) and its distribution showed cardiomyocyte hypertrophy in JQ1 and vehicle treated animals 4 and 8 weeks after TAC. Note that cardiomyocyte hypertrophy is milder in JQ1 treated animals 4 weeks after TAC compared to 8 weeks after TAC (C). Error bars indicate SEM. * = $p < 0.05$, ** = $p < 0.01$.

3.2.3 JQ1-treated animals show less wall thickening but reduced contractility

Independent from treatment with vehicle or JQ1, TAC-induced PO led to a significant decrease of ejection fraction 4 and 8 weeks After surgery (**Figure 3.7A**), left ventricular dilatation 8 weeks after surgery (**Figure 3.7B**) and an extremely significant increase of left ventricular wall thickness at both examination time points (**Figure 3.7C**). However, JQ1 treated mice showed a reduced wall thickening in comparison to vehicle treated 4 weeks after TAC ($p=0.0017$, $n=21-24$, two-way ANOVA with Tukey post hoc). In contrast to previous reports, these data do not support cardio protective effects of JQ1 after PO.

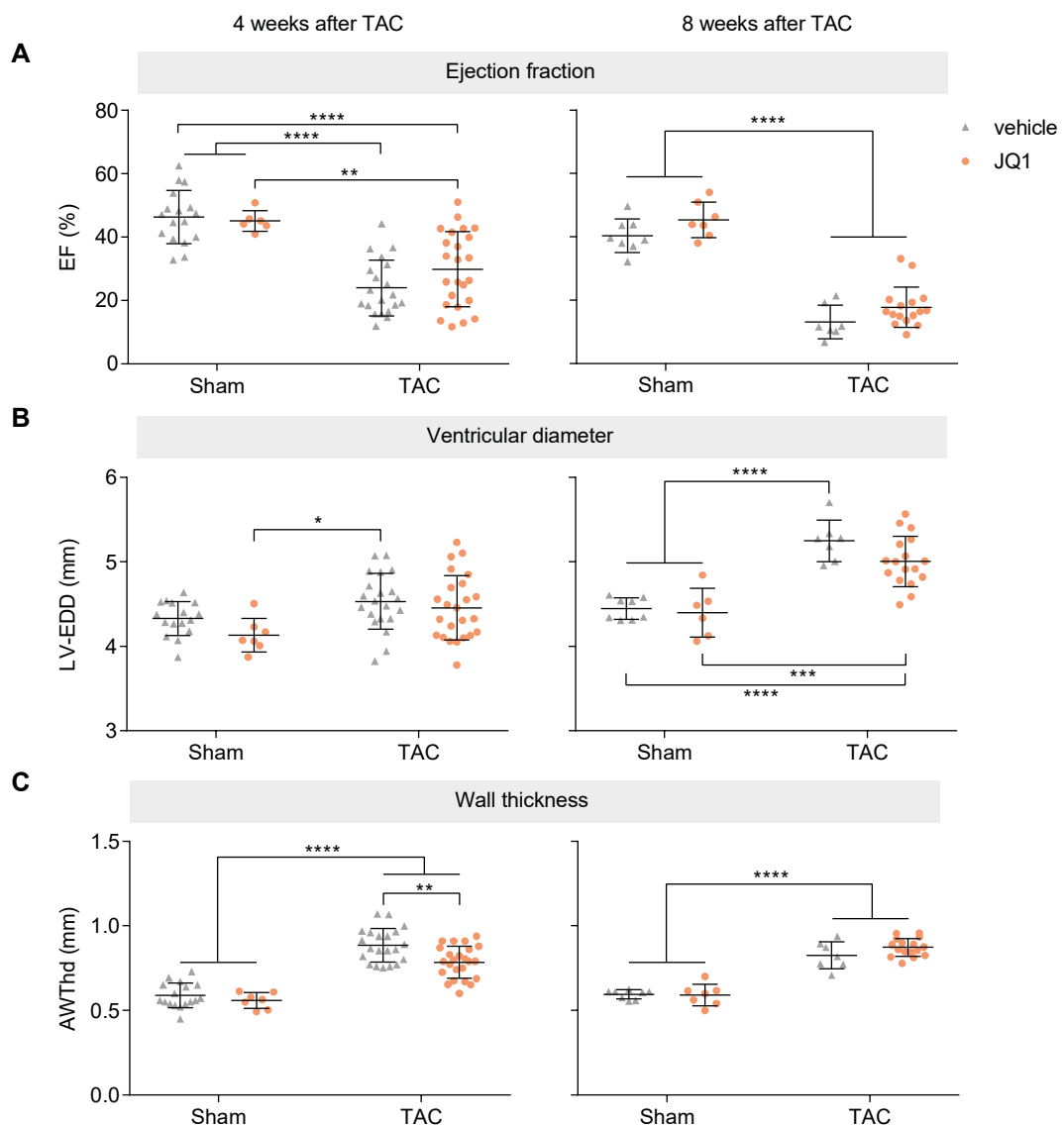


Figure 3.7: Echocardiographic phenotyping showed an overall comparable systolic dysfunction, left ventricular dilation and wall thickening in both groups after TAC.

Echocardiographic phenotyping of JQ1 and vehicle treated mice showed in both groups a significant decrease of ejection fraction 4 and 8 weeks after TAC (**A**), an increase of left ventricular diameter 8 weeks after TAC (**B**) and an extremely significant increase of left ventricular wall thickness, although JQ1 treated mice showed a reduced wall thickening in comparison to vehicle treated 4 weeks after TAC (**C**). Two-way ANOVA together with Tukey correction for multiple comparisons was used. Error bars indicate SD, * = $p < 0.05$, ** = $p < 0.01$, *** = $p < 0.001$, **** = $p < 0.0001$, each point represents the measurement for one animal.

3.2.4 JQ1 modulates the immune response, cell cycle, and muscle contraction

So far, the previously reported JQ1-mediated cardio-protection from hemodynamic stress could not be reproduced in this work. To detect subtle JQ1 effects, a molecular characterization of the left ventricular transcriptome in animals used for the previous analyses was performed. Mice of group 1 were allowed to rest for three days after echocardiographic assessment four weeks after surgery prior to sacrifice and heart dissection to avoid acute transcriptional artefacts due to handling, stress, or anesthesia. The retrograde perfused left ventricles of Sham vehicle, TAC vehicle, and TAC JQ1 were used for next-generation mRNA sequencing. In comparison to Sham vehicle, 892 differentially expressed genes (DEGs) were detected for TAC vehicle and 961 DEGs for TAC JQ1 at an adjusted p-value (p_{adj}) less than 0.05 and a \log_2FC cutoff of 0.5 (**Figure 3.8**). The DEGs of TAC vehicle were used for an overrepresentation analysis (ORA) for gene ontology (GO) terms of biological processes and showed enrichment for genes associated with tissue development, ion transport, and ECM organization ($p_{adj}<0.05$, false discovery rate (FDR) <0.05) (**Figure 3.8A-B**). To allow analysis of potentially BET-regulated genes after TAC, genes differentially expressed in TAC vehicle were removed from GO analysis (**Figure 3.8C**, intersect) and only TAC JQ1 specific DEGs were analyzed. ORA of these 418 DEGs showed strongest enrichment for immune cell activation and cell division ($p_{adj}<0.05$, FDR <0.05 , Top10 sorted according to ratio of enrichment) (**Figure 3.8C**). However, a direct comparison of expression data from TAC vehicle and TAC JQ1 revealed only 19 DEGs ($p_{adj}<0.05$, $\log_2FC\pm 0.5$) that after ORA with a less stringent cutoff showed an enrichment for processes involved in immune response and metabolic processes ($p_{adj}<0.05$, FDR <0.11 , sorted according to \log_{10} ratio of enrichment) (**Figure 3.8D**) as no biological processes was overrepresented at a FDR less than 0.05. A heatmap of RPKMs of these 19 DEGs showed clusters of genes that were only induced or repressed in TAC JQ1 hearts and a cluster of genes induced in TAC vehicle and unaffected in TAC JQ1 (**Figure 3.8E**). Among these genes detected were *Zfp948* and *Zfp185* (zinc finger proteins possibly involved in cell proliferation and differentiation), *Tfrc* (receptor for iron uptake), *Asb4* and *Asb5* (involved in vascularization), *Bach2* (transcription factor regulating apoptosis), *Ccl2* (chemotactic factor recruiting monocytes and basophils), *Cd74* (critical for antigen processing), *H2.Ab1* and *H2.Eb1* and *H2.Aa* (atypical histones). To detect functional groups of slightly differentially regulated genes that individually are discarded by cutoffs during differential expression analysis, gene set enrichment analysis (GSEA) was performed. GSEA of TAC vehicle versus TAC JQ1 revealed 49 positively enriched GO gene sets ($p_{adj}<0.05$, FDR <0.25). The GO categories were manually clustered into 'Transport', 'Translation initiation', 'Splicing', 'RNA processing', 'Ribonucleoprotein complex' and 'Biosynthesis' (**Appendix Figure 5.3**).

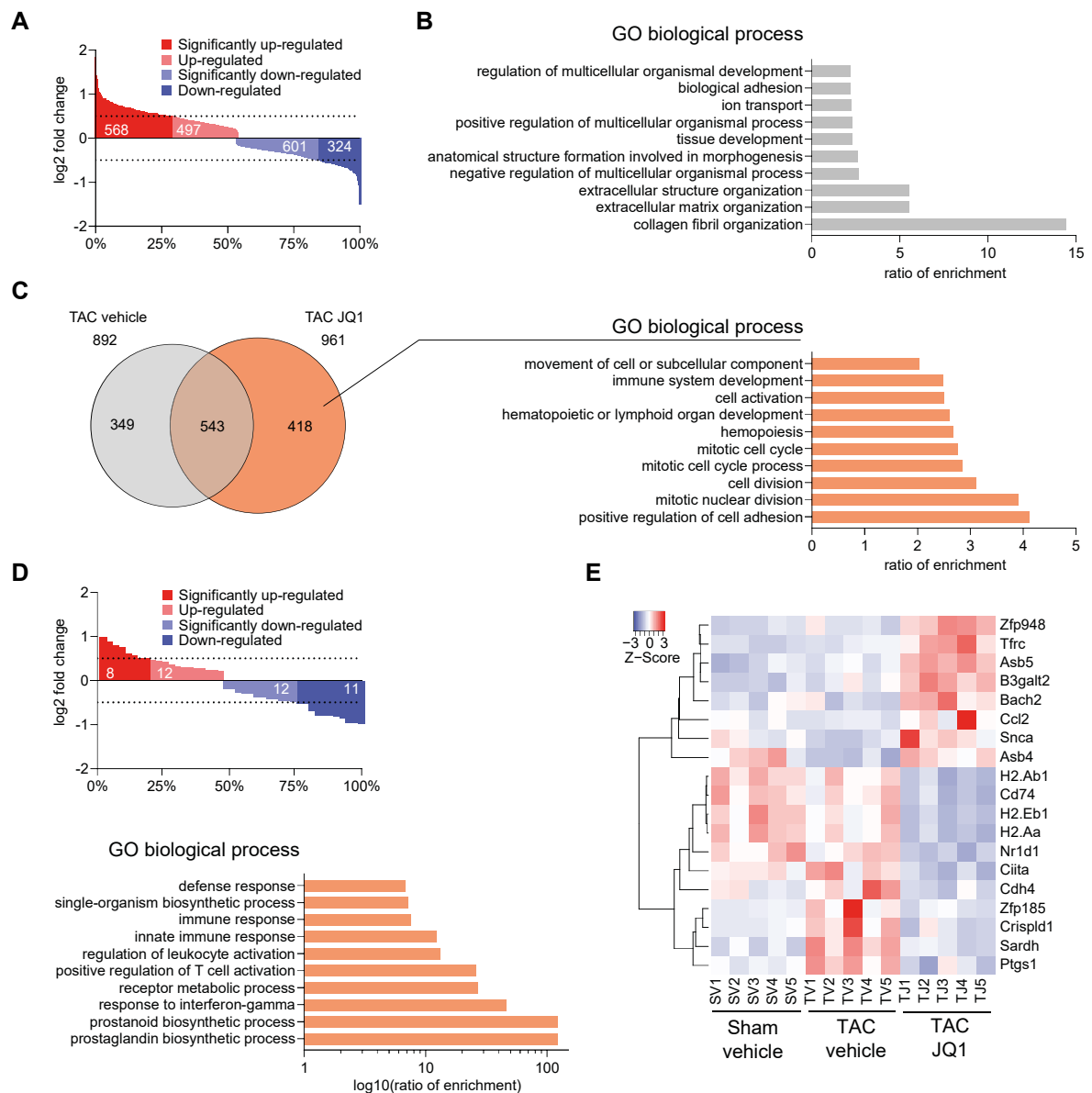


Figure 3.8: Four weeks after TAC hearts show wide gene expression changes and mild reaction to JQ1-dependent BET inhibition.

Differential expression analysis after mRNAseq of left ventricles 4 weeks after TAC and vehicle treatment versus Sham and vehicle showed 1990 differentially expressed genes (DEGs) in TAC vehicle ($p_{adj} < 0.05$; 1065 up, red; 925 down, blue) of which 892 were significant at $p_{adj} < 0.05$ and $\log_2FC \pm 0.5$ (568 up, dark red; 324 down, dark blue). White numbers indicate number of DEGs and x-axis the percent of total DEGs (**A**). Overrepresentation analysis (ORA) of gene ontology (GO) terms of biological processes for 892 significantly regulated genes in (A) showed enrichment in regulation of tissue development, ion transport, and ECM organization ($p_{adj} < 0.05$, $FDR < 0.05$, Top10 sorted according to ratio of enrichment) (**B**). Overlap for DEGs ($p_{adj} < 0.05$, $\log_2FC \pm 0.5$) in TAC vehicle (892 genes) and TAC JQ1 (961 genes), both versus Sham vehicle. 418 TAC JQ1 exclusive DEGs were identified and used for ORA of GO biological processes. This showed an enrichment of GO terms for immune cell activation and cell division ($p_{adj} < 0.05$, $FDR < 0.05$, Top10 sorted according to ratio of enrichment) (**C**). mRNA sequencing revealed 43 DEGs (20 up, red; 23 down, blue) between TAC JQ1 and TAC vehicle with $p_{adj} < 0.05$. A subsequent cutoff at $\log_2FC \pm 0.5$ resulted in 19 DEGs (8 up, dark red; 11 down, dark blue) which were used for ORA GO biological processes. Enriched GO categories ($p_{adj} < 0.05$, $FDR < 0.11$, sorted according to \log_{10} ratio of enrichment) in TAC JQ1 hearts included immune response and metabolic processes (**D**). A heatmap of the 19 TAC JQ1 DEGs was clustered via centroid linkage with Pearson method and revealed 3 clusters, JQ1 induced genes, JQ1 repressed genes, and TAC-dependent gene induction that is reversed by JQ1 (**E**).

To describe the effects of JQ1 on the stressed heart in more detail, 418 genes differentially expressed ($p_{adj} < 0.05$, $\log_2FC \pm 0.5$) in TAC JQ1 but not in TAC vehicle mice in comparison to Sham vehicle (**Figure 3.9A**) were further analyzed. Pathway analysis showed significant clusters ($p_{adj} < 0.05$) associated with T cell activation, antigen processing and cell cycle but also with sarcolemma, calcium regulation in cardiac cells, and muscle contraction (**Figure 3.9B**). Plotting of the normalized gene counts (RPKM) of the 418 DEGs in a heatmap revealed one cluster of genes up-regulated and another down-regulated after TAC for both treatments, although TAC JQ1 showed stronger difference to Sham vehicle (**Figure 3.9C**). These data demonstrate that JQ1-mediated BET inhibition has only mild effects on gene expression after TAC, mainly modulating biological processes like immune response, cell division, and RNA processing.

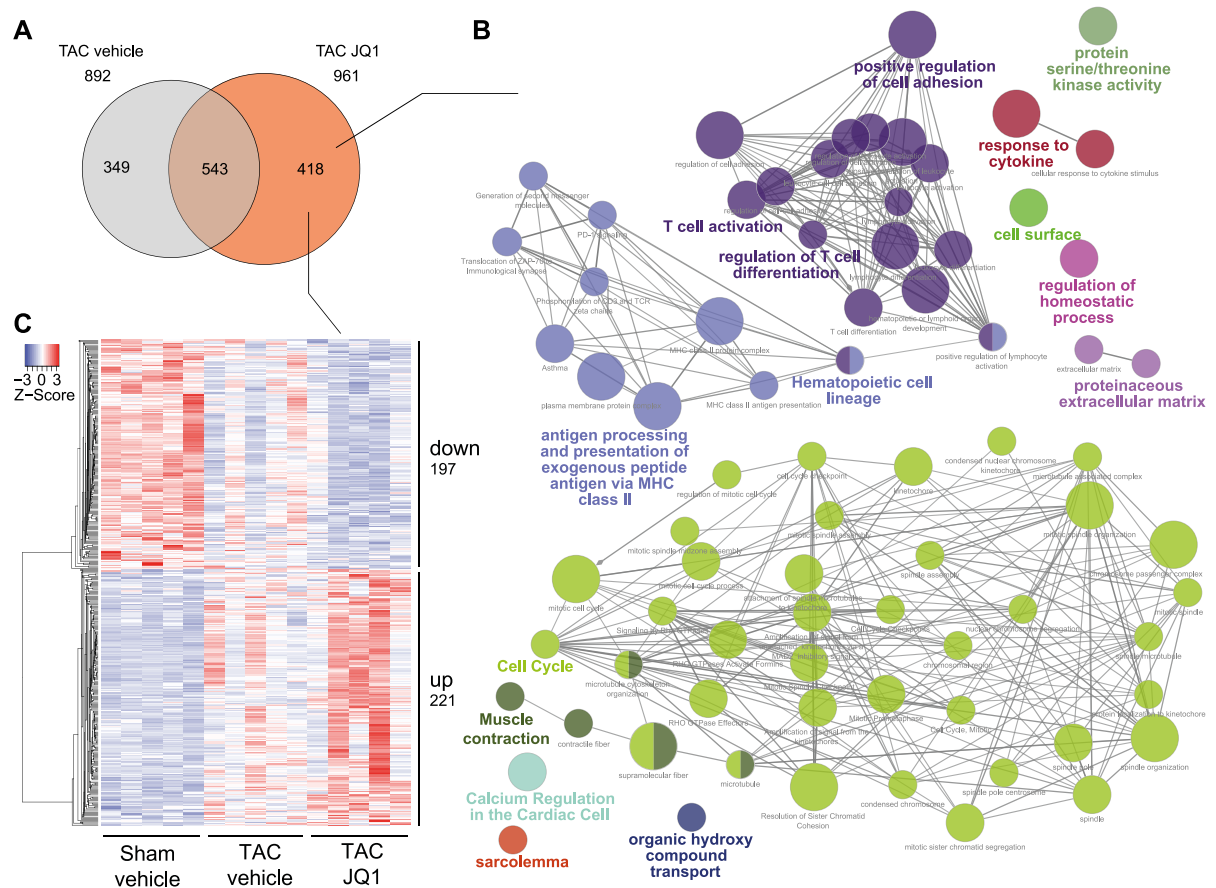


Figure 3.9: JQ1 modulates multiple biological pathways such as immune response, cell cycle, and muscle contraction.

Overlap for DEGs ($p_{adj} < 0.05$, $\log_2FC \pm 0.5$) in TAC vehicle (892 genes) and TAC JQ1 (961 genes), both versus Sham vehicle. 418 TAC JQ1 exclusive DEGs were identified (**A**). ClueGO pathway analysis of 418 DEGs from (**A**) ($p_{adj} < 0.05$, $\log_2FC \pm 0.5$) revealed enrichment for immune response, cell cycle, and cardiac muscle contraction ($p_{adj} < 0.05$, $Kappa = 0.4$). Nodes have been rearranged for better readability. Circle size represents p_{adj} (**B**). Heatmap of the 418 TAC JQ1 DEGs, clustered via centroid linkage with Pearson method (**C**).

3.2.5 JQ1 does not reverse stress-induced gene expression

The findings from this study contradict previous reports on JQ1-mediated protection of hearts after TAC (Anand et al. 2013; Spiltoir et al. 2013; Haldar and McKinsey 2014). Therefore, the previously published microarray data from Anand and colleagues (Anand et al. 2013) was reanalyzed. Differential expression analysis of 'TAC vehicle 28d' or 'TAC JQ1 28d' versus 'Sham vehicle 28d' (Anand et al. 2013) resulted in 979 DEGs (716 up, 264 down) for TAC vehicle and 1066 DEGs (118 up, 948 down) for TAC JQ1 ($p_{adj} < 0.05$, $\log_2FC \pm 0.5$). From the 408 DEGs common for both groups 391 genes were differentially regulated (**Figure 3.10A**). The comparison of these differentially regulated genes to DEGs of TAC vehicle and TAC JQ1 (4 weeks) from this study ($p_{adj} < 0.05$, $\log_2FC \pm 0.5$) identified 142 common DEGs (**Figure 3.10B**). As demonstrated by the heatmap for length normalized read counts, none of the 142 common DEG was differentially regulated in mice from this study upon vehicle or JQ1 treatment (**Figure 3.10C**). Moreover, after TAC both treatment groups of this study showed almost identical significant increase of cardiac stress marker expression such as genes encoding for natriuretic peptides (*Nppa*, *Nppb*), for embryonal isoforms of sarcomere proteins (*Acta1*, *Myh7*), for an inhibitor of calcineurin-dependent transcriptional responses (*Rcan*), for the connective tissue growth factor (*Ctgf*) expressed by vascular endothelial cells, and for a typical cytokine (*Il6*) (**Figure 3.10D**). Altogether, the previously reported cardio-protection of JQ1 administration after TAC (Anand et al. 2013; Spiltoir et al. 2013; Haldar and McKinsey 2014; Duan et al. 2017) could not be reproduced in this study.

As the quality and delivery of JQ1 was not monitored throughout this study, cardiac delivery and function is hard to prove. Therefore, I have analyzed the expression of *Hexim1*, *Serpini1*, *Zcchc24*, *Zmynd8* (Lin et al. 2017), *Myc*, *Ccr2*, *Cd180* (Yeh et al. 2017), and *Bcl2* (Hogg et al. 2016), which were previously described as BET inhibition biomarkers. However, transcriptome data from TAC JQ1 four weeks after surgery showed no differential expression for these genes (data not shown).

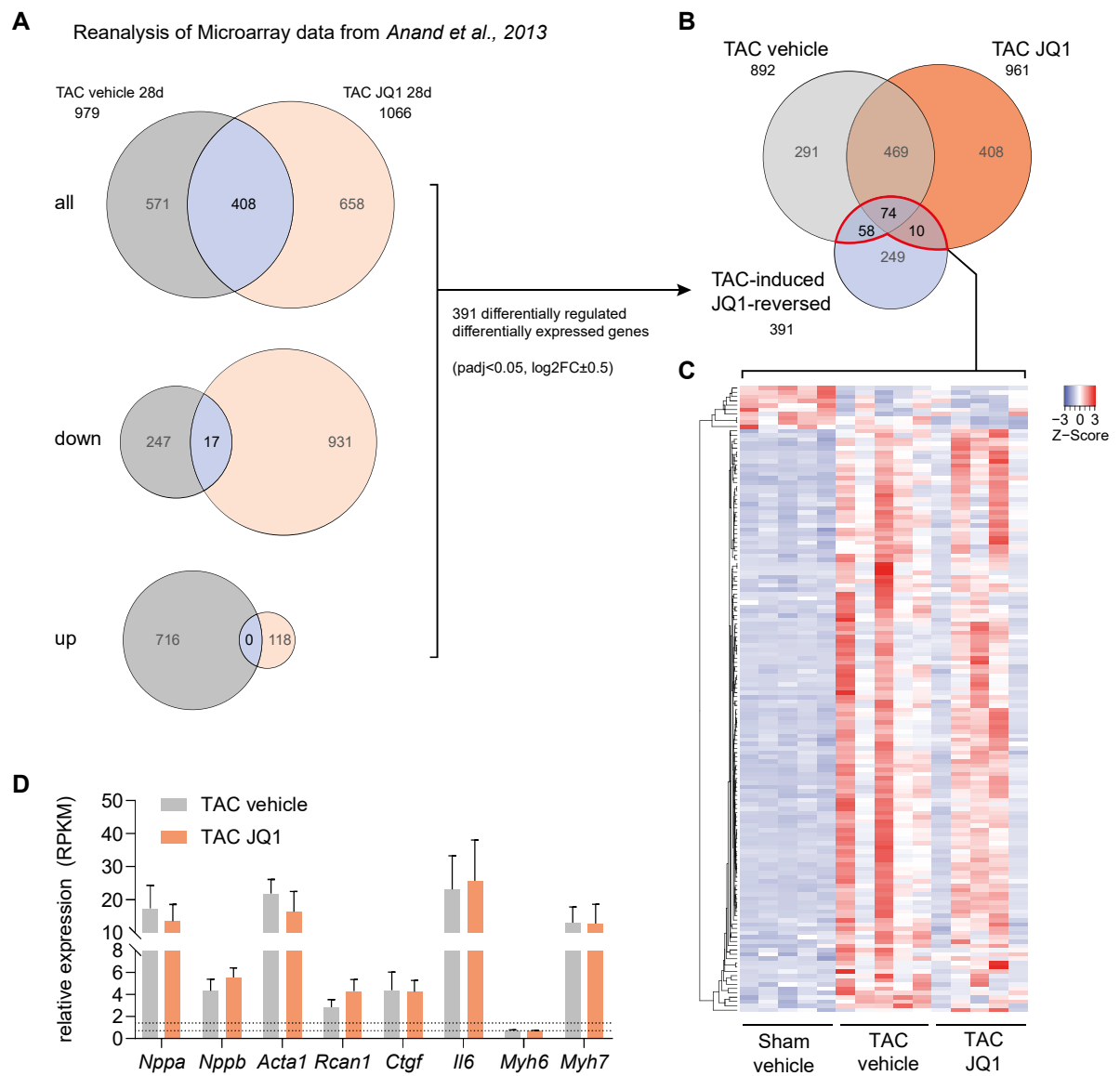


Figure 3.10: JQ1 does not reverse TAC-induced genes.

Reanalysis of previously published microarray data of TAC vehicle or TAC JQ1 versus Sham vehicle (28 days) (Anand et al. 2013) resulted in 979 DEGs for TAC vehicle and 1066 DEGs for TAC JQ1 ($\text{padj} < 0.05, \log_2\text{FC} \pm 0.5$). From the overall 408 intersecting DEGs 391 were up-regulated in TAC vehicle and down-regulated in TAC JQ1 (A). Overlap of 391 TAC-induced and JQ1-reversed DEGs from (A) with DEGs of TAC vehicle and TAC JQ1 (4 weeks) from this study ($\text{padj} < 0.05, \log_2\text{FC} \pm 0.5$). 142 intersecting DEGs were identified (B). Heatmap of expression data from this study for the 142 DEGs common with the differentially regulated DEGs from (A), clustered via centroid linkage with Pearson method (C). Relative expression of cardiac stress and remodeling markers. No significant differences between TAC vehicle and TAC JQ1 were observed. Based on RPKM normalized to Sham vehicle. Error bars indicate SEM (D).

3.3 The role of Brd2 in the healthy and diseased mouse heart

3.3.1 Generation and validation of *Brd2* knockout mice

BET-inhibition by JQ1 has been previously shown to prevent pathologic remodeling and preserve contractile function of the heart in a mouse PO model. Therefore, BET inhibitors have been proposed as potential pharmaceuticals for HF (Anand et al. 2013; Spiltoir et al. 2013; Duan et al. 2017). Under our laboratory conditions these findings could not be confirmed as JQ1 treated animals developed pathologic hypertrophy, showed decreased heart function, and died prematurely after TAC (3.2). It cannot be excluded that experimental differences between the studies such as age, sex, and genetic background of the examined mice might lead to these controversial results. To clarify the inconsistencies, to overcome the limits of systemic BET inhibition, and to evaluate the potential of BET proteins as targets for HF treatment, it is necessary to further dissect the functions of particular BET proteins specifically in cardiac cells. Therefore, it is essential to generate and to use conditional BET alleles (Haldar and McKinsey 2014).

Although *Brd2* shows the highest expression level of all BET members in the heart, its role in cardiac cells is unknown. To allow functional analyses a conditional *Brd2* allele was used, which was previously generated in our group (Benito et al. unpublished) by introduction of two loxP sites at the *Brd2* locus, one upstream of exon 3 and the other downstream of exon 4, to induce a frameshift and premature Stop after Cre-mediated recombination (**Figure 3.11A**). Homozygous male mice of this line (*Brd2* fl/fl) were crossed to female mice of the cardiomyocyte-specific Cre-line α MHC-Cre to obtain Cre-positive mice homozygous for the conditional allele (*Cre*⁺;*Brd2* fl/fl) in the F2 generation (**Figure 3.11B**). Mice homozygous for the recombined allele were viable and bred normally. DNA from tail biopsies was used to control the genetic identity of the mice (**Figure 3.11C**). All crossings produced offspring with genotypes at Mendelian frequencies with a male to female ratio of 1:1.

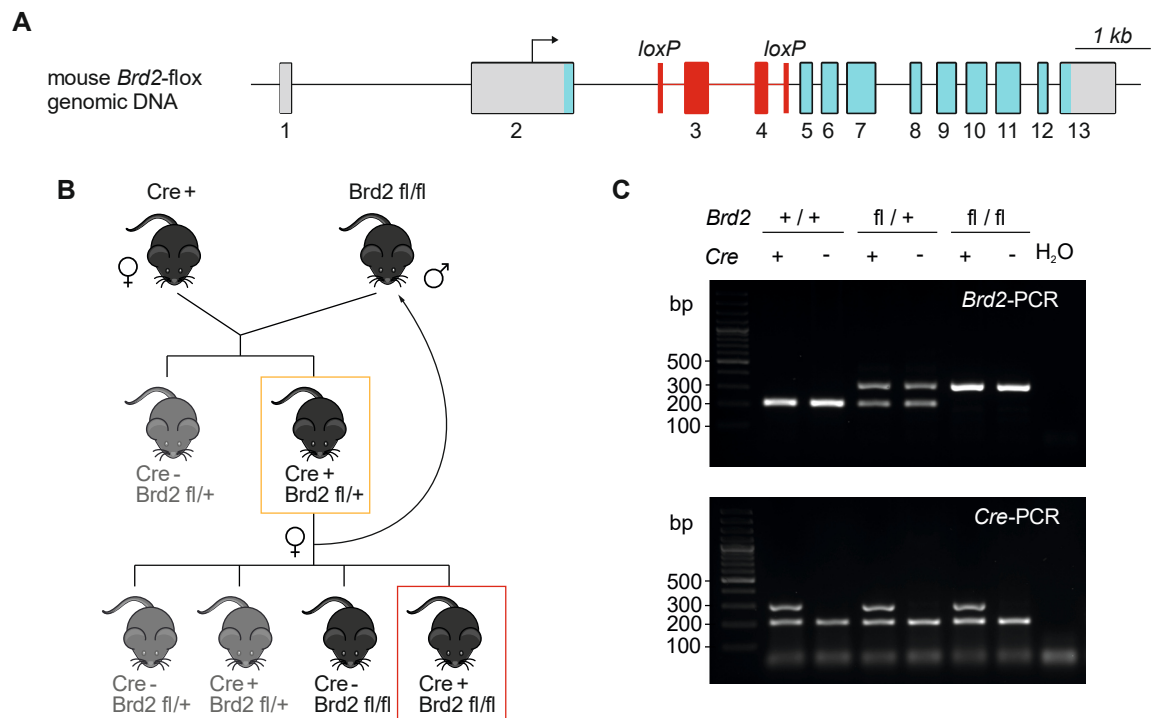


Figure 3.11: Generation of cardiomyocyte-specific *Brd2* knockout mice.

Illustration of the floxed *Brd2* allele. Boxes with numbers represent exons, blue filling represents coding region, red indicates target region excised after Cre-mediated recombination. The exon/intron proportions were maintained (bar=1 kb) (A). Paternal *Brd2*^{fl/fl} (*Brd2* fl/fl) were mated to maternal α MHC-Cre⁺ (Cre⁺) resulting in either Cre⁻; *Brd2*^{fl/+} or Cre⁺; *Brd2*^{fl/+} (orange box). Female Cre⁺; *Brd2*^{fl/+} were backcrossed to male *Brd2*^{fl/fl} to obtain Cre⁺; *Brd2*^{fl/fl} (red box) (B). Representative genotyping PCR from tail biopsies. *Brd2* primers bind to endogenous region flanking the loxP site between exons 4 and 5 and result in a PCR product of 210 bp for the wildtype allele and 320 bp for the floxed allele. In the Cre-PCR an internal control primer pair yields a smaller product of 200 bp and the Cre-primer a product of ~300 bp. H₂O served as negative control. bp=basepairs (C).

To validate the desired *Brd2* knockout in the heart, PCR-based analysis on genome and transcriptome level was performed on Cre⁻; *Brd2*^{fl/fl} (cre-) and Cre⁺; *Brd2*^{fl/fl} (cre+) animals using primer pairs annealing outside or at the target site (Figure 3.12B). Standard PCR with DNA from left ventricles and primers flanking the target site at the *Brd2* locus confirmed successful Cre-mediated deletion of *Brd2* exons 3 and 4 (Figure 3.12A). The deletion led to a significant reduction of *Brd2* mRNA levels containing exons 3 and 4 in left ventricle (p<0.05) and isolated cardiomyocytes (p<0.001). But interestingly, *Brd2* mRNA levels downstream of the target site remained unchanged in total RNA from left ventricle and isolated cardiomyocytes (Figure 3.12C). Hence, the mutant *Brd2* allele is expressed as putative truncated mRNA.

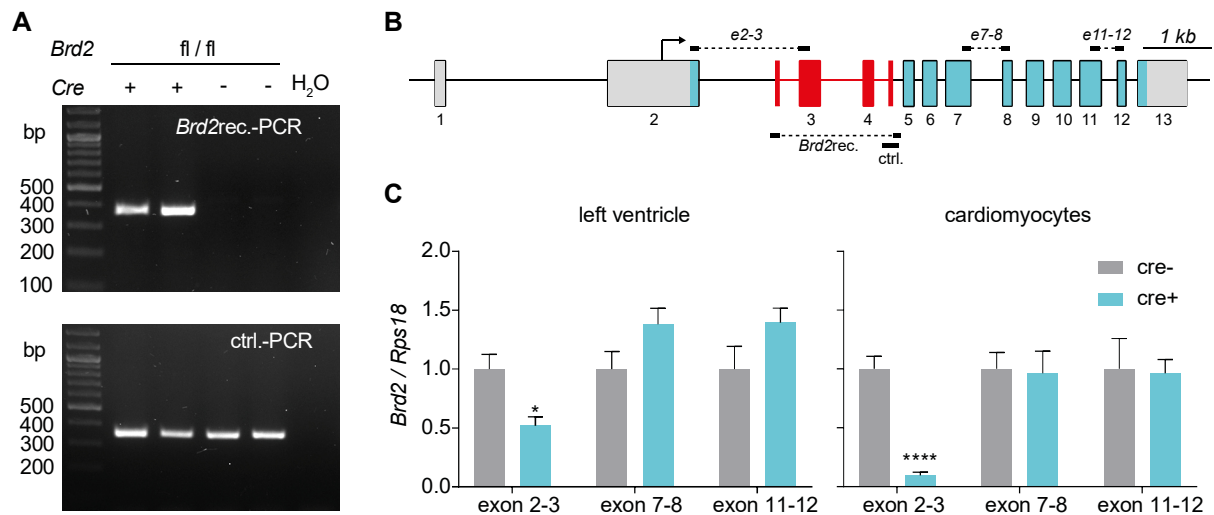


Figure 3.12: The Cre-mediated recombination in the *Brd2* locus leads to the expression of a *Brd2* mRNA with a deletion of the target exons 3 and 4.

Representative genotyping PCRs from heart biopsies. *Brd2* recombination primers result in a ~ 380 bp PCR product after successful recombination whereas the control PCR yields a ~ 350 bp product for the floxed allele regardless recombination. H₂O served as negative control (**A**). Illustration of the floxed *Brd2* allele with target sites of recombination and RT-qPCR primers. Dashed lines are not amplified during PCR. Boxes with numbers represent exons, blue filling represents coding region, red indicates target region excised after Cre-mediated recombination. The exon/intron proportions were maintained (bar=1 kb) (**B**). After recombination, the expression of the targeted *Brd2* exons 3 and 4 was significantly decreased but downstream exons showed no expression changes when analyzing total RNA from left ventricle (**C, left**) and from isolated cardiomyocytes (RT-qPCR, n=5-6) (**C, right**). Unpaired two-tailed t-test was used. Error bars indicate SEM, * = p<0.05, **** = p<0.0001.

Western blotting was used to check if the truncated *Brd2* mRNA leads to the translation of a residual protein. Using total protein extracts from left ventricle, the full-length BRD2 (~110 kDa) was detected in both, Cre⁺; *Brd2*^{fl/fl} animals and the Cre-negative littermates (**Figure 3.13A left**) at comparable levels (quantification not shown). But only in the Cre⁺; *Brd2*^{fl/fl} samples an additional protein band at approximately 90 kDa was detected (**Figure 3.13A right**). The α MHC-Cre mice express Cre-recombinase exclusively in cardiomyocytes, that is why other cells in the heart of Cre⁺; *Brd2*^{fl/fl} still express full-length BRD2. Therefore, the analysis was repeated with total protein from isolated cardiomyocytes to exclude non-cardiomyocyte protein. Western blot analysis of these samples revealed that the full-length BRD2 was only detectable in samples from cre-negative mice, whereas in Cre⁺; *Brd2*^{fl/fl} only a shorter protein at about 90 kDa was observed (**Figure 3.13A right**). The specificity of the antibody against BRD2 was assured in vitro using *siBrd2* (**Appendix Figure 5.2**) (Ana Kutschat and Feda Hamdan, unpublished). Immunocytochemistry of isolated *Brd2* Δ BDI cardiomyocytes (data not shown) showed no difference to wildtype (**Figure 3.1**). Neither wildtype BRD2 nor a truncated BRD2 were detectable in protein samples from left ventricle and isolated cardiomyocytes from *Brd2* Δ BDI and control mice using Orbitrap liquid chromatography-mass spectrometry after excision from polyacrylamide gel at the respective molecular weights (data not shown) (Christian Schiffmann, personal correspondence). To analyze the identity of the transcript and

check if it could yield a truncated protein, the mutant mRNA was reverse transcribed and resulting cDNA sequenced. Alignment of the sequencing results to the annotated full-length *Brd2* cDNA (**Appendix Table 5.4**) revealed that the Cre-mediated recombination in the *Brd2* locus leads to a transcript that is alternatively spliced from exon 2 to exon 5 (**Figure 3.13B**). An in-frame ATG in the beginning of exon 5 could be used as alternative start codon (**Figure 3.13B**). Thus, the mutant *Brd2* mRNA could potentially be translated and result in a truncated BRD2 protein, which lacks the first bromodomain (BDI) but contains the inter-bromodomain region, the second bromodomain, and the whole C-terminus. In the following the Cre⁺; *Brd2*^{fl/fl} mice will be referred to as *Brd2*ΔBDI.

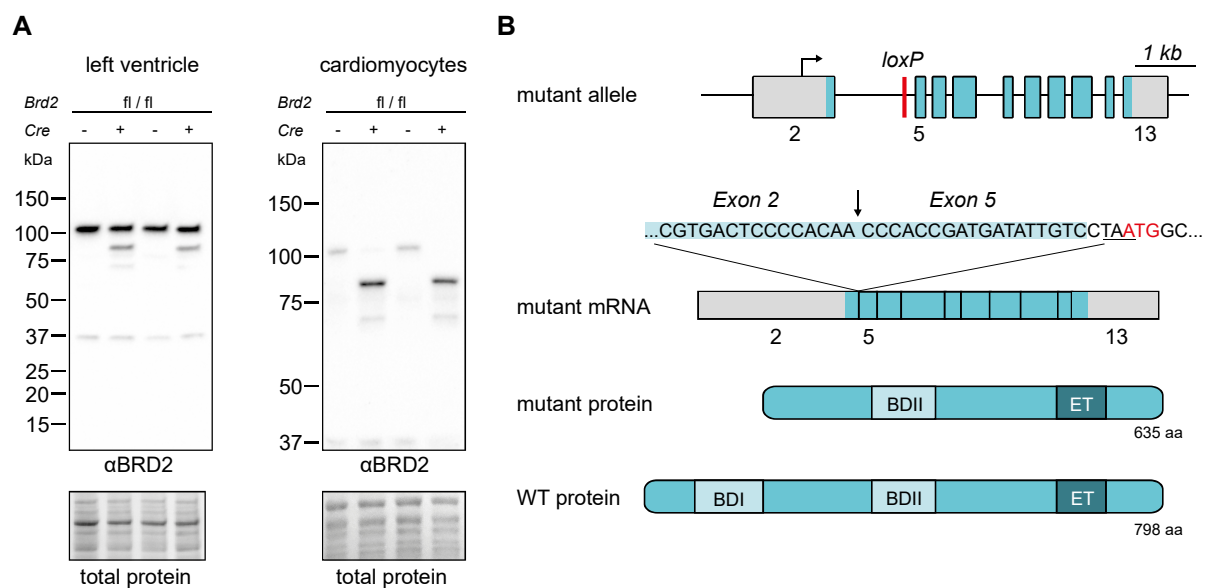


Figure 3.13: The deletion of *Brd2* exons 3 to 4 results in the expression of a truncated protein. Western blot analysis revealed the expression of a truncated protein after deletion of *Brd2* exons 3-4 in total protein from left ventricle (**A, left**) and isolated cardiomyocytes (**A, right**). Splicing of the mutant *Brd2* mRNA and the predicted protein. cDNA of the mutant mRNA was generated and sequenced to elucidate the identity of the transcript and the putative truncated protein. The original translation start codon (ATG) is located in exon 2 (not depicted) but yields no protein due to a frameshift and premature stop in exon 5 (underscored). The sequence encoding BDI is highlighted in light blue. Exon 5 contains an in-frame ATG (red). The mutant allele is referred to as *Brd2*ΔBDI (**B**). WT= wild type

3.3.2 Characterization of *Brd2*ΔBDI mutant mice

Distinct functions of the two bromodomains of BET proteins have previously been demonstrated using BET inhibitors with higher specificity for the first (Gacias et al. 2014; Cheung et al. 2017a) or the second bromodomain (Picaud et al. 2013; Gilham et al. 2016) and by expression of mutant BET proteins lacking one of the bromodomains *in vitro* (Gamsjaeger et al. 2011; Shi et al. 2014) and *in vivo* (Shang et al. 2007). Therefore, I decided to continue with the characterization of the newly generated *Brd2*ΔBDI mice to examine the phenotypic and functional effects after deletion of the first bromodomain of BRD2 in the heart.

Mice of the α MHC-Cre line positive for the Cre recombinase (cre control) and our newly generated Brd2 Δ BDI animals were compared in context of heart morphology, function and physiology to identify possible alterations in animals lacking the first bromodomain of BRD2 in cardiomyocytes. Cre control and Brd2 Δ BDI hearts showed no signs of fibrosis and no differences in Masson's trichrome stainings at the age of three months. Notably, Cre-dependent degenerative vacuoles in cardiomyocytes were observed in 6 month old animals of both groups (**Figure 3.14 A-B**). Furthermore, no alterations in LV-weight-to-body-weight (LV-W/BW) ratio were observed at the age of 3 and 6 months (**Figure 3.14 C**). Likewise, cardiomyocyte dimensions of WGA-stained cre control and Brd2 Δ BDI heart cross sections also did not show any differences in mean minimal fiber diameters (MFD) and their distributions (**Figure 3.14 D-F**). To analyze *in vivo* heart dimensions and function, echocardiography of cre control and Brd2 Δ BDI animals was performed. No significant alterations in ejection fraction (EF), left ventricular end-diastolic diameter (LV-EDD), and wall thickness were revealed between both groups (**Figure 3.14 G-I**). However, mice of both groups that were used for basal echocardiographic characterization mostly died by the age of 45 to 50 weeks (data not shown).

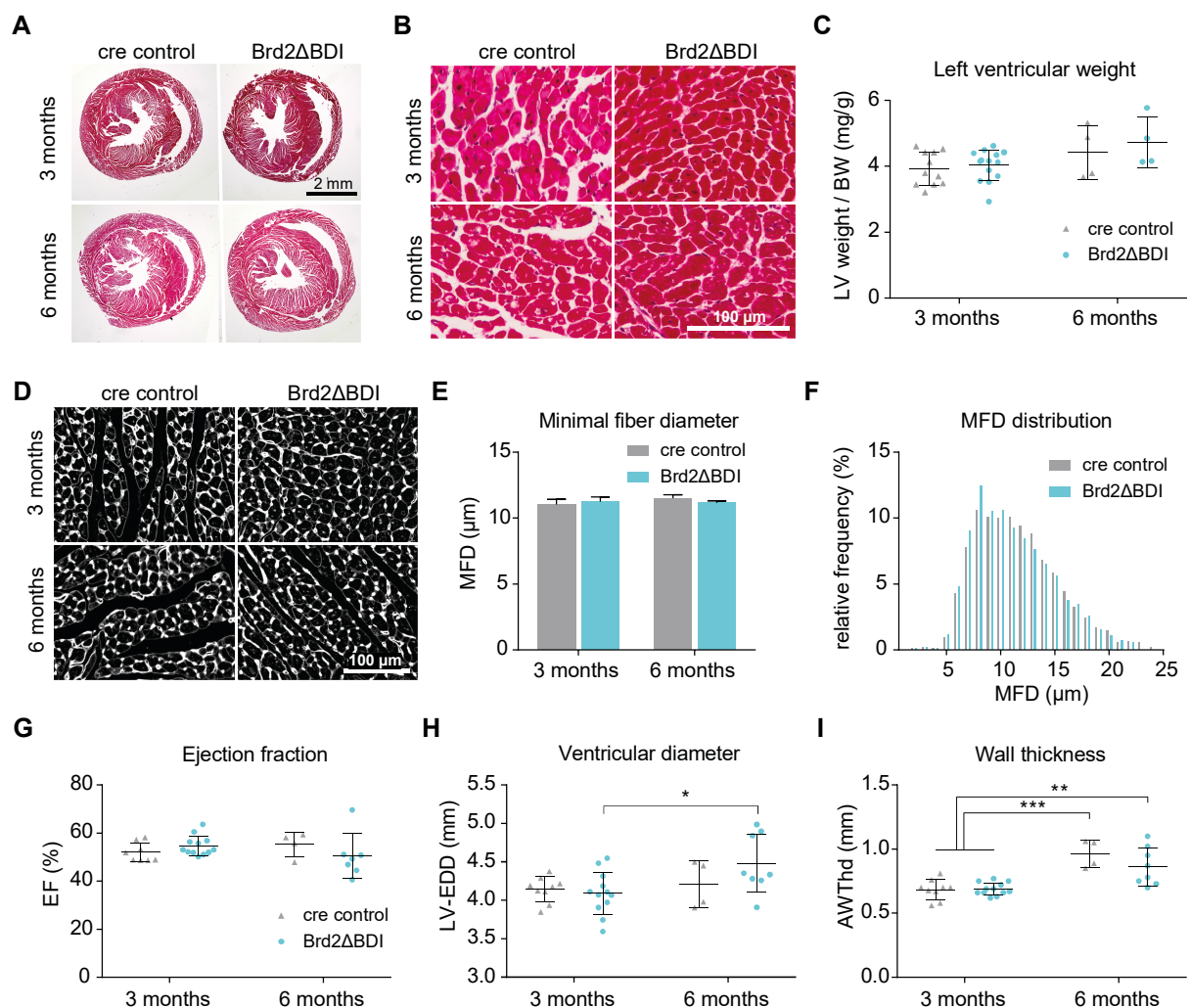


Figure 3.14: Morphometric characterization and echocardiographic analysis of Brd2 Δ BDI mice showed no differences to cre control mice.

Masson's trichrome stain shows no difference in heart dimension (bar=2 mm) (A) and no fibrosis in 3 and 6 months old Brd2 Δ BDI mutant and cre control mice. Note the degenerative vacuoles (white spots) in 6 months old animals (both groups) (bar=100 μ m) (B). Basal left ventricular weight was not changed upon Brd2 exon 3-4 deletion (C). Representative pictures of Wheat Germ Agglutinin staining (D), analysis of the minimal fiber diameter (error bars indicate SEM, n=2-6) (E) and its distribution analysis showed no changes of cardiomyocyte dimensions in Brd2 Δ BDI mutant mice (F). Echocardiographic phenotyping of cre control vs. Brd2 Δ BDI mutant mice at 3 and 6 months of age showed no changes in ejection fraction (G) a slight increase of left ventricular diameter in Brd2 Δ BDI from 3 to 6 months of age (H) and a comparable increase of left ventricular wall thickness in 6 months old animals of both groups (I). Two-way ANOVA together with Tukey correction for multiple comparisons was used. Error bars indicate SD if not stated otherwise, *= p<0.05, **= p<0.01, ****= p<0.0001. Each point represents the measurement for one animal.

3.3.3 The survival of Brd2 Δ BDI mice is slightly reduced after TAC

To examine the impact of BRD2 Δ BDI on cardiac remodeling and development of HF, Cre⁻; Brd2^{fl/fl} (control), Cre⁺; Brd2^{fl/fl} (Brd2 Δ BDI) and α MHC-Cre⁺ (cre control) mice were bred as depicted in Figure 3.15 A. The animals of all three groups underwent TAC or Sham surgery at the age of 8 weeks. To monitor heart function and dimensions, the animals were analyzed by echocardiography one and five weeks after TAC or Sham surgery and either sacrificed afterwards for histological and molecular analyses or monitored regarding their survival after TAC for up to 4 months (Figure 3.15B).

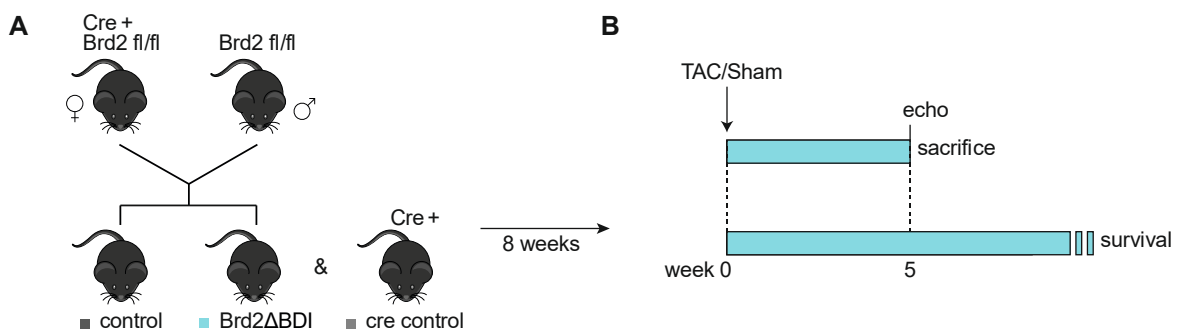


Figure 3.15: Brd2 Δ BDI mating scheme and experimental design.

Mating scheme of parental transgenic mouse lines and resulting offspring genotypes, Cre⁻; Brd2^{fl/fl} (control), Cre⁺; Brd2^{fl/fl} (Brd2 Δ BDI) and α MHC-Cre⁺ (cre control) mice. The animals underwent TAC or Sham surgery at the age of 8 weeks (A). Experimental design: the animals were analyzed by echocardiography 1 and 5 weeks after TAC or Sham surgery and either sacrificed afterwards for molecular testing or monitored regarding their survival after TAC for up to 4 months (B).

To ensure that the TAC was successful and comparable between groups the pressure gradient across the constriction was measured 24 to 72 hours after surgery by Doppler echocardiography. The average fractional flow reserve values were comparable and showed an almost 14-fold TAC-dependent increase (p<0.0001, two-way ANOVA with Tukey test) from about 5 mmHG at baseline (Sham) to 70 mmHG (\pm 20SD) in the control group and 68 mmHG (\pm 16SD) in Brd2 Δ BDI animals (Figure 3.16A). Operated animals that were not sacrificed for

molecular testing 5 weeks after TAC were monitored for their survival and analyzed using a Kaplan-Meier curve. Despite comparable fractional flow reserves, *Brd2* Δ BDI animals showed a significantly higher mortality after TAC in comparison to control ($p=0.0129$, $n=34$) but not to cre control, which showed an 'intermediate' mortality.

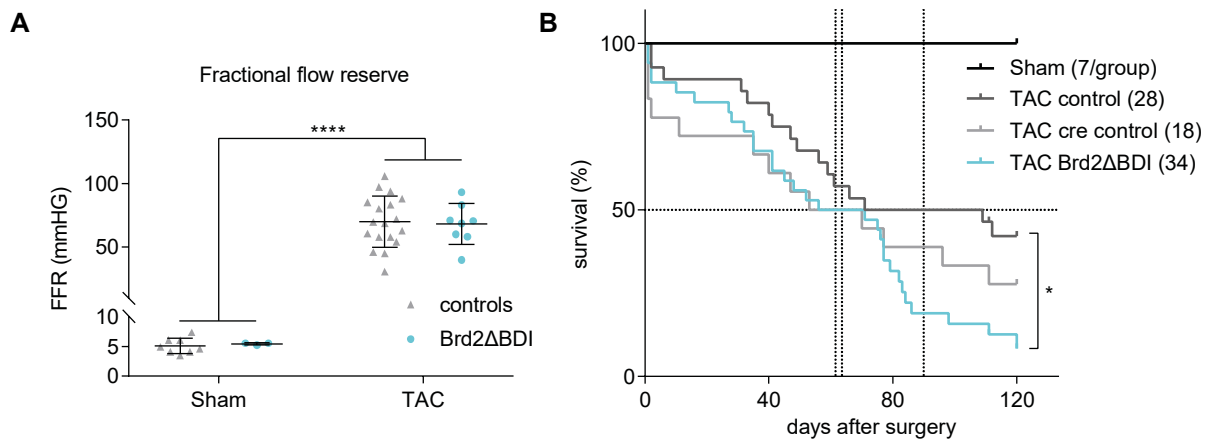


Figure 3.16: The survival after TAC is reduced in *Brd2* Δ BDI mutant mice compared to control but not to cre control.

The successful TAC was ensured by measurement of the fractional flow reserve 24 to 72 hours after surgery which was comparably increased in *Brd2* Δ BDI and controls after TAC (data presented as mean +SD, each point represents the measurement for one animal, ****= $p < 0.0001$, two-way ANOVA with Tukey test) (**A**). Kaplan-Meier curve showing the percent of living animals for the time after TAC or Sham without first 48 hours after surgery (Log-rank Mantel-Cox test, *= $p < 0.05$, numbers in brackets represent animals examined, dotted lines indicate median survival) (**B**).

3.3.4 *Brd2* Δ BDI and control mice show comparable cardiac remodeling

Masson's trichrome stain and LV-W/BW ratio showed left ventricular enlargement 5 weeks after TAC in *Brd2* Δ BDI and control mice, respectively (**Figure 3.17 A-B**). The mRNA levels of the cardiac stress markers *Nppa* and *Nppb* were increased 5 weeks after TAC in comparison to Sham in both groups (**Figure 3.17C-D**). Notably, *Brd2* Δ BDI hearts showed 5.5-fold higher *Nppa* levels than control (**Figure 3.17C**, $p < 0.01$, two-way ANOVA). The data suggest that the expression of *BRD2* Δ BDI does not alter the response to TAC-induced PO.

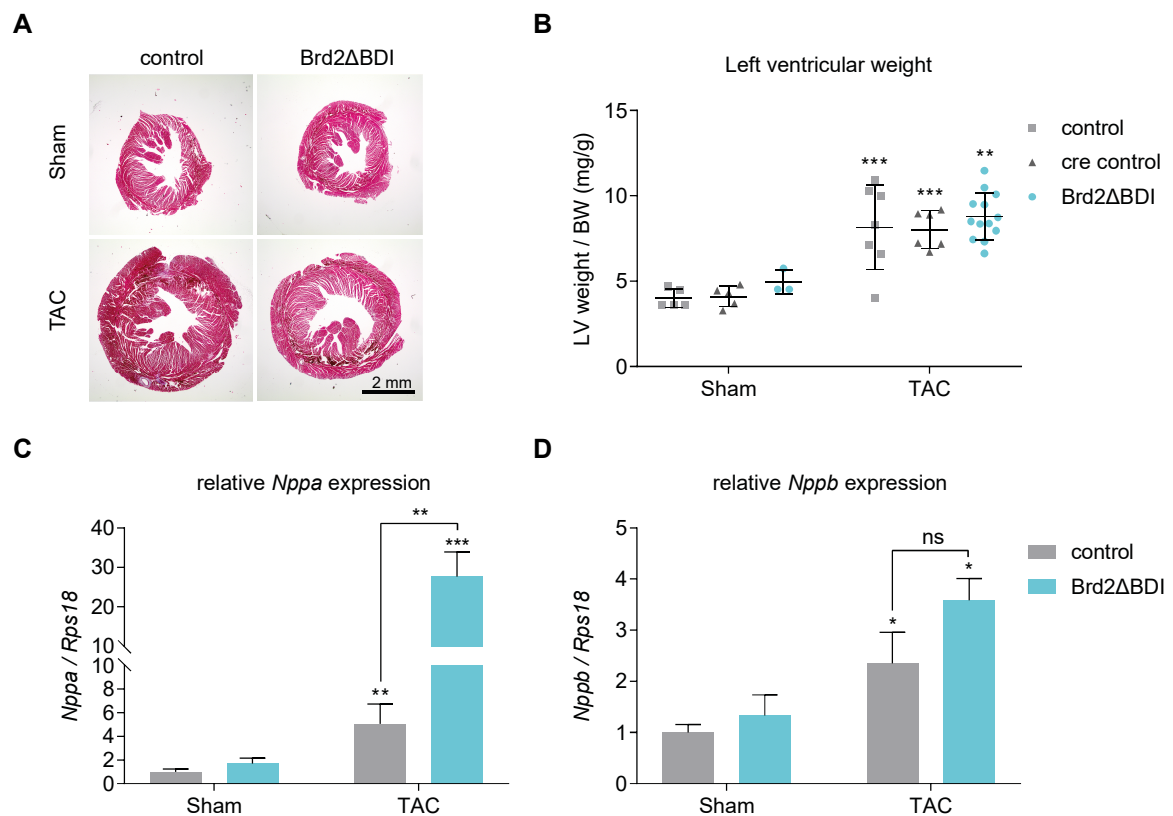


Figure 3.17: Brd2 Δ BDI and controls show comparable cardiac remodeling and cardiac stress marker expression 5 weeks after TAC.

Masson's trichrome stain showed increase in size of the left ventricle after TAC in Brd2 Δ BDI and control mice, respectively (bar=2 mm) (**A**). Control groups and Brd2 Δ BDI showed a comparable increase of left ventricular weight 5 weeks after TAC in comparison to Sham (error bars indicate SD) (**B**). *Nppa* mRNA expression levels were increased 5 weeks after TAC in comparison to Sham for control ($F(1,14) = 9,718$, $p=0,0076$) and significantly stronger for Brd2 Δ BDI mice ($\# = p < 0.001$ to Sham Brd2 Δ BDI, $\$ = p < 0.01$ to TAC control) (**C**), whereas *Nppb* mRNA expression was comparably increased for both groups after TAC (RT-qPCR, $n=3-5$) (**D**). Two-way ANOVA together with Tukey correction for multiple comparisons was used. Error bars indicate SEM if not stated otherwise, * = $p < 0.05$, ** = $p < 0.01$, *** = $p < 0.001$.

Echocardiographic phenotyping of control and Brd2 Δ BDI mutant mice 5 weeks after surgery showed an extremely significant decrease of ejection fraction after TAC across all groups (**Figure 3.18A**), no significant change of left ventricular diameter, although some individuals had dilated ventricles, (**Figure 3.18B**) and a comparable increase of left ventricular wall thickness in all groups (**Figure 3.18C**). Consequently, Brd2 Δ BDI does not influence heart dimensions and function after TAC.

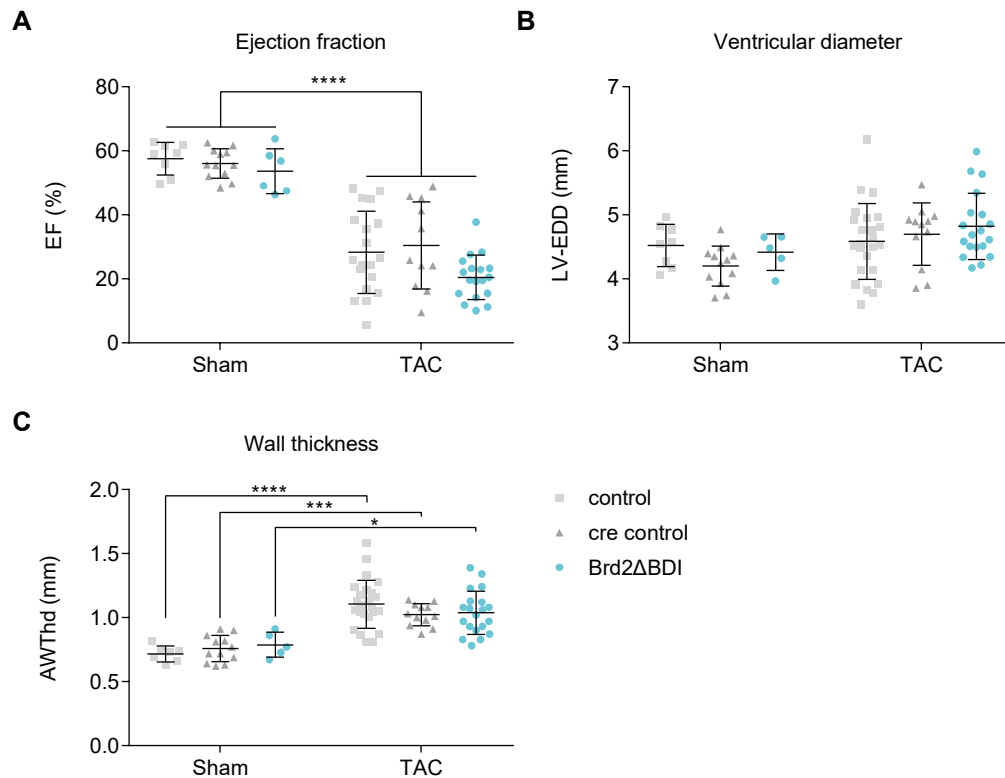


Figure 3.18: Echocardiographic phenotyping shows no significant differences between *Brd2*ΔBDI, control and cre control mice 5 weeks after TAC.

Echocardiographic phenotyping of control and *Brd2*ΔBDI mutant mice 5 weeks after surgery showed an extremely significant decrease of ejection fraction after TAC across all groups (A) no significant change of left ventricular diameter (B) and a comparable increase of left ventricular wall thickness in all groups (C). Two-way ANOVA together with Tukey correction for multiple comparisons was used. Error bars indicate SEM if not stated otherwise, * = $p < 0.05$, *** = $p < 0.001$, **** = $p < 0.0001$, each point represents the measurement for one animal.

3.4 The role of *Brd4* in the healthy and diseased mouse heart

3.4.1 Generation and validation of *Brd4* knockout mice

Once a conditional *Brd4* allele was available in our group (Benito et al. unpublished), which contained two loxP sites at the *Brd4* locus, one upstream of exon 6 and the other downstream of exon 7 (Figure 3.19A), matings with the cardiomyocyte-specific Cre-line were set up. Therefore, male mice heterozygous for the floxed *Brd4* allele (*Brd4*^{fl/+}) were crossed to female mice of the α MHC-Cre (Cre⁺). DNA from tail biopsies was used to control the genetic identity of the mice (Figure 3.19C). Genotypes of the F1 generation showed a Mendelian distribution and mice heterozygous for the recombined allele were viable and dissected hearts showed no obvious abnormalities (data not shown). Next, female Cre⁺;*Brd4*^{fl/+} mice were backcrossed to male *Brd4*^{fl/+} mice to produce homozygous *Brd4* knockout mice (Figure 3.19B). Five of these matings produced 17 litters with 94 pups in total but only one Cre-positive mouse was identified as homozygous for the conditional *Brd4* allele (Cre⁺;*Brd4*^{fl/fl}) (Figure 3.19D). This female died prematurely 6 weeks after birth. The actual genotype frequencies in the F2 generation (Figure

3.19D) were not Mendelian (Figure 3.19B) and suggested embryonic lethality of mice homozygous for the recombined *Brd4* allele.

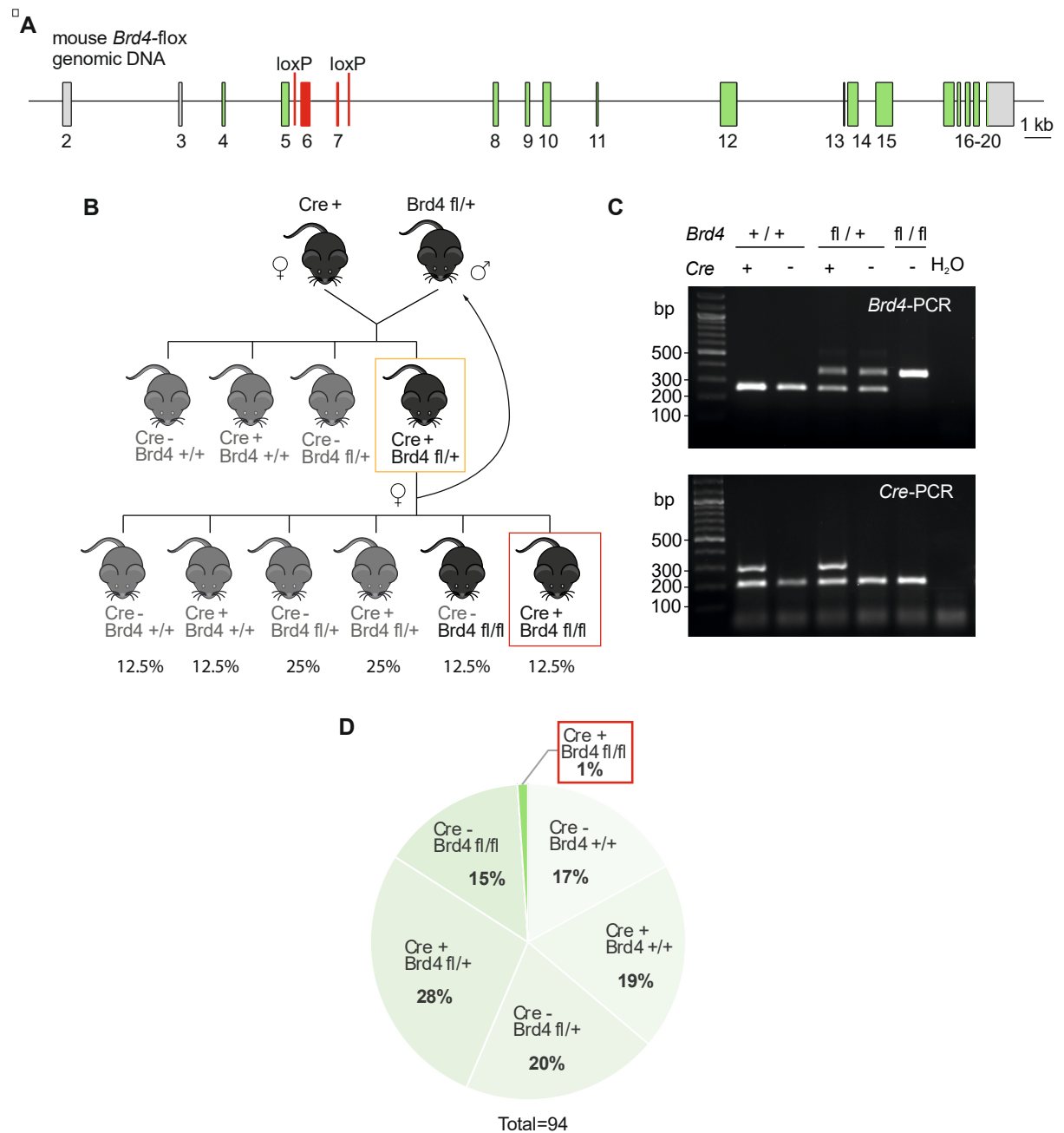


Figure 3.19: Generation of cardiomyocyte-specific *Brd4* knockout mice.

Illustration of the floxed *Brd4* allele. Boxes with numbers represent exons, green filling represents coding region, red indicates target region excised after Cre-mediated recombination. The exon/intron proportions were maintained (bar=1 kb) (A). Paternal *Brd4*^{fl/+} were mated to maternal α MHC-Cre⁺ (Cre⁺) resulting in either Cre⁻; *Brd4*^{fl/+} or Cre⁺; *Brd4*^{fl/+} (orange box). Female Cre⁺; *Brd4*^{fl/+} were backcrossed to male *Brd4*^{fl/+} to obtain Cre⁺; *Brd4*^{fl/fl} (red box). Expected Mendelian genotype frequencies of F2 genotypes are presented in % (B). Representative genotyping PCR from tail biopsies. *Brd4* primers bind to endogenous region flanking the loxP site between exons 7 and 8 and result in a PCR product of 250 bp for the wildtype allele and 360 bp for the floxed allele. In the Cre-PCR an internal control primer pair yields a smaller product of 200 bp and the Cre-primer a product of ~300 bp. H₂O served as negative control. bp=basepairs (C). Genotype distribution for matings of female Cre⁺; *Brd4*^{fl/+} and male *Brd4*^{fl/+} animals visualized as pie chart (D).

It was previously reported that the α MHC-Cre mice might transiently express the Cre-recombinase during early embryonic development in the heart and, depending on the target gene, could lead to developmental defects and lethality (Davis et al. 2012). My findings support this report. To overcome this limitation, the Tamoxifen-inducible α MHC-MerCreMer mice were used in a second approach. These mice express a fusion protein of Cre-recombinase with two copies of a modified estrogen-receptor ligand-binding domain (MerCreMer) in cardiomyocytes. Only upon application of Tamoxifen, the fusion-Cre-recombinase is translocated from cytosol into the nucleus enabling loxP-site-specific recombination (Sohal et al. 2001; Lexow et al. 2013). Therefore, male $Brd4^{fl/fl}$ ($Brd4^{fl/fl}$) were mated to female $MerCreMer^+$ mice resulting in either $MerCreMer^- ; Brd4^{fl/+}$ or $MerCreMer^+ ; Brd4^{fl/+}$ pups. Female $MerCreMer^+ ; Brd4^{fl/+}$ animals were further backcrossed to male $Brd4^{fl/fl}$ to obtain $MerCreMer^+ ; Brd4^{fl/fl}$ (Figure 3.20A). DNA from tail biopsies was used to control the genetic identity of the mice (Figure 3.20B) and showed a Mendelian distribution of genotypes with 1:1 female to male ratio. All Cre-positive mice hetero- or homozygous for the floxed *Brd4* allele were viable and bred normally.

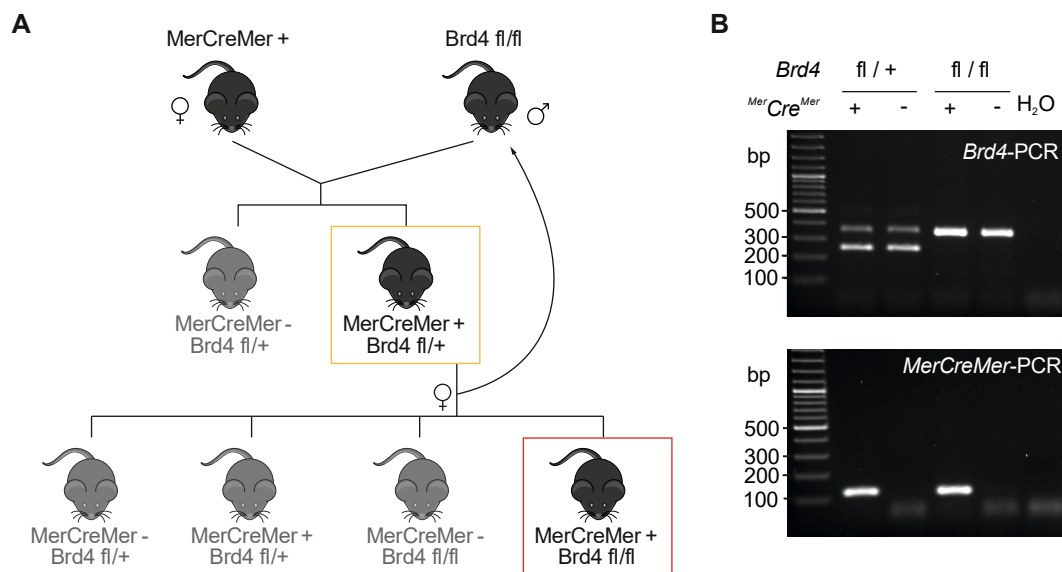


Figure 3.20: Generation of inducible cardiomyocyte-specific *Brd4* knockout mice.

Paternal $Brd4^{fl/fl}$ were mated to maternal α MHC-MerCreMer⁺ ($MerCreMer^+$) resulting in either $MerCreMer^- ; Brd4^{fl/+}$ or $MerCreMer^+ ; Brd4^{fl/+}$ (orange box). Female $MerCreMer^+ ; Brd4^{fl/+}$ were backcrossed to male $Brd4^{fl/fl}$ to obtain $MerCreMer^+ ; Brd4^{fl/fl}$ (red box) (A). Representative genotyping PCR from tail biopsies. *Brd4* primers bind to endogenous region flanking the loxP site between exons 7 and 8 and result in a PCR product of 250 bp for the wildtype allele and 360 bp for the floxed allele. In the *MerCreMer*-PCR the *MerCreMer*-primer result in a product of ~120 bp. H₂O served as negative control. bp=basepairs (B).

For further validation, 5 weeks old $MerCreMer^+ ; Brd4^{fl/fl}$ mice either received Tamoxifen (2.1.4) on three consecutive days at the dosage of 30 mg/kg/day by intraperitoneal injection (*Brd4* KO), or were not treated (control). Administration of 3 x 30 mg/kg tamoxifen caused 10-20% mortality in comparison to not injected animals (data not shown) which is consistent with

previous findings (Bersell et al. 2013), but the remaining *Brd4* KO mice lived for over one year without incidents or unusual observations (data not shown).

The successful *Brd4* knockout was validated by standard PCR on the genome and by RT-qPCR on the transcriptome level using primer pairs specific for the target site or transcript variants (**Figure 3.21A**). Standard PCR, with DNA from left ventricles and primers flanking the target site at the *Brd4* locus, confirmed successful Cre-mediated deletion of *Brd4* exons 6 and 7 (**Figure 3.21B**). As demonstrated by RT-qPCR, the deletion led to an extremely significant reduction of total *Brd4* mRNA levels in left ventricle ($p < 0.0001$, unpaired two-tailed t-test, $n = 8-9$) and even stronger in isolated cardiomyocytes ($p < 0.0001$, unpaired two-tailed t-test, $n = 3-6$) (**Figure 3.21C**). This means that the Cre-mediated deletion of exons 6 and 7 of *Brd4* leads to a complete depletion of the full-length *Brd4* short and long isoforms in cardiomyocytes.

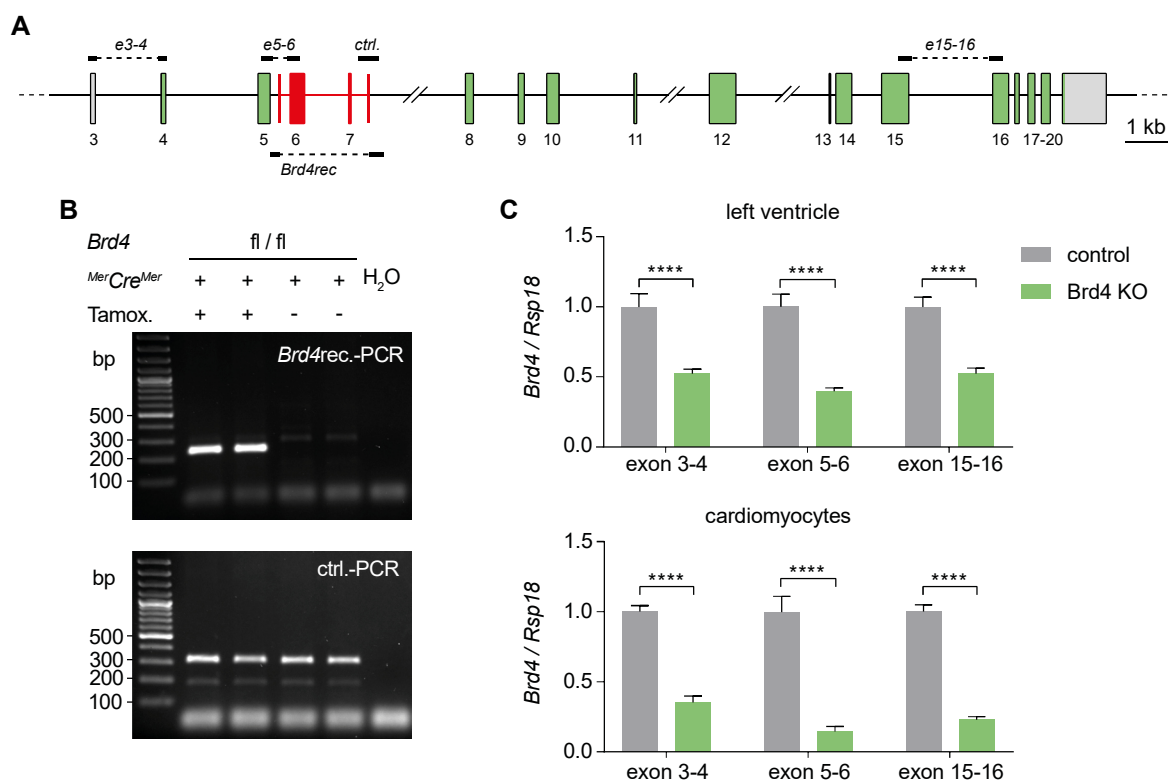


Figure 3.21: Tamoxifen-induced deletion of exons 6 and 7 in the *Brd4* locus via MerCreMer leads to decreased *Brd4* expression in the heart.

Illustration of the floxed *Brd4* allele with target sites of recombination and RT-qPCR primers. Dashed lines are not amplified during PCR. Boxes with numbers represent exons, green filling represents coding region, red indicates target region excised after MerCreMer-mediated recombination. Long introns were discontinued (bar=1 kb) (**A**). Representative genotyping PCRs from heart biopsies. *Brd4* recombination primers result in a ~ 250 bp PCR product after successful recombination whereas the control PCR yields a ~ 320 bp product for the floxed allele regardless recombination. H₂O served as negative control (**B**). After recombination, the overall expression of *Brd4* was significantly decreased when analyzing total RNA from left ventricle (RT-qPCR, $n = 8-9$) (**C, top**) and from isolated cardiomyocytes (RT-qPCR, $n = 3-6$) (**C, bottom**). Unpaired two-tailed t-test was used. Error bars indicate SEM, ****= $p < 0.0001$.

Western blot analysis of nuclear and chromatin-bound protein fractions from left ventricles of 3-month-old control and *Brd4* KO animals showed no difference in BRD4 protein levels (**Figure**

3.22A). But a slight but not significant reduction in the nuclear fraction from isolated cardiomyocytes was observed in Brd4 KO samples (**Figure 3.22B-C**). Immunocytochemistry of isolated Brd4 KO cardiomyocytes (data not shown) showed no difference to wildtype (**Figure 3.1**). Despite various efforts, the absence of BRD4 after knockout could not be clearly verified by immunoblotting. This might be due to residual fibroblasts and 10-20% of not recombined cardiomyocytes, which still express BRD4. The western blot conditions might be further improved in future studies but the slight reduction of BRD4 levels in Brd4 KO cardiomyocytes together with the depletion of *Brd4* mRNA were promising indications for the intended knockout.

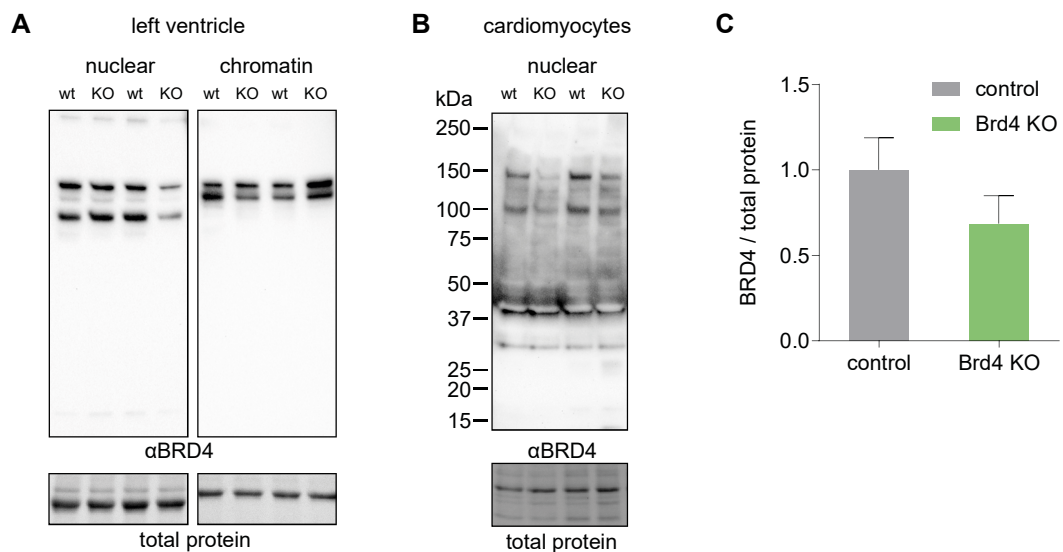


Figure 3.22: Successful *Brd4* knockout could not be clearly validated by immunoblotting.

Western blot showed that BRD4 was present in subcellular fractions for nuclear and chromatin-bound protein from left ventricles of 3 months old control and Brd4 KO mice (**A**) but slightly reduced in the nuclear fraction from isolated cardiomyocytes using anti-BRD4 (ab128874) (**B**). Quantification of BRD4 intensities normalized to total protein (not significant, unpaired two-tailed t-test, $n=3$) (**C**). Data presented as mean +SEM.

3.4.2 *Brd4* knockout mice show basal concentric hypertrophy

Morphometric and echocardiographic characterization was performed to investigate the basal effect of *Brd4* depletion from cardiomyocytes. Therefore, MerCreMer⁺;Brd4^{fl/fl} mice that were not induced (control) or that received Tamoxifen (Brd4 KO) as previously described (2.1.4) were compared in context of heart morphology, function and physiology in 3 and 6 month old animals. At both timepoints, Brd4 KO hearts showed slightly enlarged ventricular walls in Masson's trichrome stainings (**Figure 3.23A**), which led to increased left ventricular to body weight ratios in three month old animals in comparison to control ($p=0.0005$, two-way ANOVA with Tukey post-hoc, $n=16-19$) (**Figure 3.23B**). Six months old control animals showed a significant increase compared to three month old control ($p=0.0002$, two-way ANOVA with Tukey post hoc, $n=16-18$) but not to Brd4 KO as their left ventricles did not change with age

(Figure 3.23B). WGA-stained heart cross sections showed increased mean MFDs ($F(1,13) = 6.711$, $p=0.0224$, two-way ANOVA, $n=4-5$) and a distribution shift towards larger cardiomyocytes in Brd4 KO compared to control mice (Figure 3.23 C-E).

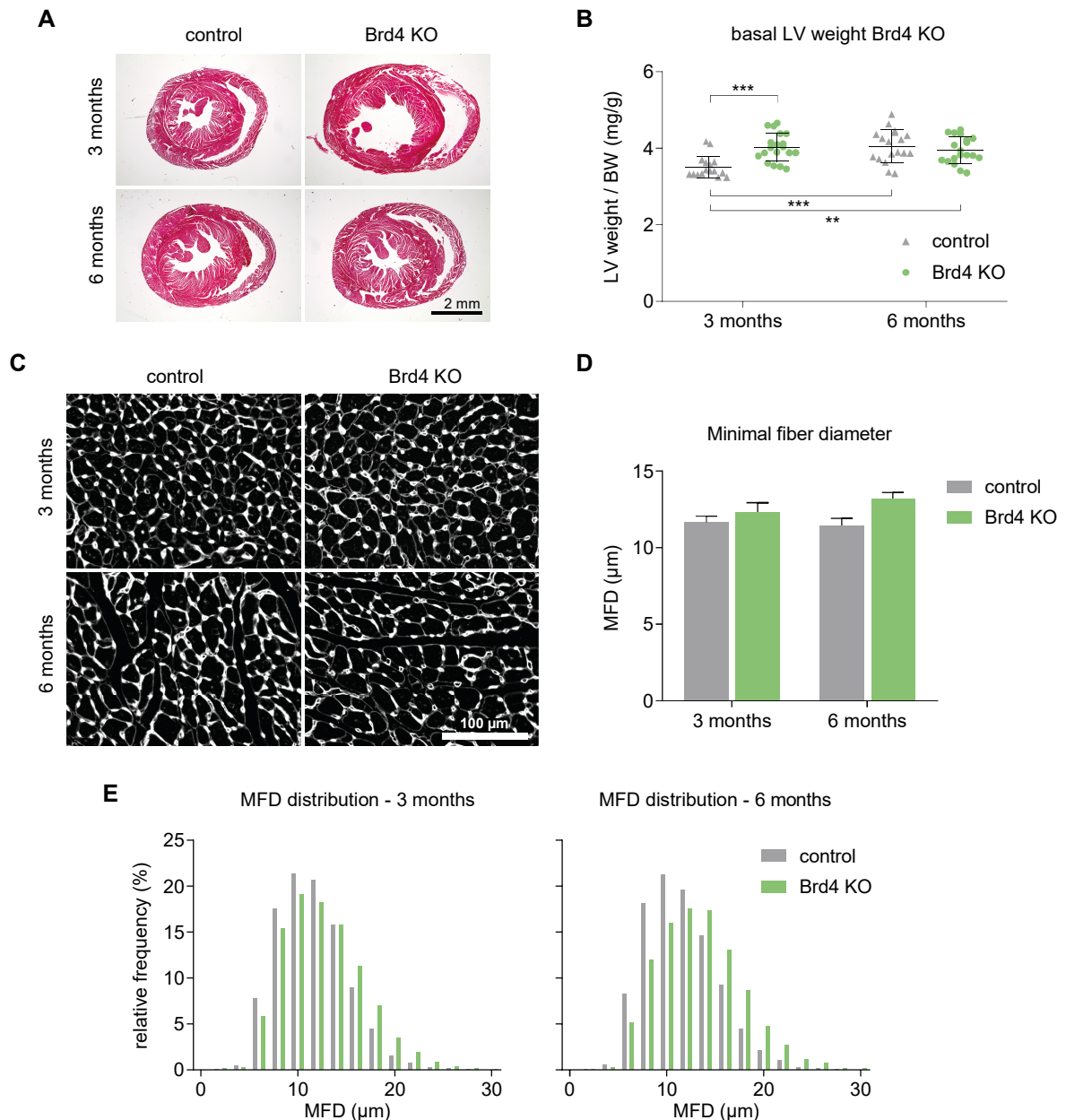


Figure 3.23: Morphometric characterization of *Brd4* knockout mice showed concentric hypertrophy in comparison to control mice.

Masson's trichrome stain showed slightly enlarged hearts in 3 and 6 months old Brd4 KO vs. control mice (bar=2 mm) (A). Basal left ventricular weight to body weight ratio was not changed upon Brd4 knockout (each point represents the measurement for one animal, error bars indicate SD, two-way ANOVA with Tukey) (B). Representative pictures of Wheat Germ Agglutinin staining (C), analysis of the minimal fiber diameter (error bars indicate SEM) (two-way ANOVA with Tukey, $F(1,13) = 6.711$, $p=0.0224$, $n=4-5$) (D) and its distribution analysis showed cardiomyocyte hypertrophy in Brd4 knockout mice (E). Two-way ANOVA together with Tukey correction for multiple comparisons was used. Error bars indicate SD if not stated otherwise, **= $p<0.01$, ***= $p<0.001$.

3.4.3 *Brd4* KO mice show thicker ventricular walls but normal cardiac function

To challenge these findings, additional basal echocardiographic phenotyping was performed including Tamoxifen-induced α MHC-MerCreMer positive mice (MerCreMer⁺) to rule out possible Tamoxifen or Cre activity related effects. MerCreMer⁺, control and Brd4 KO mice at 3 and 6 months of age showed no significant differences in ejection fraction, although Brd4 KO mice had slightly higher ejection fractions with 3 months that significantly decreased to control levels with 6 months ($p=0.0002$, two-way ANOVA, $n=16-19$) (**Figure 3.24A**). No left ventricular dilation was observed (**Figure 3.24B**) but with 3 months left ventricular wall thickness was significantly increased in Brd4 KO to control ($p<0.0001$, two-way ANOVA with Tukey post hoc, $n=14-17$) and to MerCreMer⁺ ($p=0.0013$, two-way ANOVA with Tukey post hoc, $n=7-14$). With 6 months left ventricular wall thickness of MerCreMer⁺ animals slightly increased ($p=0.0103$, two-way ANOVA with Tukey post hoc, $n=7$) and stayed stable in Brd4 KO mice but was still significantly thicker compared to control ($p<0.0001$, two-way ANOVA with Tukey post hoc, $n=16-18$) (**Figure 3.24C**).

These data showed that with induction at postnatal week 5, Brd4 KO mice are viable and develop basal concentric hypertrophy, which had no adverse effects on heart function nor on survival. Furthermore, echocardiographic examination of MerCreMer⁺ control animals demonstrated that the Brd4 KO effects were not attributed to Tamoxifen application or Cre-activity in 3- and 6-months old animals. Therefore, MerCreMer⁺ animals were not included in the following experiments.

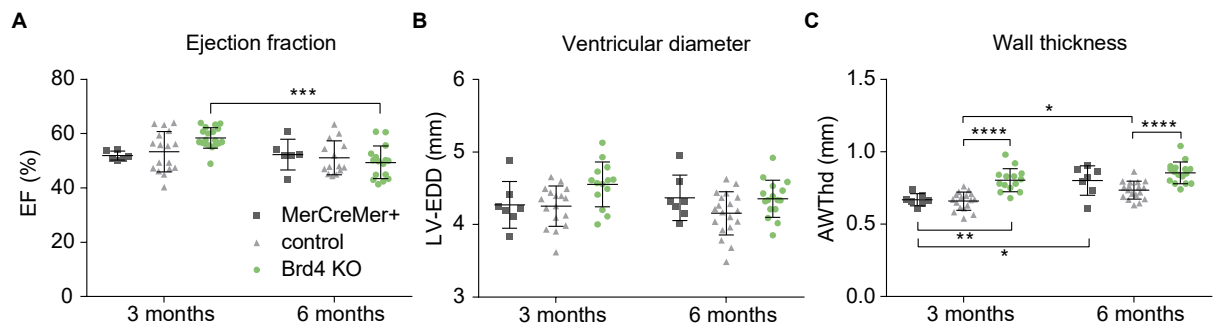


Figure 3.24: Basal echocardiographic phenotyping showed increased left ventricular wall thickness in Brd4 KO mice.

Echocardiographic phenotyping of MerCreMer⁺, control and Brd4 KO mice at 3 and 6 months of age showed no significant differences in ejection fraction between groups, although Brd4 KO mice show slightly higher ejection fraction with 3 months that significantly decreases to control levels with 6 months (**A**). No difference in left ventricular diameter was observed (**B**). Left ventricular wall thickness was significantly increased in Brd4 KO to both controls in 3 months old animals. With 6 months left ventricular wall thickness of MerCreMer⁺ animals slightly increased and stayed stable in Brd4 KO mice but was still significantly thicker compared to control (**C**). Two-way ANOVA together with Tukey correction for multiple comparisons was used. Error bars indicate SD, * = $p<0.05$, ** = $p<0.01$, *** = $p<0.001$, **** = $p<0.0001$. Each point represents the measurement for one animal.

3.4.4 *Brd4* KO mice show higher mortality after TAC

To examine *Brd4* KO mice for cardiac phenotypes after TAC-induced PO, female *MerCreMer*⁺; *Brd4*^{fl/fl} mice were crossed with male *Brd4*^{fl/fl} mice. Only *MerCreMer*-positive offspring was used for further examination. With 5 weeks 50% of animals received 30mg/kg/d Tamoxifen on three consecutive days via intraperitoneal injection (*Brd4* KO), whereas the other half was not induced (control) (**Figure 3.25A**). It was previously described that transient cardiac phenotypes can occur in *MerCreMer*⁺ animals shortly after Tamoxifen-application but are normalized within one to three weeks after the last dosage (Hougen et al. 2010). For that reason, I decided to induce *MerCreMer*-mediated recombination by applying Tamoxifen at the age of 5 weeks, 3 weeks before TAC or Sham surgery. Animals of the control and *Brd4* KO group underwent TAC or Sham at the age of 8-10 weeks and were analyzed by echocardiography 1 and 5 weeks after surgery. Afterwards, the animals were either sacrificed for molecular testing or received an additional echo 10 weeks after surgery and were monitored regarding their survival after TAC for up to 6 months (**Figure 3.25B**).

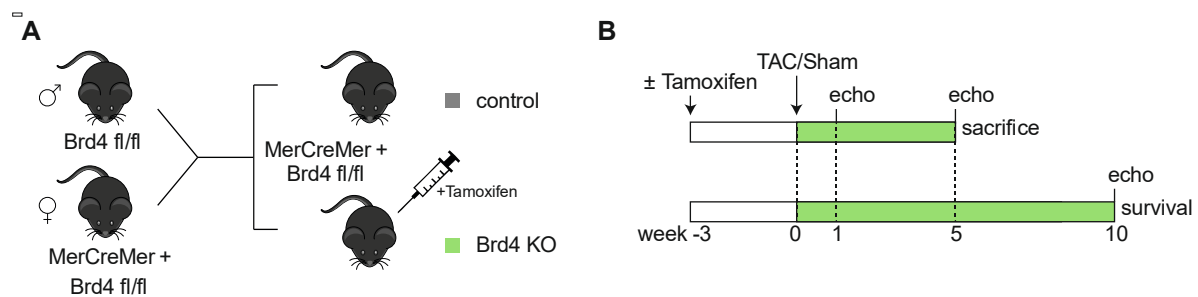


Figure 3.25: *Brd4* KO mating scheme and experimental design.

Mating scheme of parental transgenic mouse lines. Only *MerCreMer*⁺; *Brd4*^{fl/fl} offspring was used for further examination. With 5 weeks 50% of animals received 30mg/kg/d Tamoxifen on three consecutive days via intraperitoneal injection (*Brd4* KO). The other half was not induced (control). The animals underwent TAC or Sham surgery at the age of 8-10 weeks (**A**). Experimental design: the animals were analyzed by echocardiography 1 and 5 weeks after TAC or Sham surgery and either sacrificed afterwards for molecular testing or received additional echo 10 weeks after surgery and were monitored regarding their survival after TAC for up to 6 months (**B**).

After surgeries the pressure gradients across the transverse aorta were controlled by Doppler echocardiography, to ensure the consistency of constrictions. Both, control and *Brd4* KO animals showed normally distributed 10- to 20-fold higher ($p < 0.0001$, two-way ANOVA with Tukey post hoc) fractional flow reserve after TAC than after Sham (**Figure 3.26A**). In total, 78 mice that underwent surgical intervention were monitored for the outcome of the surgeries. All death events were documented in a Kaplan-Meier curve. No Sham mouse of either group died within the time frame of the observation. *Brd4* KO mice showed a significantly increased mortality after TAC, especially within the first 40 days. The median survival of *Brd4* KO mice was 36.5 days and, thus 3.6 times lower than that of the control group ($p = 0.0188$, Gehan-Breslow-Wilcoxon test, $n = 30-38$) (**Figure 3.26B**).

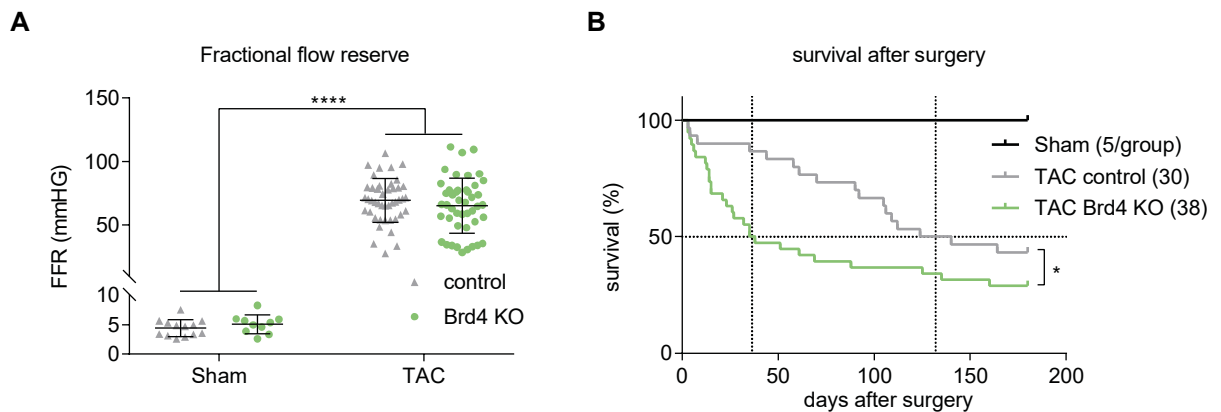


Figure 3.26: The survival after TAC is reduced in Brd4 KO mice compared to control with the strongest mortality in the early phase after TAC.

The successful TAC was ensured by measurement of the fractional flow reserve 24 to 72 hours after surgery which was comparably increased in Brd4 KO and control after TAC (data presented as mean +SD, each point represents the measurement for one animal, ****= $p < 0.0001$, two-way ANOVA with Tukey test) (**A**). Kaplan-Meier curve (without the first 48 hours after surgery) showing a significantly increased mortality of Brd4 KO mice, especially within the first 40 days after TAC. Median survival in the Brd4 KO group was 36.5 days and 132 days in the control group (Gehan-Breslow-Wilcoxon test, * $p = 0.0188$, numbers in brackets represent animals examined, dotted lines indicate median survival) (**B**).

3.4.5 *Brd4* KO attenuates cardiac remodeling after TAC

Morphometric characterization confirmed that left ventricles of Brd4 KO mice showed moderate concentric hypertrophy at baseline (Sham) and revealed that left ventricular mass did not significantly increase within 5 weeks after TAC in these animals. In contrast, left ventricles of control animals were dramatically enlarged 5 weeks after TAC and were significantly larger than left ventricles of TAC-operated Brd4 KO mice ($p < 0.01$, two-way ANOVA with Tukey post hoc test) (**Figure 3.27 A-B**). RT-qPCR was performed to determine mRNA levels of *Nppa* and *Nppb* and showed an extremely significant increase of both stress markers ($p < 0.0001$, two-way ANOVA with Tukey post hoc test) in control and Brd4 KO hearts 5 weeks after TAC (**Figure 3.27 C-D**). Notably, Brd4 KO animals that underwent Sham surgery had already significantly higher cardiac *Nppa* levels than the control animals after Sham ($p < 0.01$) (**Figure 3.27C**).

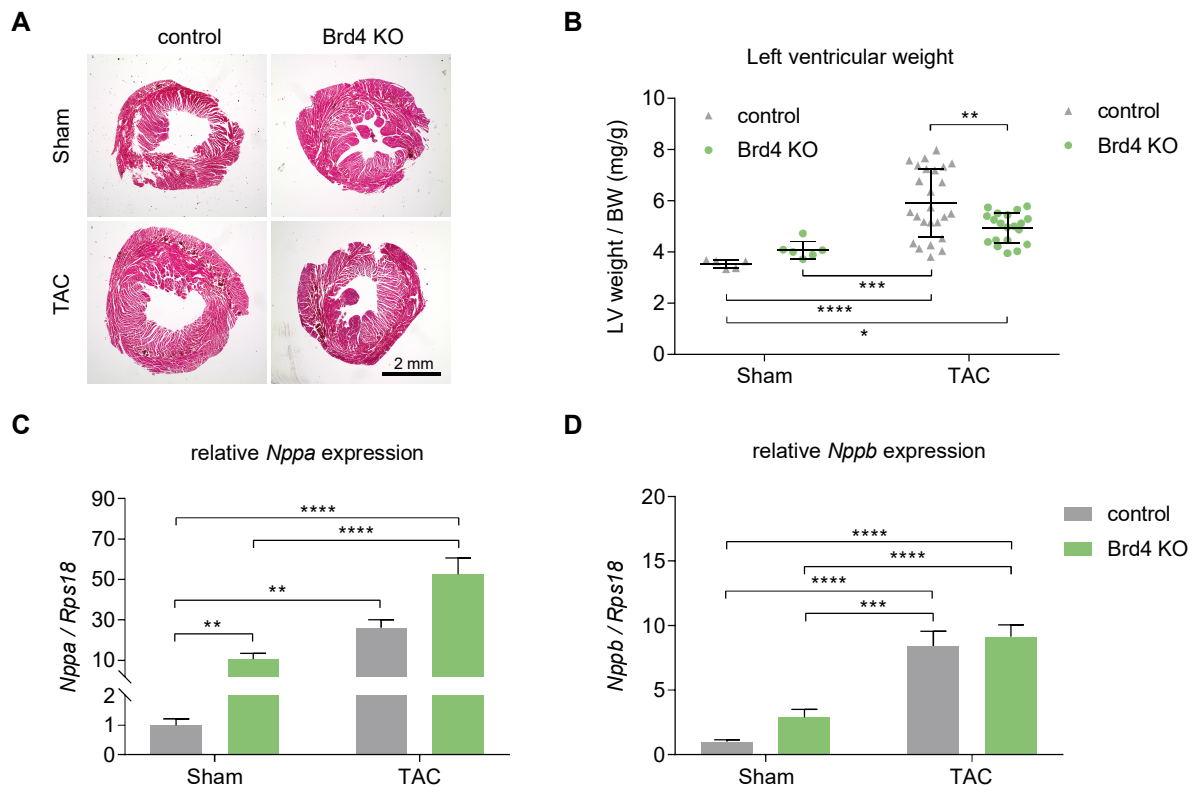


Figure 3.27: Brd4 KO and control mice show increased cardiac stress marker expression 5 weeks after TAC, but Brd4 KO mice do not develop cardiomegaly.

Masson's trichrome stain showed increase in size of the left ventricle after TAC in control but not in Brd4 KO mice (bar=2 mm) (**A**). The left ventricular weight to body weight ratios were increased 5 weeks after TAC in both groups but significantly higher in control animals (error bars indicate SD) (**B**). *Nppa* mRNA expression was significantly increased in Brd4 KO Sham and both TAC groups (**C**), whereas *Nppb* mRNA expression was only significantly increased after TAC in Brd4 KO and control hearts (RT-qPCR, n=4-6) (**D**). Two-way ANOVA together with Tukey correction for multiple comparisons was used. Error bars indicate SEM if not stated otherwise, **= $p < 0.01$, ***= $p < 0.001$, ****= $p < 0.0001$.

Next, the size of cardiomyocytes was determined as MFD from histological WGA staining of heart cross sections (**Figure 3.28**). The comparison of the average MFDs and their distributions showed a significant enlargement of cardiomyocytes in control animals after TAC in comparison to Sham control ($p < 0.05$, two-way ANOVA with Fischer's LSD test, n=4-6), whereas the size of larger Brd4 KO cardiomyocytes at baseline did not further increase after TAC (**Figure 3.28 B-C**).

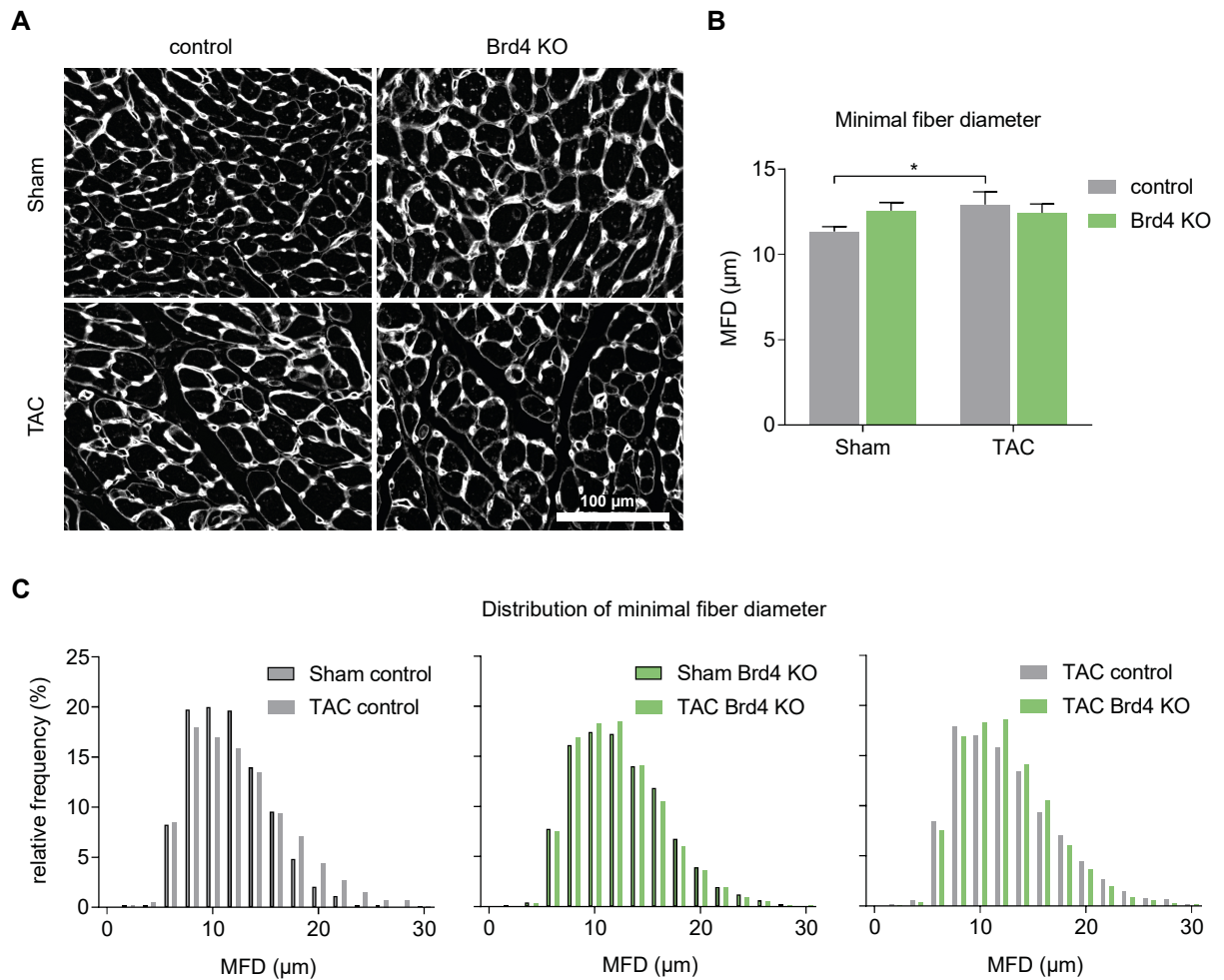


Figure 3.28: The basal cardiomyocyte hypertrophy in Brd4 KO animals does not change after TAC.

Representative pictures of Wheat Germ Agglutinin staining (**A**), analysis of the minimal fiber diameter (error bars indicate SEM) (two-way ANOVA with Fischer's LSD test, $*= p < 0.05$, $n=4-6$) (**B**) and its distribution confirmed basal cardiomyocyte hypertrophy in Brd4 KO animals and showed that cell size does not further increase after TAC (**C**).

3.4.6 Brd4 KO hearts show basal fibrosis that increases after TAC

Picro Sirius Red staining was used to visualize collagen type I and III in heart sections from control and Brd4 KO mice following Sham or TAC surgery allowing to measure interstitial fibrosis (**Figure 3.29A**). Semi-automated analysis revealed that in control $18\% \pm 3.4\text{SEM}$ and in Brd4 KO hearts $19\% \pm 3.8\text{SEM}$ of the cross-sectional area were fibrotic five weeks after TAC, which was almost 5-fold higher compared to Sham control hearts ($p < 0.05$, two-way ANOVA with Tukey post hoc testing, $n=4-6$). However, Brd4 KO mice that underwent Sham surgery already showed mild fibrosis of about 12% in a direct comparison to Sham-control ($p=0.0442$, two-way ANOVA Fischer's LSD test, $n=4-6$) (**Figure 3.29B**). These data suggest a basal activation of cardiac remodeling in Brd4 KO animals, leading to hypertrophy, expression of cardiac stress markers and mild fibrosis. After TAC, Brd4 KO and control mice showed comparable *Nppa/Nppb* levels, cardiomyocyte diameters, and fibrosis but hearts of control

animals were significantly larger. Moreover, Brd4KO mice showed significantly higher mortality within the first 40 days after TAC. This further suggests a limited capacity for cardiac remodeling after PO as well as a decreased compensatory potential in the acute phase after TAC in Brd4 KO animals.

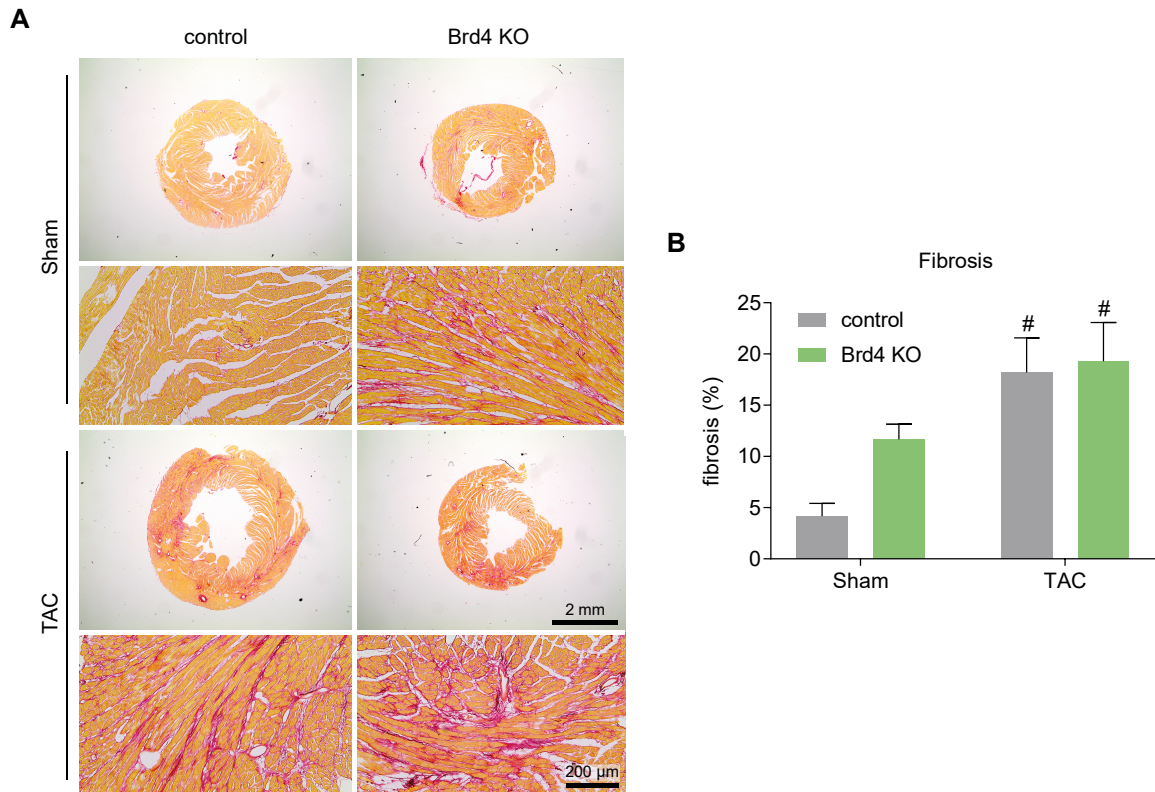


Figure 3.29: Brd4 KO hearts showed mild fibrosis after Sham that increased after TAC.

Representative heart sections stained with Picro Sirius Red from a control and Brd4 KO mouse following Sham or TAC surgery (bars: overview=2 mm, detailed=200 μ m) (A). Quantification of myocardial fibrosis in control and Brd4 KO hearts 5 weeks after Sham or TAC surgery. (B). Two-way ANOVA together with Tukey correction for multiple comparisons was used. Error bars indicate SEM. # = $p < 0.01$ to Sham control, $n = 4-6$.

3.4.7 Brd4 KO mice show partially preserved heart function after TAC

Analysis of echocardiographic images revealed differences in heart function and dimensions between control and Brd4 KO mice after pressure overload. Control animals showed a typical decrease of a basal ejection fraction of 52.5% (± 6.2 SD) to 41.1% (± 10.4 SD) ($p = 0.0018$, two-way ANOVA with Tukey, $n = 11-36$) 5 weeks and 30.4% (± 9.1 SD) ($p < 0.0001$, two-way ANOVA with Tukey, $n = 5-19$) 10 weeks after TAC. In contrast, Brd4 KO animals showed a milder reduction of the heart function starting at an ejection fraction of 58% (± 7.7 SD), it decreased to 46.9% (± 8.1 SD) ($p = 0.0247$, two-way ANOVA with Tukey, $n = 12-20$) 5 weeks and to 42.3% (± 5.4 SD) ($p = 0.0102$, two-way ANOVA with Tukey, $n = 5-10$) 10 weeks after TAC. Interestingly, Brd4 KO mice had significantly higher ejection fraction 10 weeks after TAC compared to TAC control ($p = 0.0018$, two-way ANOVA with Tukey, $n = 10-19$) (Figure 3.30A). Furthermore, left ventricular inner diameter significantly decreased within the first week after TAC in BRD4 KO

animals ($p < 0.01$, two-way ANOVA with Tukey, $n = 4-26$) and stayed significantly lower in Brd4 KO compared to control animals at all three time points after TAC (**Figure 3.30B**). Brd4 KO mice showed slightly thicker ventricular walls at baseline and almost no further wall thickening after TAC. Control animals, on the other hand, showed significant wall thickening one week after TAC ($p = 0.0061$, two-way ANOVA with Tukey, $n = 4-20$), which further increased with the duration of pressure overload ($p < 0.0001$, two-way ANOVA with Tukey) (**Figure 3.30C**). The echocardiographic phenotyping confirms a basal concentric hypertrophy that leads to a slightly increased basal ejection fraction in Brd4 KO mice and suggests that those animals have a limited remodeling capacity as demonstrated by no to little wall thickening and dilatation. Nevertheless, after pressure overload heart function seems to be somehow preserved in Brd4 KO animals or progression of HF slowed as ejection fraction decrease was not as dramatic as in the control group.

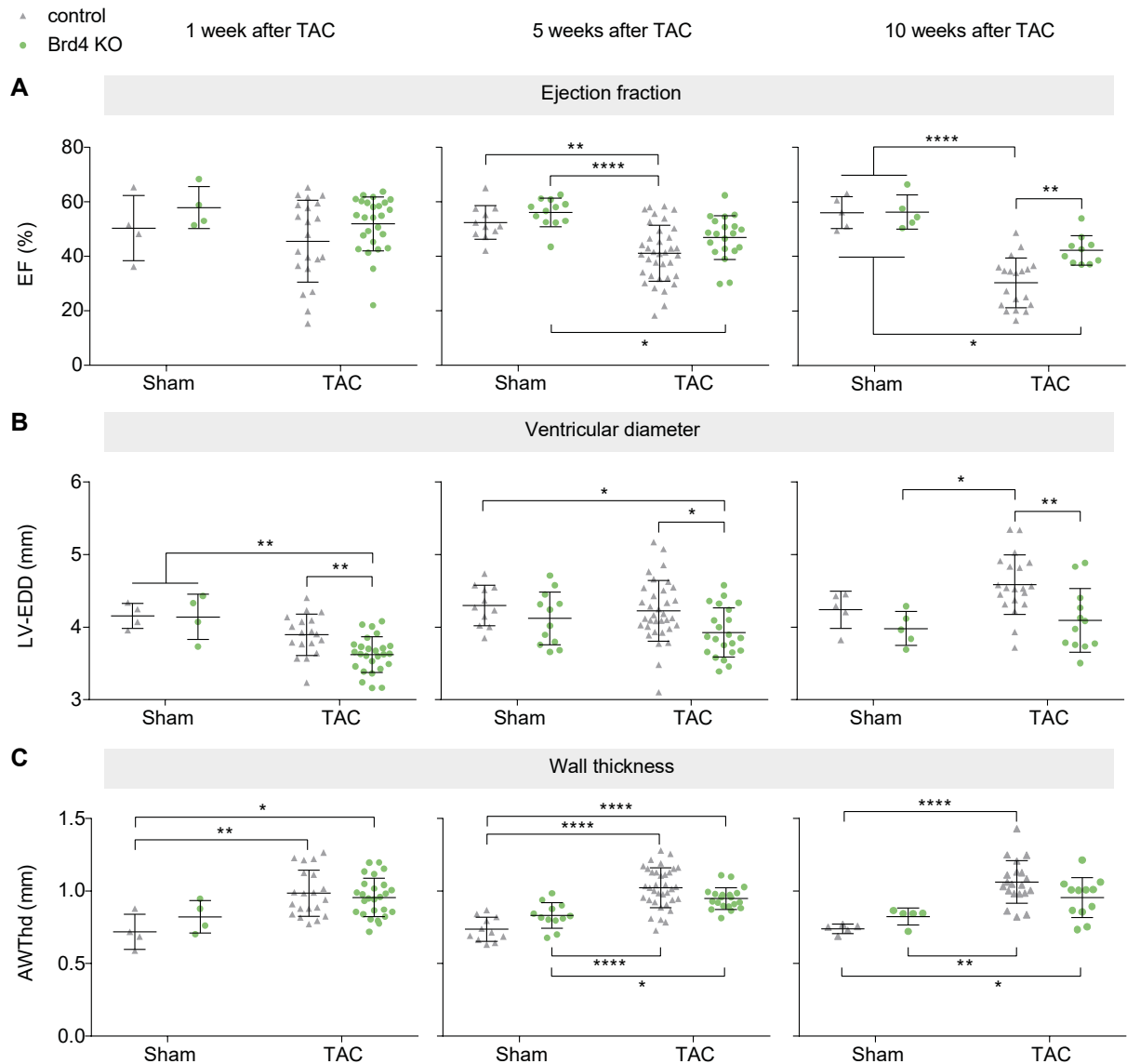


Figure 3.30: Brd4 KO animals show limited remodeling capacity after TAC and slightly preserved ejection fraction.

Echocardiographic phenotyping showed a mild ejection fraction reduction after TAC in Brd4 KO animals with significantly higher ejection fraction 10 weeks after TAC compared to TAC control (**A**). After TAC, left ventricular inner diameter was significantly lower in Brd4 KO compared to control animals (**B**). Brd4 KO mice showed less wall thickening after TAC compared to control (**C**). Two-way ANOVA together with Tukey correction for multiple comparisons was used. Error bars indicate SD, *= $p < 0.05$, ** = $p < 0.01$, *** = $p < 0.001$, **** = $p < 0.0001$, each point represents the measurement for one animal. grey triangles = control, green dots = Brd4 KO.

3.4.8 *Brd4* KO induces differential expression of genes involved in ECM organization, energy metabolism, and cardiac muscle contraction

The cardiomyocyte-specific knockout of *Brd4* in adolescent murine hearts led to the development of concentric hypertrophy, fibrosis, and the expression of cardiac stress markers but ventricular diameter, ejection fraction, and viability remained unchanged. After TAC, however, Brd4 KO mice showed increased mortality but otherwise little changes in response to cardiac stress. And although the ejection fraction of Brd4 KO mice decreased, it remained higher than that of TAC control animals. To understand the effects of BRD4 absence in cardiomyocytes at baseline and after stress-induction hearts of Brd4 KO and control animals were allowed to rest for three days after the echocardiographic examination five weeks after Sham or TAC surgery before they were sacrificed, and their hearts dissected. The so obtained hearts were retrogradely perfused to remove residual blood and left ventricles of all four experimental groups used for subsequent mRNA sequencing.

First, the basal impact of *Brd4* deletion on transcription was analyzed. Differential expression analysis of Sham Brd4 KO to Sham control revealed 2902 DEGs (1317 up, dark red; 1585 down, dark blue) ($\text{padj} < 0.05$, $\log_2\text{FC} \pm 0.5$) (**Figure 3.31A**). The RPKMs of the 2902 DEGs were plotted on a heatmap and showed 4 main gene clusters, Brd4 KO induced, Brd4 KO repressed, TAC and Brd4 KO induced, and TAC and Brd4 KO repressed (**Figure 3.31B**). Pathway analysis of the 1317 up-regulated genes in Sham Brd4 KO ($\text{padj} < 0.05$, $\log_2\text{FC} \pm 0.5$) showed an enrichment of genes involved in ECM organization, dilated cardiomyopathy, and AGE-RAGE signaling pathway ($\text{padj} < 0.05$, $\text{Kappa} = 0.4$) (**Figure 3.31C**). However, the 1585 down-regulated genes showed enrichment for GO terms associated with energy metabolism, oxidative phosphorylation, and cardiac muscle contraction ($\text{padj} < 0.05$, $\text{Kappa} = 0.4$) (**Figure 3.31D**). Moreover, left ventricles of Sham Brd4 KO mice showed significantly increased expression of cardiac stress markers ($\text{padj} < 0.05$, $\log_2\text{FC} \pm 0.5$) in comparison to Sham control (**Figure 3.31E**). Consequently, transcriptome analysis provides a link between the phenotypic and functional observations and Brd4 KO mediated differential expression of genes associated with cardiac remodeling, alters ECM organization, energy metabolism, and cardiac muscle contraction.

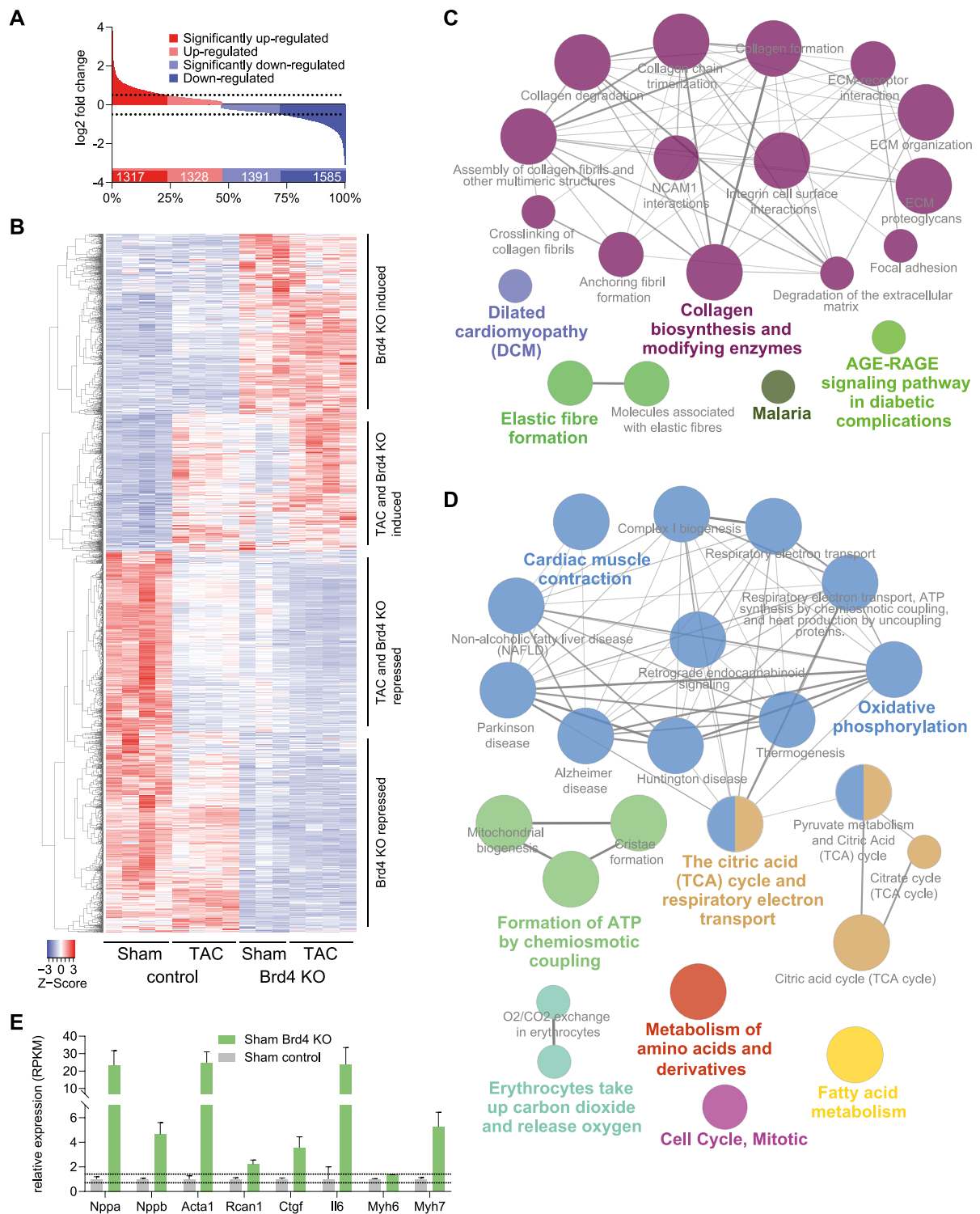


Figure 3.31: Depletion of Brd4 from cardiomyocytes induces cardiac remodeling, alters ECM organization, energy metabolism, and cardiac muscle contraction.

mRNA sequencing revealed 5621 DEGs (2645 up, red; 2976 down, blue) between Sham control and Sham Brd4 KO with $\text{padj} < 0.05$. A subsequent cutoff at $\log_2\text{FC} \pm 0.5$ resulted in 2902 DEGs (1317 up, dark red; 1585 down, dark blue). X-axis indicates number and percent of total DEG (A). A heatmap of the 2902 Sham Brd4 KO DEGs was clustered via centroid linkage with Pearson method and revealed 4 clusters (B). ClueGO pathway analysis of 2902 DEGs from (A) ($\text{padj} < 0.05$, $\log_2\text{FC} \pm 0.5$) showed GO terms enriched for ECM organization, dilated cardiomyopathy, and AGE-RAGE signaling pathway for up-regulated genes (C) and enrichment of GO terms for energy metabolism, oxidative phosphorylation, and cardiac muscle contraction for down-regulated genes ($\text{padj} < 0.05$, $\text{Kappa} = 0.4$). Circle size represents padj (D). Relative expression of cardiac stress and remodeling markers is increased for Sham Brd4 KO. Based on RPKM normalized to Sham control. Error bars indicate SEM (E).

The basal Brd4 KO effects resemble main features of hypertrophic cardiomyopathy (HCM) (Marian and Braunwald 2017). For validation, DEGs for Sham Brd4 KO versus Sham control were mapped to the according KEGG HCM pathway (red= up-regulated, blue= down-regulated) (Figure 3.32). Upon *Brd4* deletion, the expression of sarcomere genes (*Myh7*, *Mybpc3*, *Tnnt2*, *Tnni3*, *Actc1*) and of genes encoding ion channels involved in membrane repolarization (*RyR2*, *SERCA2a*) is modulated. The absence of BRD4 further led to increased expression of integrins, intermediate filaments (Dystrophin and Desmin) as well as the induction of factors like IGF-1, TGF- β , TNF- α , and IL-6. The underlying gene expression changes provide a causal link to the observed basal Brd4 KO effects.

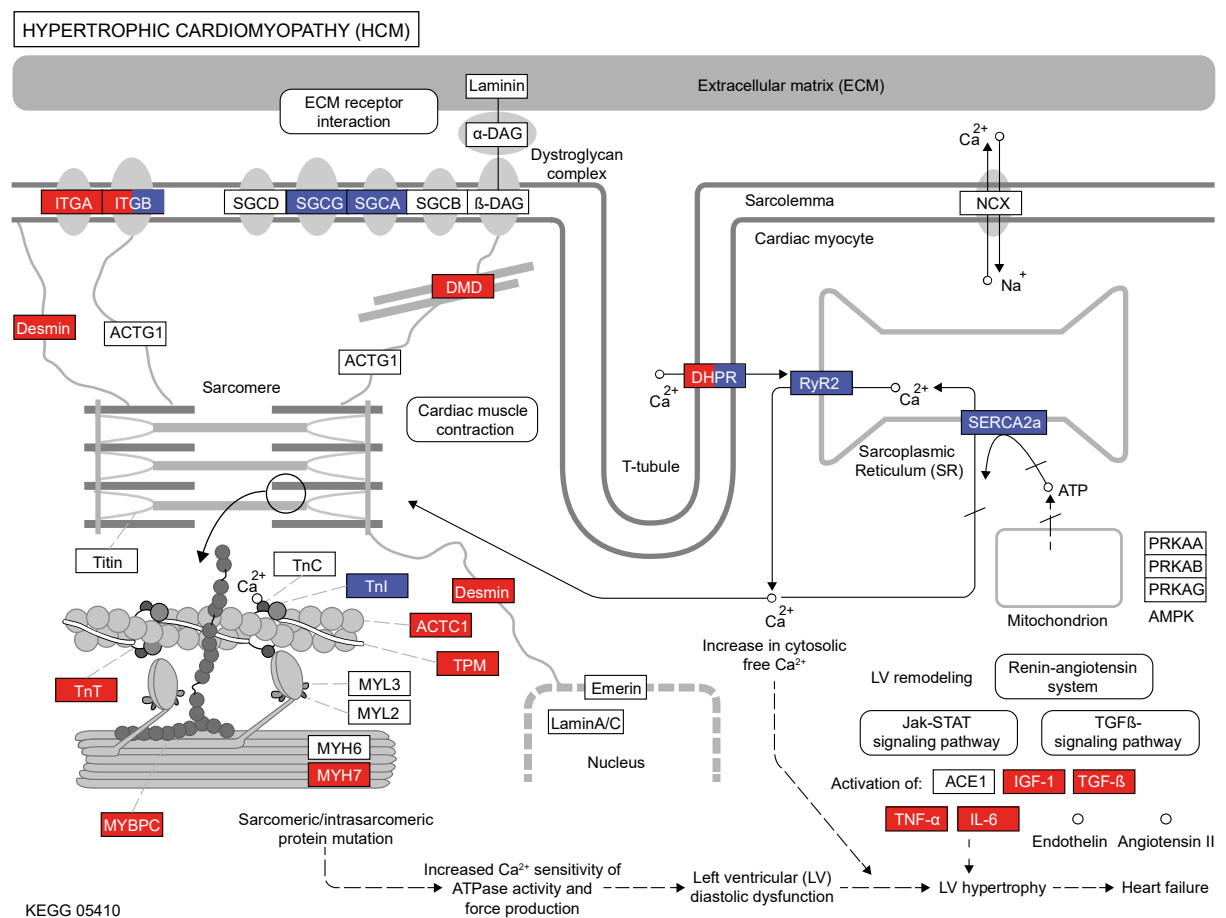


Figure 3.32: Brd4 KO animals show gene expression changes associated with HCM.

Schematic view of a cardiomyocyte with key proteins associated with the KEGG pathway map (05410) for hypertrophic cardiomyopathy (HCM). Differentially expressed genes for Sham Brd4 KO versus Sham control are highlighted (red= up-regulated, blue= down-regulated). Upon Brd4 deletion, sarcomere composition and Ca²⁺ handling is modulated which leads to activation of signaling pathways associated with cardiac remodeling such as hypertrophy, fibrosis, and heart failure. ACE1= angiotensin I-converting enzyme; ACTC1= actin; ACTG1= actin beta/gamma 1; DAG= dystroglycan 1; DHPR= voltage-dependent calcium channel; DMD= dystrophin; IGF-1= insulin-like growth factor 1; IL6= interleukin 6; ITG= integrin; MYBPC3= myosin-binding protein C; MYH6= myosin heavy chain 6; MYH7= myosin heavy chain 7; Myl2= myosin regulatory light chain 2; Myl3= myosin light chain 3; NCX= solute carrier family 8 (sodium/calcium exchanger); PRKA= AMP-activated protein kinase; RyR= ryanodine receptor 2; SERCA2a= ATPase sarcoplasmic/endoplasmic reticulum Ca²⁺ transporting 2; SGC= sarcoglycan; TGF- β = transforming growth factor beta-1; TnC= troponin C; TNF- α = tumor necrosis factor superfamily, member 2; TnI= troponin I; TnT= troponin T.

3.4.9 BRD4 depletion blunts the response to TAC-induced cardiac stress

The basal effects of *in vivo* *Brd4* depletion from cardiomyocytes as well as underlying biological processes have already been elaborated and revealed wide expression changes mainly associated with energy metabolism and cardiac muscle contraction that in turn most likely lead to the development of HCM. Subsequently, the impact of *Brd4* KO on stress response was analyzed using our mRNA sequencing data.

The comparison of DEGs for TAC control (2063 genes), TAC *Brd4* KO (3882 genes), and Sham *Brd4* KO (2901 genes) all versus Sham control ($p_{adj} < 0.05$, $\log_2FC \pm 0.5$) showed 1011 genes common for all three groups (**Figure 3.33A**). This intersect included e.g. cardiac stress and remodeling markers such as *Nppa*, *Nppb*, *Acta1*, *Rcan1*, *Ctgf*, *Il6*, and *Myh7*, which were significantly increased in all three groups in comparison to Sham control ($p_{adj} < 0.05$, $\log_2FC \pm 0.5$), although Sham *Brd4* KO showed slightly lower expression than the TAC groups (**Figure 3.33B**). Additional differential expression analyses were performed to enable the identification of genes differently regulated in TAC control and TAC *Brd4* KO animals as well as to describe transcriptional changes in *Brd4* KO mic in response to cardiac stress. For TAC control versus TAC *Brd4* KO 2121 DEGs (926 up, dark red; 1195 down, dark blue) were detected (**Figure 3.33C**), whereas for Sham *Brd4* KO and TAC *Brd4* KO only 34 DEGs (19 up, dark red; 15 down, dark blue) were identified ($p_{adj} < 0.05$, $\log_2FC \pm 0.5$) (**Figure 3.33D**). KEGG pathway analysis of the 2121 DEGs between both TAC groups identified 42 enriched pathways that were manually assigned to the respective KEGG orthology categories. Thus, 21 metabolic pathways (blue), 10 pathways associated with organismal systems (green), 8 associated with human diseases (orange), and 3 associated with other KEGG categories (black) ($p_{adj} < 0.05$, $FDR < 0.05$) were detected. In contrast, the 34 DEGs from the comparison of *Brd4* KO mice after Sham versus TAC showed no enrichment (**Figure 3.33E**). These analyses showed only marginal transcriptional changes after TAC in *Brd4* KO hearts, but a wide range of differentially expressed genes mainly associated with metabolism and human diseases between TAC *Brd4* KO and TAC control.

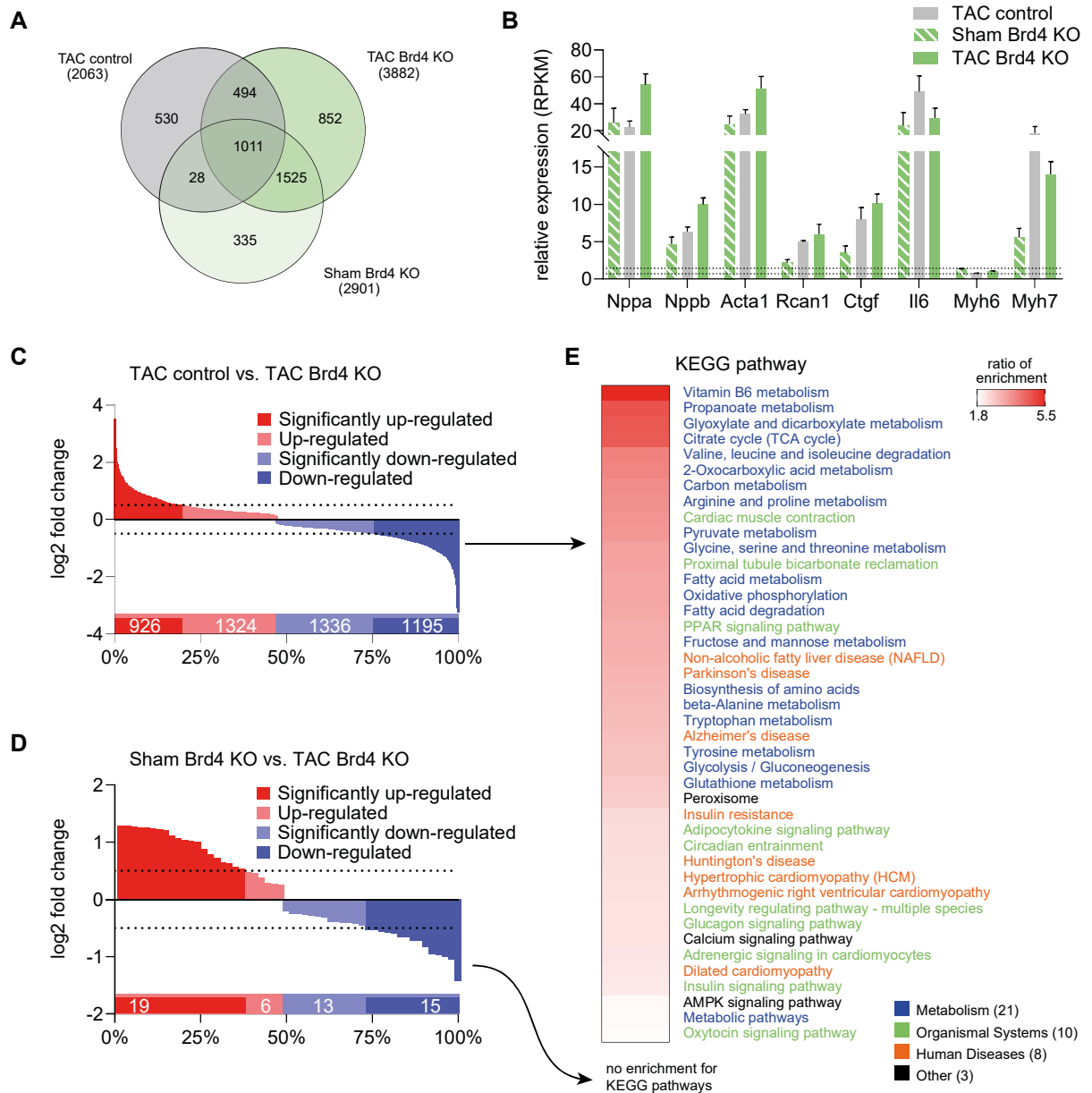


Figure 3.33: Brd4 KO hearts show marginal transcriptional changes after TAC, but a wide range of genes associated with metabolism and human diseases is differentially expressed between TAC Brd4 KO and TAC control.

Overlap for DEGs ($p_{adj} < 0.05$, $\log_2FC \pm 0.5$) in TAC control (2063 genes) and TAC Brd4 KO (3882 genes) and Sham Brd4 KO (2901 genes), all versus Sham control (**A**). Relative expression of cardiac stress and remodeling markers is increased after TAC and after Brd4 depletion. Based on RPKM normalized to Sham control. Error bars indicate SEM (**B**). Differential expression analysis revealed 2121 DEGs (926 up, dark red; 1195 down, dark blue) between TAC control and TAC Brd4 KO (**C**) and 34 DEGs (19 up, dark red; 15 down, dark blue) between Sham Brd4 KO and TAC Brd4 KO at a cutoff of $p_{adj} < 0.05$ and $\log_2FC \pm 0.5$. X-axis indicates number and percent of total DEG (**D**). KEGG pathway analysis ($p_{adj} < 0.05$, $FDR < 0.05$) with TAC Brd4 KO DEGs from (**C**) shows enrichment for 21 metabolic pathways (blue), 10 pathways associated with organismal systems (green), 8 associated with human diseases (orange), and 3 associated with other KEGG categories (black). The 34 DEGs from the comparison of Sham Brd4 KO to TAC Brd4 KO from (**D**) showed no enrichment for KEGG pathways ($p_{adj} < 0.05$, $FDR < 0.05$) (**E**).

Finally, for a more precise description of Brd4 KO specific gene regulation, the resulting DEGs from six differential expression analyses were compared with a Venn diagram to identify subsets of genes. For further examination three clusters of genes were picked that are regulated only upon Brd4 deletion and independent of the surgery (Cluster #1), differentially regulated in Brd4 KO mice in comparison to TAC control (Cluster #2), and regulated in TAC control but not affected by Brd4 KO (Cluster #3) (**Figure 3.34A**). Cluster #3 resulted in 176 genes regulated only in the TAC control group but did not show significant enrichment for any GO terms. I have identified 163 differentially regulated DEGs in Cluster #2, which showed an enrichment for biological processes such as ion transport, membrane repolarization, and muscle contraction. In Cluster #1 742 Brd4 KO exclusive DEGs were detected that showed an enrichment for mitochondrial membrane organization and metabolism (**Figure 3.34**). A subsequent pathway analysis revealed that Brd4 KO altered the energy metabolism, the response to mechanical stimulus, and cardiac muscle contraction (**Appendix Figure 5.4**) suggesting that BRD4 is important for the regulation of those processes in cardiomyocytes. These results demonstrate that BRD4 mostly affects energy metabolism and membrane repolarization and thus plays a crucial role in cardiac muscle contraction and heart function in general.

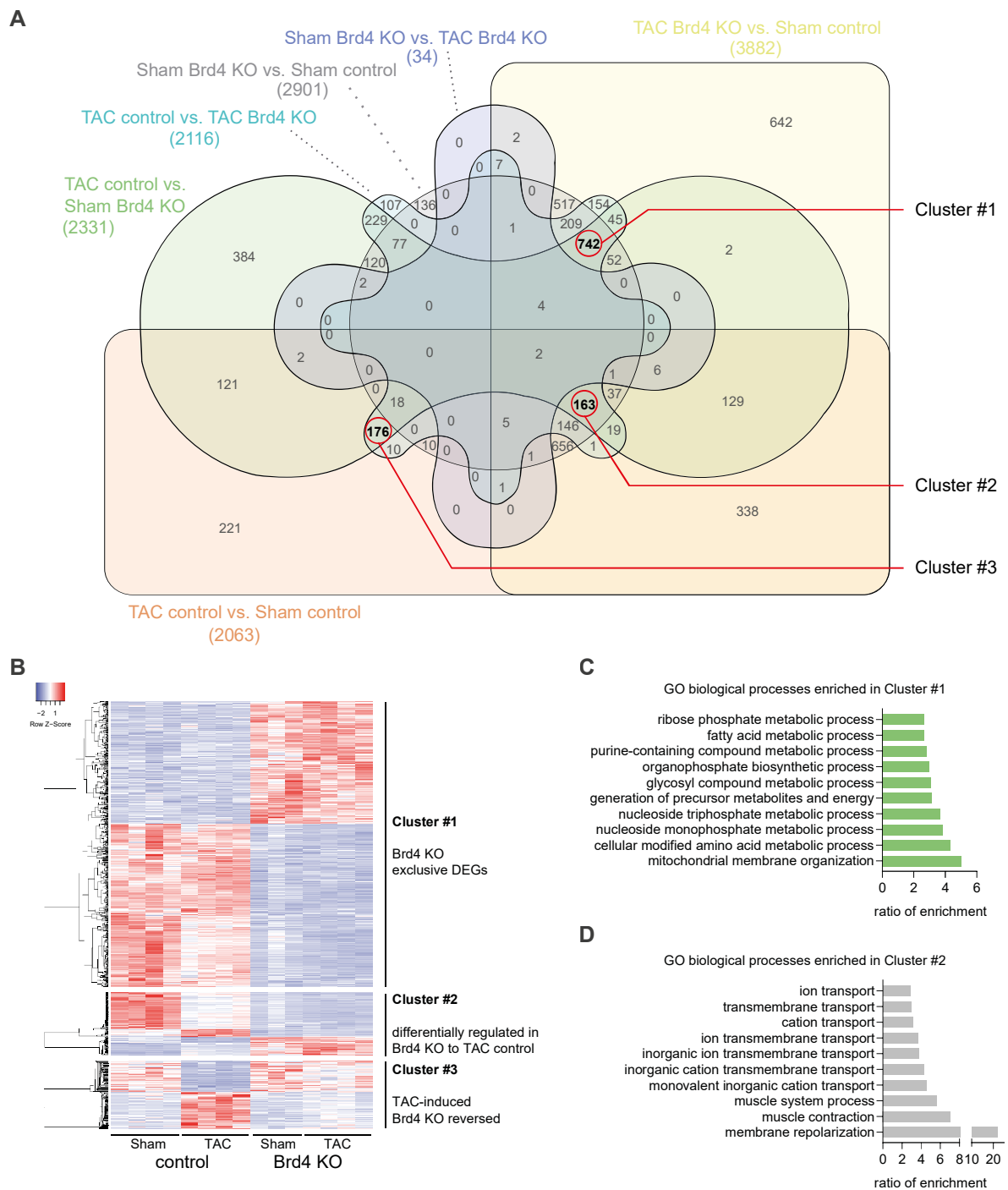


Figure 3.34: Deletion of Brd4 mostly affects energy metabolism and membrane repolarization. Overlap for DEGs ($\text{padj} < 0.05$, $\log_2\text{FC} \pm 0.5$) from all 6 possible comparisons for the 4 sequencing groups Sham control, TAC control, Sham Brd4 KO, and TAC Brd4 KO. Three subgroups of DEGs are highlighted: Brd4 KO exclusive DEGs (Cluster #1), DEGs differentially regulated in Brd4 KO and TAC control (Cluster #2), and TAC-regulated and Brd4 KO reversed DEGs (Cluster #3) (A). A heatmap of the three DEG clusters depicted in (A) was clustered via centroid linkage with Pearson method (B). Overrepresentation analysis (ORA) of gene ontology (GO) terms of biological processes for 742 significantly regulated genes in Cluster #1 (A-B) showed enrichment in mitochondrial membrane organization and metabolic processes ($\text{padj} < 0.05$, $\text{FDR} < 0.05$, Top10 sorted according to ratio of enrichment) (C). ORA of GO terms of biological processes for 163 significantly regulated genes in Cluster #2 (A-B) showed enrichment in ion transport, membrane repolarization, and muscle contraction ($\text{padj} < 0.05$, $\text{FDR} < 0.05$, Top10 sorted according to ratio of enrichment) (D).

4 Discussion

Heart failure (HF) is a multifactorial disease with a high prevalence and poor prognosis and therefore poses a socioeconomic burden for the whole population. It is the leading cause of hospitalizations and healthcare expenditures, which are predicted to double by the year 2030 (Heidenreich et al. 2013). ACE inhibitors and β -blockers are used for over 20 years to treat HF, but novel therapeutic strategies are needed as morbidity and mortality are still unacceptably high. Despite classical gene regulation by transcription factors, hemodynamic and hormonal stress can be implemented by epigenetic mechanisms like chromatin remodeling and acetylation to drive pathologic changes of the heart (Lee et al. 2017). The chromatin readers of the Bromo- and extraterminal domain (BET) protein family recognize acetylated histone residues associated with active transcription (Filippakopoulos et al. 2010). The small molecule JQ1 was shown to displace those readers from chromatin, to prevent pathologic cardiac remodeling, and to preserve heart function when applied in a mouse transverse aortic constriction (TAC) induced pressure-overload model (PO) (Anand et al. 2013; Spiltoir et al. 2013). In conclusion, BET proteins have been reported to control pathological cardiac hypertrophy (Spiltoir et al. 2013) by mediating transcriptional pause release in heart failure (Anand et al. 2013). But it remains elusive if JQ1 improves the outcome of PO, if it directly or indirectly affects the heart and what the individual functions of particular BET members are, as JQ1 is administered systemically and was shown to inhibit all proteins of the BET family.

To help elucidate the individual roles of particular BET members in cardiac cells I first described their expression in the healthy and diseased adult mouse heart to validate and complement previous findings. Second, I examined the survival of JQ1 treated mice after TAC to test if BET inhibition does lead to an improved outcome after PO. Next, I used conditional alleles from our group to generate mice with cardiomyocyte specific knockout of *Brd2* and *Brd4*, respectively. After validation and characterization of the newly generated mice, I investigated how these animals respond to TAC-induced PO and if they are protected from maladaptive cardiac remodeling as described for BET inhibition by JQ1.

4.1 Expression of BET members in the healthy and diseased heart

To characterize the basal expression of BET protein members in the healthy murine heart transcriptome analysis and immunoblotting using left ventricles of adult wildtype mice (FVB/N) was performed. Cardiac expression of *Brd2*, *Brd3*, and *Brd4* was confirmed but in contrast to literature (Anand et al. 2013), *Brd2* showed 4-fold higher mRNA levels than *Brd3* and *Brd4*, respectively (**Figure 3.1A**). Human transcriptome data support these findings (Khadjeh, unpublished results). For all further experiments of this project I decided to focus on two BET

members, *Brd2* as the highest expressed member in the heart, and *Brd4* as the most interesting candidate in non-cardiac analyses.

Immunocytochemistry confirmed that *Brd2* (Spiltoir et al. 2013) and *Brd4* (Anand et al. 2013; Spiltoir et al. 2013) are translated in cardiomyocytes and the proteins localized in the nucleus (**Figure 3.1B-C**). Using left ventricular total protein from adult mice for immunoblotting, BRD2 was detected at about 110 kDa. As BRD4 shows low abundance in cardiac total protein (data not shown), subcellular protein fractions were obtained from left ventricle (2.2.8). BRD4 was detected at 100 kDa in the nuclear fraction and at 125 kDa in chromatin-bound protein (**Figure 3.1C**). The higher molecular weight in the chromatin fraction is probably due to phosphorylation that has previously been described to act as trigger for the targeting of BRD4 to chromatin (Wu et al. 2013; Shu et al. 2016). These results confirm previous reports (Anand et al. 2013; Spiltoir et al. 2013) of BET expression in the murine heart as well as the nuclear localization of BRD2 and BRD4 but in contrast to the literature not *Brd4* (Anand et al. 2013) but *Brd2* shows strongest cardiac expression.

Moreover, to check if and how BET proteins are regulated upon PO induction, gene expression and protein levels were analyzed. Gene expression analyses showed that mRNA levels of *Brd2*, *Brd3*, and *Brd4* are not regulated by TAC-induced hemodynamic stress (**Figure 3.2A**). However, RT-qPCR showed a significant prevalence for the short *Brd4* isoform in the Sham group but a net shift towards the long isoform after TAC (**Figure 3.2E**). Immunoblotting supports the induction of the presumably long isoform of BRD4 after TAC. BRD2 protein levels, however, are not altered after the induction of PO. These results are in contrast to the previously reported TAC-mediated decrease of BRD2 and increase of BRD4 protein levels (Spiltoir et al. 2013; Haldar and McKinsey 2014), although the published whole blots show multiple (>9) unspecific protein bands that compromise the author's conclusions.

Nevertheless, there are some experimental differences that make direct comparisons of both studies difficult. In this study left ventricle from female FVB/N mice eight weeks after Sham or TAC surgery were used, whereas Spiltoir and colleagues examined left ventricles from male mice of the BL6/J strain four weeks after surgeries. Possible explanations for the differences might be sexual dimorphic gene expression (Isensee et al. 2008) or influence of the genetic background (Barnabei et al. 2010). Another explanation might be differential BET expression at different stages during disease progression as in my hands mice show advanced pathologic remodeling with signs of HF by 4-5 weeks and manifested HF by 8 weeks following TAC.

However, my finding on the TAC-induced expression of the long *Brd4* isoform can be complemented with functional data from a previous study. Schröder and colleagues showed that the short BRD4 associates with an inactive P-TEFb complex containing HEXIM1 and 7SK snRNA and that the long BRD4 can activate P-TEFb by blocking its interaction with HEXIM1-7SK (Schröder et al. 2012). Thus, the BRD4-dependent activation of pathologic gene

expression in cardiac remodeling and HF (Anand et al. 2013; Spiltoir et al. 2013; Haldar and McKinsey 2014) might be mediated by stress-induced isoform shift from short to long *Brd4* with the according binding of active P-TEFb. Indeed, HEXIM1 has already been suggested as endogenous inhibitor of hypertrophy (Haldar and McKinsey 2014) but has not been linked to BRD4 isoforms so far.

4.2 Cardio protective effects of JQ1 could not be reproduced

BET bromodomain inhibition by JQ1 has been described to protect the murine heart from pathologic cardiac remodeling and to preserve ventricular function after TAC (Anand et al. 2013; Spiltoir et al. 2013) and was described as an effective treatment for preestablished HF, more recently (Duan et al. 2017). But it was not reported if BET inhibition does also improve the prognosis after PO induction. Beside cardio protective properties, the final proof for an effective treatment of HF would be an improved outcome. To investigate if BET inhibition could decrease the TAC-mediated mortality, eight weeks old female mice of the C57BL/6N inbred strain were subjected to TAC or Sham and treated with JQ1 (50 mg/kg/day vs. vehicle control) daily for four weeks, beginning one day after surgery. The consistency of all TAC surgeries was demonstrated by comparable pressure gradients across the aortic constriction (**Figure 3.4**). Survival analysis revealed that BET inhibition does not improve the outcome of TAC-induced PO as JQ1 and vehicle treated animals showed comparable mortality after TAC (**Figure 3.4**). JQ1 treated mice showed pathologic cardiomegaly, myocardial expression of cardiac stress marker genes (**Figure 3.5**), and cardiomyocyte hypertrophy (**Figure 3.6**) after TAC. Moreover, echocardiography showed TAC-dependent systolic dysfunction, ventricular dilation, and wall thickening in JQ1 treated animals (**Figure 3.7**). The pathologic changes were comparable in JQ1 and vehicle treated mice, four and eight weeks after TAC. The only difference between the treatment groups was the significantly lower wall thickness four weeks after TAC in the JQ1 group, which was still significantly higher than in Sham control. These results contradict previous reports on cardio protective effects of JQ1 in the mouse PO model (Anand et al. 2013; Spiltoir et al. 2013; Duan et al. 2017).

To further evaluate my findings and to validate JQ1-mediated BET inhibition, I analyzed the left ventricular gene expression profiles of vehicle or JQ1-treated animals 4 weeks after TAC via mRNA sequencing. After differential expression analysis to Sham vehicle and subtraction of differentially expressed genes (DEGs) from TAC vehicle, I found JQ1-dependent expression of genes involved in biological processes such as immune system development, cell activation, mitotic cell cycle, and cell division (**Figure 3.8C**). Pathway analysis further confirmed the influence of JQ1 on the immune response and cell cycle, but in addition revealed an effect on ECM, sarcolemma, and muscle contraction (**Figure 3.9**). Direct comparison of TAC vehicle to TAC JQ1 sequencing data revealed only 19 DEGs (cutoff $\text{padj} < 0.05$, $\log_2\text{FC} \pm 0.5$) that are

mostly involved in immune response (**Figure 3.8D**). These findings are consistent with previous reports of BRD4 being involved in cell cycle regulation (Dey et al. 2009; Filippakopoulos et al. 2010), proliferation (Houzelstein et al. 2002), immune cell differentiation (Cheung et al. 2017a; Cheung et al. 2017b), and inflammation (Duan et al. 2017).

Moreover, gene set enrichment analysis (GSEA) of TAC vehicle and TAC JQ1 showed a positive enrichment for ribonucleoprotein complex formation involved in splicing, RNA processing, and translation (**Appendix Figure 5.3A**). This is in line with previous reports of BRD4 regulating stress-induced splicing (Hussong et al. 2017) and miRNA processing (Suzuki et al. 2017) and suggests that BRD4 might be important for the response to metabolic and oxidative stress in the heart, although in this study no phenotypic or functional differences were observed after JQ1-treatment.

Due to the controversies between this study and findings from Anand and colleagues we re-analyzed the deposited microarray data of mice that received JQ1 or vehicle for 28 days after TAC surgery (Anand et al. 2013) and specifically screened for DEGs, which were differentially regulated in the treatment groups. Of the 391 TAC-induced and JQ1-reversed genes from Anand's study 142 were differentially expressed in our data but not differentially regulated upon vehicle or JQ1 treatment (**Figure 3.10**). In addition, typical marker genes of cardiac remodeling are expressed in TAC vehicle and TAC JQ1 alike. Overall, these findings are consistent with our morphometric and functional data but contradict previous reports of JQ1-mediated cardio-protection after TAC (Anand et al. 2013; Spiltoir et al. 2013).

To confirm successful BET inhibition, the expression of BET inhibition biomarkers known from cancer research such as *Hexim1*, *Serpini1*, *Zcchc24*, *Zmynd8* (Lin et al. 2017), *Myc*, *Ccr2*, *CD180* (Yeh et al. 2017), or *Bcl2* (Hogg et al. 2016) was examined but none of the genes were differentially expressed in TAC JQ1 animals four weeks after surgery (data not shown). It is likely that BET proteins have tissue specific targets, which might explain why none of the described biomarkers were regulated in our cardiac samples. Nevertheless, it cannot be fully excluded that our batch of JQ1 might have been decomposed despite special attention to storage, handling, and preparation according to the instructions from the Bradner lab. Future studies could repeatedly analyze the compounds integrity or collect blood samples for serum level measurements to ensure the proper quality and delivery of JQ1.

As this study was not explicitly designed for direct comparison to previous work, the experimental setup shows some differences that might partially attribute to the contrary results. While I investigated female mice of the inbred strain C57BL/6N, Spiltoir, Anand, Duan and colleagues used male mice of the C57BL/6J strain (Anand et al. 2013; Spiltoir et al. 2013; Duan et al. 2017). Several studies describe the genetic background of mouse models as confounding factor in cardiovascular research (Barnabei et al. 2010; Garcia-Menendez et al. 2013; Simon et al. 2013). Comparison of C57BL/6 sub-strains revealed that e.g. blood

pressure and heart weight normalized to tibia length are significantly higher in healthy C57BL/6J than in C57BL/6N mice but did not detect any basal structural or functional differences by echocardiography (Simon et al. 2013). More importantly in context of this study, C57BL/6N mice were reported to show significantly lower survival and cardiac function but increased heart weight, lung weight, and *Nppb* levels after TAC when compared with C57BL/6J (Garcia-Menendez et al. 2013). In addition, sex-specific differences in cardiac gene expression such as elevated *Nppb* levels (2.7-fold) in female mice have been described, although older animals were examined in that study (Isensee et al. 2008). Furthermore, in this study mice were subjected to TAC at the age of 8 to 9 weeks, not at 10-12 (Anand et al. 2013) or 10 to 11 weeks (Duan et al. 2017). Although age, sex, or genetic background might alter pathogenesis or the sensitivity to pharmaceuticals such as BET inhibitors, it seems unlikely that these factors could entirely prevent the previously published strong cardioprotective effects of JQ1.

Another explanation for the conflicting results might be the overall experimental variability of TAC, which together with a low number of replicates might lead to statistical artefacts. TAC surgeries in this work and previous studies on BET protein members in the heart (Anand et al. 2013; Spiltoir et al. 2013; Duan et al. 2017) were performed according to the most common procedure originally described by Rockman and colleagues. Thus, by tying a ligature around the transverse aorta and a 27 G needle as spacer and carefully removing the needle, the aorta is constrained to the diameter of the needle and a gaged aortic stenosis is produced (Rockman et al. 1991). Following TAC, mice show a significant aortic gradient and develop concentric hypertrophy within one to two weeks (Rockman et al. 1991; deAlmeida et al. 2010). However, this technique has two major downsides. First, the same spacer (27 G) is used for constriction regardless of the sex, body weight and aortic dimensions of the animals, thus, causing variability in the degree of constriction among individual animals (Merino et al. 2018). Secondly, the tightness of the ligature has an influence on the degree of constriction as well (Merino et al. 2018). Both factors introduce a significant variability into resulting pressure gradients and the development of cardiac hypertrophy. Therefore, it is crucial to report pressure gradients for possibly all animals included in further analysis to assure successful and consistent TACs, especially if this could falsify the working hypothesis. This is the major shortcoming of previous studies that report cardio protective effects of BET inhibition by JQ1, of which only Anand and colleagues (Anand et al. 2013) reported pressure gradients for four animals per group. Conversely, in this study I report pressure gradients for all JQ1 or vehicle-treated animals following Sham (n=7-17) or TAC (n=29-39) surgery.

Moreover, beside factors such as anesthesia (Roth et al. 2002), sex, age, and bodyweight, echocardiographic analysis is subject to intra- and inter-observer as well as technical variability (Donner et al. 2018; Lindsey et al. 2018). Interventions such as TAC further increase this variability due to differences in surgical performance as well as the disease progression of

individual animals. Using echocardiographic data from our previous studies for power calculations, I determined a sample size of fourteen (n=14) animals to allow a sufficient statistical power for the mouse PO model (**Appendix Figure 5.1**). Consequently, I report echocardiographic data for 6-17 Sham and 20-24 TAC animals 4 weeks after surgery treated either with vehicle or JQ1, whereas previous studies reported data for seven (Duan et al. 2017), six to ten (Spiltoir et al. 2013), and ten animals (Anand et al. 2013) after surgeries.

A future comparative study on BET inhibition by JQ1 after PO in age-matched male and female mice of C57BL/6/N and C57BL/J strains could address these conflicting results and possibly neglect or confirm sex-specific or genetic differences in the cardiac function of BETs.

4.3 Functional analysis of Brd2 and Brd4 in the murine heart

The previously reported cardio-protective effects of BET inhibition by JQ1 after PO were not confirmed but also not disproved in this study as it cannot be excluded that experimental differences such as age, sex, and genetic background might lead to discrepant results. To evaluate the potential of BET proteins as targets for HF treatment and to overcome the limits of systemic and simultaneous inhibition of all BET members, it is necessary to further dissect the functions of particular BET proteins specifically in cardiac cells. In this work, I used two murine conditional BET alleles, *Brd2^{fllox}* and *Brd4^{fllox}*, which were previously generated in our group (Eva Benito, unpublished), to induce Cre-mediated recombination in cardiomyocytes and to analyze the respective loss of *Brd2* and *Brd4* function *in vivo*.

4.3.1 Generation of mice with cardiomyocyte-specific deletion of the first bromodomain of BRD2

Breeding of mice carrying our conditional *Brd2* allele with mice of the α MHC-Cre line, which express a constitutively active Cre recombinase exclusively in cardiomyocytes (Agah et al. 1997), resulted in progeny with a genomic deletion of *Brd2* exons three and four (**Figure 3.11**). All mice bred normally, and the litters showed Mendelian genotype distribution. Cre-positive mice homozygous for the mutant allele are viable. The deletion of exons three and four does not lead to the intended nonsense-mediated decay but to the expression of a truncated *Brd2* mRNA (**Figure 3.12**). Sequence data and immunoblotting strongly suggest that exon 2 of the truncated mRNA is omitted leading to in-frame translation from an internal start codon downstream of the region encoding for the first bromodomain (**Figure 3.13**). Therefore, the Cre-mediated deletion of exons three and four generated a mutant allele of *Brd2* that expresses a truncated BRD2 protein lacking the first bromodomain (BRD2 Δ BDI).

Several studies reported gene targeting approaches using the CRISPR/Cas9 (Kapahnke et al. 2016; Mou et al. 2017; Sharpe and Cooper 2017) or the Cre/loxP system (Yang et al. 2009) to produce mRNAs that express a residual protein through exon skipping rather than the intended

knockout allele. Interestingly, this has also been described for the BET protein member *Brdt*. In the attempt to produce a null allele of the testis specific *Brdt* in mouse, Shang and colleagues deleted exons two, three, and four and generated a mutant allele that expresses a truncated BRDT protein lacking the first bromodomain (BDI). This accidental deletion allowed the first functional analysis of an individual BET bromodomain *in vivo* and demonstrated that BRDT-BDI is necessary for sperm differentiation as male mice homozygous for this mutant *Brdt* allele produce fewer and abnormal sperm, thus, becoming infertile (Shang et al. 2007).

Distinct functions of the two bromodomains of BET proteins were later reported in various other studies. For example, it was shown that BRD3 directly interacts with the acetylated hematopoietic transcription factor GATA binding factor 1 (GATA1) via its BDI and that this interaction is essential for the recruitment of GATA1 to its target sites on the chromatin as demonstrated by BET inhibition via GW841819X (Gamsjaeger et al. 2011; Lamonica et al. 2011). In a different study, Shi and colleagues reported individual functions for the BRD4 bromodomains, with BDI binding to acetylated histone 4 residues and BDII linked to di-acetylated transcription factor Twist. The BRD4-Twist complex controls WNT5A expression in breast cancer, and BET inhibitors JQ1 and MS417 were demonstrated to dissociate this complex and to suppress tumorigenicity (Shi et al. 2014).

With the development of more specific molecules that selectively inhibit individual BET bromodomains, the therapeutic value of BET inhibition increases. Furthermore, these BET inhibitors of the 'second generation' help to further establish distinct roles for BDI and BDII. Olinone, a BET BDI inhibitor, was described to induce the differentiation of oligodendrocytes, whereas inhibition of both BET bromodomains had an opposite effect (Gacias et al. 2014). The small molecule RVX-208 selectively inhibits BET BDII (Picaud et al. 2013), is currently in phase III clinical trials for treating atherosclerotic cardiovascular disease, and was linked to the decrease of major adverse cardiac events (Gilham et al. 2016).

In contrast to BRD3, BRD4, and BRDT, functional information for BRD2 bromodomains is sparse, although BRD2 was described to couple histone acetylation to transcription (LeRoy et al. 2008). In particular, BRD2 was shown to recognize acetylated H4 tails via its BDI (Nakamura et al. 2007; Filippakopoulos et al. 2010; Umehara et al. 2010; Filippakopoulos et al. 2012) and to recruit proteins such as E2F and HDACs to chromatin (Houzelstein et al. 2002; Fu et al. 2015). Based on the reported link between BRD2-BDI and transcription, I decided to further characterize the newly generated *Brd2 Δ BDI* mice to examine morphologic and functional consequences upon the loss of the first bromodomain of BRD2 in the healthy adult heart and after induction of PO.

4.3.2 Heart development, function and remodeling are independent from the first bromodomain of BRD2

The newly generated Brd2 Δ BDI mice were used to examine the functional role of the first bromodomain of *Brd2* in cardiomyocytes regarding heart development, morphology, function, and its response to TAC-induced PO. Homozygous Brd2 Δ BDI mice are viable, have normal sized hearts and cardiomyocytes and do not show any defects or abnormalities of the heart by the age of 3 months. Further, echocardiography revealed normal heart dimensions and systolic function with three and six months but a slightly increased left ventricular diameter in six months old animals (**Figure 3.14**). These findings suggest that the development of the murine heart as well as its size, shape, and function are independent from the first bromodomain of BRD2. Conversely, BRD2 might be substituted with BRD2 Δ BDI or other proteins to maintain its possible, if any, functions in cardiomyocytes. Future studies could examine and compare the chromatin occupation of BRD2 and BRD2 Δ BDI by e.g. chromatin immunoprecipitation and subsequent sequencing to clarify if the first bromodomain is needed to bind specific BRD2 target regions in cardiomyocytes.

However, Brd2 Δ BDI and cre control mice mostly died by the age of 45 to 50 weeks (data not shown). In addition, histology revealed the formation of degenerative vacuoles in cardiomyocytes of six months old animals in both groups (**Figure 3.14B**). Such vacuoles have been linked to cardiotoxicity (An et al. 2017) and are probably due to chronic Cre-recombinase activity. Cre-dependent cardiotoxicity has been previously described (Davis et al. 2012) and was also shown to cause mortality (Bersell et al. 2013). The cardiotoxic effect is dependent on Cre recombinase levels in the nucleus as well as on the duration of its nuclear localization (Bersell et al. 2013; Lexow et al. 2013), and is probably due to Cre off-target activity at cryptic loxP sites in the genome (Loonstra et al. 2001, Semprini et al. 2007).

I further investigated if the first bromodomain of *Brd2* contributes to cardiac remodeling in response to PO. Therefore, eight to ten weeks old Brd2 Δ BDI mice were subjected to TAC, analyzed by echocardiography five weeks after surgery, and either sacrificed for subsequent histological and molecular testing or monitored for their survival for up to 120 days after surgery. Five weeks after PO induction Brd2 Δ BDI animals showed pathologic hypertrophy and systolic dysfunction without any significant differences to the Cre-negative littermates and the cre control group (**Figure 3.17 and Figure 3.18**). Brd2 Δ BDI mice showed TAC-induced cardiac stress marker expression with *Nppa* levels being significantly higher compared to TAC control (**Figure 3.17 and Figure 3.18**). These findings suggest BRD2-BDI to be dispensable for the response to hemodynamic stress and for the according morphologic and functional changes of the heart. Based on the elevated *Nppa* levels one might speculate that Brd2 Δ BDI possibly regulates *Nppa* expression but this needs further investigation. Furthermore, TAC-dependent mortality was higher in Brd2 Δ BDI and cre control animals (**Figure 3.16**). Based on previous

reports and my own observations discussed before, the increased mortality is likely a Cre-dependent effect. This is a limitation I did not expect and that could be overcome in future studies by using an inducible Cre-line to reduce nuclear Cre levels or by using a CRISPR/Cas9 mediated gene targeting approach.

The deletion of the first BRD2 bromodomain did not elicit phenotypic changes neither in the healthy heart nor after PO induction, although chromatin acetylation in general has previously been shown to play an important role in the development of HF (Bucks and Olson 2006) and as BRD2 was demonstrated to bind e.g. acetylated lysine 12 on histone 4 (H4K12ac) (Kanno et al. 2004). Chromatin binding has been especially linked to the first bromodomain of BRD2 as it was shown to form homodimers and to recognize H4K12ac in the context of H4K8ac, which binds a cavity at the dimer interface of BRD2-BDI (Umehara et al. 2010). In addition, the first bromodomain of BRD2 was shown to bind a tetra-acetylated H4 peptide at lysins 5, 8, 12, and 16 with a 10-fold higher affinity than the second bromodomain of BRD2 and, thus, Brd2-BDI was proposed to be responsible for the recognition of H4 tails (Filippakopoulos et al. 2012). Consequently, the mutant BRD2 Δ BDI described in this work is probably unable to recognize and bind acetylated chromatin but it might maintain specific functions of the second bromodomain such as scaffolding of enhancer complexes. Such function can be derived from a recent study in T helper 17 cells. Cheung and colleagues nicely demonstrated that BRD2 supports enhancer assembly at *cis*-regulatory elements by binding to acetylated signal transducer and activator of transcription 3 (STAT3) via its second bromodomain (Cheung et al. 2017b). It is possible that the second bromodomain is sufficient for the heart-specific function of BRD2.

Altogether, my findings suggest that proper heart development, normal heart function, and cardiac remodeling in response to hemodynamic stress are independent from the first bromodomain of BRD2. This was unexpected as CaMKIIa-Cre-mediated targeting of our conditional *Brd2* allele and, thus, hippocampal BRD2 Δ BDI expression was shown to have a strong effect on cognition by impairing spatial learning (Eva Benito, unpublished). These differences indicate tissue-specific functions for individual BET bromodomains and might have therapeutic potential. With the development of novel BET inhibitors, selective targeting of particular BET bromodomains became available and could be used specifically in the context of a given disease and target tissue. This work suggests that the first bromodomain of BRD2 might not be a promising therapeutic target for cardiac hypertrophy and HF and, consequently, that therapeutic use of BET-BDI inhibitors for non-cardiac diseases possibly has no adverse effects on cardiomyocytes, at least in the context of *Brd2*. To further evaluate *Brd2* as potential therapeutic target, future studies could investigate its role in more detail by using a null allele or by deleting the second bromodomain in cardiac cells. Maybe this would partially resemble the reported cardio-protective effects of JQ1 administration, as it was shown to have a

three-fold higher affinity to the second of the two BRD2 bromodomains (Filippakopoulos et al. 2010).

4.3.3 Successful generation of cardiomyocyte-specific *Brd4* knockout mice

JQ1-dependent BET inhibition was described to prevent features of pathologic cardiac remodeling such as the activation of stress-induced transcription, pathologic hypertrophy, interstitial fibrosis, and systolic dysfunction after pressure overload (PO). This led to the hypothesis that BET proteins promote HF by co-activation of target genes in response to pathologic stress in the heart (Haldar and McKinsey 2014).

However, JQ1 acts systemically and simultaneously inhibits all BET members and thus does not allow precise conclusions on the function of particular BET members in a certain tissue- or cell-type. To challenge the proposed HF promoting function of BET proteins and to overcome limitations of previous studies, my aim was to examine the loss-of-function of *Brd4* in cardiomyocytes *in vivo* and especially after induction of PO using a genetic approach. This work presents the first *in vivo* insight into the function of *Brd4* in cardiomyocytes and its consequences on heart development, function, and on pathologic cardiac remodeling.

At the beginning of this thesis, no conditional *Brd4* allele was available, but recently two groups reported independent generation of such alleles in mouse. Lee and colleagues generated two conditional *Brd4* alleles by flanking exon three or exon five with two loxP sites, respectively, and used the resulting mice to disrupt *Brd4* in adipocytes and myocytes. *Brd4* deficient mice died after birth and showed severe reduction of brown adipose tissue and muscle mass. In subsequent analyses, *Brd4* was shown to bind active enhancers and to control differentiation of adipocytes but to be dispensable in maintaining terminally differentiated adipose tissue (Lee et al. 2017). Bao and colleagues targeted exon three to deplete *Brd4* in myeloid-lineage cells and found *Brd4* to modulate the innate immune response (Bao et al. 2017).

However, in order to allow the examination of *Brd4* functions *in vivo*, our group generated mice carrying a *Brd4^{fl/fl}* allele. To disrupt *Brd4* function in cardiomyocytes, mice carrying our conditional *Brd4* allele with floxed exons six and seven were crossed to aMHC-Cre mice (Agah et al. 1997), which express a constitutively active Cre recombinase from early embryonic development throughout the animals lifespan (Davis et al. 2012). Mice with a heterozygous *Brd4* knockout in cardiomyocytes were viable and showed no cardiac defects (data not shown). This suggests that a single copy of *Brd4* is sufficient for its cardiac function and is consistent with previous reports that did not observe any cardiac phenotype in mice with a heterozygous global *Brd4* knockout (Houzelstein et al. 2002). However, progeny of the F2 generation showed non-Mendelian genotype distribution as only one out of almost 100 pups was Cre-positive and carried two copies of the floxed allele (Cre⁺ ; *Brd4^{fl/fl}*) (**Figure 3.19**) but died prematurely at postnatal week six. This suggests embryonic lethality upon homozygous *Brd4* deletion in cardiomyocytes and is consistent with observations in mouse embryos with a global

homozygous *Brd4* knockout that died shortly after implantation at about embryonic day 5.5 (E5.5) (Houzelstein et al. 2002; Gyuris et al. 2009).

The heart is the first organ formed during organogenesis and the main steps of its development are the establishment of the cardiac mesoderm at E7.5, the development of the heart tube at E8, looping of the heart at E8.5, the formation of the heart chambers at E10.8, and the formation of the four-chambered heart at E14.5 (Nandi and Mishra 2015). Impaired expression of genes involved in cardiac differentiation and development leads to fetal heart failure, cardiac arrest and *in-utero* death by E14.5 (Nandi and Mishra 2015). The dysregulation of genes crucial for proper cardiogenesis after deletion of *Brd4* is the most likely explanation for the observed embryonic lethality as BRD4 has been previously described to be essential for cell differentiation (Houzelstein et al. 2002; Lee et al. 2017). The birth of the only Cre⁺ ; *Brd4*^{fl/fl} mouse might be due to later onset of Cre-expression, incomplete Cre-dependent recombination during embryogenesis or an unknown genetic factor. The role of *Brd4* in cardiogenesis has not been further examined as this work focused on BET protein function in the adult heart.

Therefore, the Tamoxifen-inducible α MHC-MerCreMer mouse line (Sohal et al. 2001) was used to allow *Brd4* disruption at a later timepoint (**Figure 3.20**). Lexow and colleagues previously demonstrated that Tamoxifen itself has no effect in MerCreMer-negative animals and that cytosolic MerCreMer alone is not toxic (Lexow et al. 2013). However, MerCreMer translocation into the nucleus and, thus, activity increases dependent on the dose of Tamoxifen and may induce cardiomyocyte apoptosis, myocardial fibrosis, and cardiac dysfunction (Bersell et al. 2013). To achieve efficient Cre-mediated recombination on one hand but to minimize cardiotoxic effects of nuclear Cre recombinase on the other hand, Tamoxifen has been administered at the previously proposed optimal concentration of 30 mg/kg/day on three consecutive days (Bersell et al. 2013). Tamoxifen administration caused 10-20% mortality within the first two weeks after injection (data not shown), which is a known limitation of the inducible Cre-loxP-system and has been previously described as a loxP independent DNA damage response that leads to myocardial dysfunction and death (Bersell et al. 2013). However, the remaining Tamoxifen-induced animals were viable and lived for over one year. Further, to account for this acute mortality and to allow the reversion of any transient effects of Tamoxifen-induced MerCreMer activation (Higashi et al. 2009; Hougen et al. 2010) animals were administered to Tamoxifen at postnatal week five and thus at least three weeks prior to further interventions or measurements.

The breeding of mice carrying our conditional *Brd4* allele to α MHC-MerCreMer mice resulted in progeny with Mendelian genotype frequencies. All mice hetero- or homozygous for the conditional *Brd4* allele and positive for the inducible Cre recombinase were viable and bred normally suggesting that no transient or spontaneous Cre activity occurred. Tamoxifen-

induced MerCreMer-mediated deletion of exons 6 and 7 of *Brd4* led to an extremely significant depletion of *Brd4* mRNA (**Figure 3.21**) demonstrating the successful knockout of *Brd4* in cardiomyocytes. However, *Brd4* knockout could not be demonstrated on protein level. Western blot analysis showed no BRD4 reduction in left ventricular protein fractions, whereas nuclear protein from isolated cardiomyocytes of Brd4 KO animals showed only a slight reduction of BRD4 protein levels (**Figure 3.22**). This might be due to limitations such as the overall low abundance of BRD4 in the heart, BRD4 from residual non-cardiomyocytes in nuclear protein from isolated cardiomyocytes, and residual BRD4 expression in 10-20% of cardiomyocytes without Cre-mediated recombination. The western blot conditions and, thus, the proof of BRD4 depletion might be improved in the future by optimizing the purity of isolated cardiomyocytes or performing immune precipitation prior to western blotting.

Nevertheless, the extremely decreased *Brd4* mRNA levels in cardiomyocytes demonstrate successful and complete *Brd4* disruption and were convincing enough to proceed with the first *in vivo* study of Brd4 *loss-of-function* in the mouse heart.

4.3.4 BRD4 is necessary to suppress hypertrophic genes in the healthy heart

The newly generated Brd4 KO mice were characterized using morphometric and echocardiographic methods, to investigate if the loss of *Brd4* in cardiomyocytes alters cardiac morphology or function, and, thus, to determine if *Brd4* is involved in maintaining the adult heart. The deletion of *Brd4* was induced by tamoxifen injection at postnatal week five. The resulting knockout mice were viable and usually lived for more than 12 months. Brd4 KO mice showed left ventricular wall thickening, increased left ventricular to body weight ratios, and increased cardiomyocyte diameters in three and six months old animals, whereas left ventricles were non-dilated (**Figure 3.23 -Figure 3.24**). However, the systolic function of Brd4 KO, which is presented as ejection fraction (EF), was not altered in comparison to controls. Furthermore, echocardiographic examination of tamoxifen-induced MerCreMer+ control animals demonstrated that the left ventricular wall thickening in Brd4 KO mice is not attributed to tamoxifen or Cre-activity (**Figure 3.24**). Thus, mice lacking BRD4 in cardiomyocytes develop a basal concentric hypertrophy with preserved ejection fraction and no adverse effect on survival.

These findings suggest a basal growth-regulating function for BRD4 in the adult heart. On the one hand, this is consistent with previous studies that demonstrated the association of BRD4 with enhancer and promoter regions of pro-hypertrophic genes (Anand et al. 2013; Spiltoir et al. 2013; Haldar and McKinsey 2014; Duan et al. 2017). On the other hand, these studies proposed BRD4-dependent transcriptional activation of pro-hypertrophic genes in response to cardiac stress, whereas my data suggest a basal suppression of hypertrophy genes by BRD4. Together these findings point towards two distinct roles of BRD4 in the heart, a basal negative regulation of pro-hypertrophic genes and a stress-induced activation of pathologic gene

expression that might be implemented by a shift from the short to the long BRD4 isoform upon cardiac stress as previously discussed (4.1).

A basal negative regulation of target genes in the healthy heart might be conveyed through recruitment of transcriptional repressors by BRD4 as recently reported in pancreatic cells, in which a complex of the Euchromatic Histone Lysine Methyltransferase 2 (EHMT2) with BRD4 represses autophagy and lysosome genes (Sakamaki et al. 2017). Furthermore, the short isoform of BRD4 has been described to co-repress HIV transcription through interaction with SWI/SNF nucleosome remodelers (Conrad et al. 2017). Very recently, Lambert and colleagues also reported a repressive function of BRD4 possibly through interaction with negative transcriptional regulators such as nucleosome remodeling and deacetylase (NuRD) or negative elongation factor (NELF) (Lambert et al. 2018).

In the heart, a basal negative regulatory BRD4 function is further supported by molecular and histologic analyses of Sham Brd4 KO mice, which showed that the disruption of *Brd4* in cardiomyocytes leads to the basal expression of cardiac stress markers (**Figure 3.27C**) and the development of a mild fibrosis (**Figure 3.29**). In addition, transcriptome analysis revealed that Brd4 KO leads to differential expression of a wide range of genes involved in biological processes such as cell cycle, ECM organization, energy metabolism, oxidative phosphorylation, cardiac muscle contraction, and dilated cardiomyopathy (**Figure 3.31**). Consistent with these findings, BRD4 was demonstrated to bind promoters of genes involved in mitochondrial bioenergetics and oxidative phosphorylation *in vitro* using human cytoplasmic hybrid cells (Barrow et al. 2016). In contrast to this work, Barrow and colleagues demonstrated the induction of the according genes upon *Brd4* depletion, but the difference might be due to tissue-specific function of BRD4. Moreover, Brd4 KO mice show the reactivation of fetal genes such as the fetal myosin heavy chain 7 (*Myh7*), atrial natriuretic peptide (*Nppa*), or actin alpha 1 (*Acta1*) (**Figure 3.31E**), which are common markers for cardiac remodeling and hypertrophy (Hill and Olson 2008; van Berlo et al. 2013; Nakamura and Sadoshima 2018).

Nevertheless, it remains unclear which factors activate the transcription of *Brd4* target genes in Brd4 KO mice. One can speculate that the remaining BET members BRD2 and BRD3 occupy BRD4 binding sites in its absence and promote transcription of the *Brd4* target genes. Indeed, no left ventricular wall thickening or cardiomyocyte hypertrophy was observed after displacement of all BET members from chromatin by JQ1 in Sham animals neither in this work nor in previous studies (Anand et al. 2013; Duan et al. 2017). A future study could address this open question by JQ1 administration in Brd4 KO mice to test if BET inhibition might rescue the basal concentric hypertrophy phenotype.

Furthermore, pathway analysis of the Sham Brd4 KO expression data showed regulation of genes encoding for sarcomere proteins (*Myh7*, *Mybpc3*, *Tnnt2*, *Tnni3*, *Actc1*) and ion channels involved in membrane repolarization (**Figure 3.32**), which might lead to increased Ca^{2+}

sensitivity of myofilaments, abnormal Ca^{2+} levels and an energy deficit (Fatkin and Graham 2002). The analysis further revealed altered expression of integrins, intermediate filaments (Dystrophin and Desmin) as well as the activation of factors like IGF-1, TGF- β , TNF- α , and IL-6. Such dysregulation might lead to left ventricular diastolic dysfunction, hypertrophy and eventually to heart failure (Fatkin and Graham 2002).

Altogether, the observed Brd4 KO effects in the adult murine heart resemble characteristics of hypertrophic cardiomyopathy (HCM). HCM is an inheritable cardiac condition that is characterized by concentric hypertrophy of the left ventricle without any stimulant pressure or volume overload, a non-dilated left ventricle, and normal or increased ejection fraction (Marian and Braunwald 2017). HCM is caused by mutations in genes encoding sarcomere proteins and is mostly inherited (Marian and Roberts 1998; Marian and Braunwald 2017). However, HCM shows a broad spectrum of phenotypic expression even in patients with mutations in the same gene, which is likely due to differences in genetic background and epigenetic factors (Marian 2002; Zhao et al. 2015; Marian and Braunwald 2017). As the Brd4 KO mouse presented in this work develops basal HCM without any known sarcomeric mutation, one could speculate that a certain sarcomere protein composition or expression of certain isoforms might induce HCM. Therefore, our Brd4 KO mice could be used in future studies to identify specific factors that drive development or lead to phenotypic variations of HCM.

An example for another mouse that spontaneously develops a concentric hypertrophy is the mitogen-activated protein kinase kinase 1 (MEK1) transgenic mouse, which expresses an activated form of MEK1 under the control of the α -MHC promoter. The MEK1 mouse was reported to sustain the hypertrophic phenotype with increased heart function, and survival for over 12 months, and to show increased *Nppa*, *Nppb*, *Actc1* as well as *Myh7* mRNA levels (Bueno et al. 2000). In contrast to our Brd4 KO mouse, however, MEK1 does not show signs of interstitial fibrosis. Nevertheless, it is possible that the deletion of *Brd4* somehow leads to activation of the MEK1-ERK1/2 pathway, which in turn might drive the development of a concentric hypertrophy observed in Brd4 KO animals. This possible explanation could be examined in the future by e.g. immunoblotting and quantification of total and phosphorylated ERK.

4.3.5 *Brd4* is necessary for the PO-induced remodeling and hypertrophy

I further investigated if *Brd4* depletion from cardiomyocytes influences cardiac remodeling in response to PO to challenge previous findings on cardio protective effects of JQ1-mediated BET inhibition (Anand et al. 2013; Spiltoir et al. 2013). Therefore, eight to ten weeks old Brd4 KO mice were subjected to TAC, analyzed by echocardiography one and five weeks after surgery and either sacrificed for subsequent histological and molecular testing or received another echo 10 weeks after surgery and were monitored for their survival for up to 180 days (Figure 3.25).

Consistent with the basal characterization, BRD4 KO mice subjected to Sham showed concentric hypertrophy but, in addition, significantly higher *Nppa* levels (**Figure 3.27**) and mild interstitial fibrosis (**Figure 3.29**) when compared to Sham control. In comparison, five weeks after TAC Brd4 KO and control mice showed no significant differences in *Nppa/Nppb* levels, cardiomyocyte diameters, and fibrosis although hearts of control animals were significantly larger (**Figure 3.27**). However, Brd4KO mice showed significantly higher mortality within the first 40 days after TAC (**Figure 3.26**). Nevertheless, heart function seems to be partially preserved in surviving Brd4 KO animals after PO or progression of HF slowed as ejection fraction decrease was not as dramatic as in the control group (**Figure 3.30**). These findings demonstrate that Brd4 KO animals have a limited capacity for cardiac remodeling after PO as well as a decreased compensatory potential in the acute phase after TAC. This suggests that *Brd4* is necessary for the response to hemodynamic stress, which is consistent with previous reports (Anand et al. 2013; Spiltoir et al. 2013).

Interestingly, similar observations were reported for the chromatin remodeling protein Brg1, which plays an important role in gene regulation, differentiation and growth of cardiac cells in embryos (Hang et al. 2010). Brg1 is silenced in adults but gets re-expressed upon cardiac stress to drive hypertrophy and isoform switch from adult (*Myh6*) to embryonic myosin heavy chain (*Myh7*) in complex with HDAC and poly (ADP ribose) polymerase (PARP) (Hang et al. 2010). However, a knockout of Brg1 prevents hypertrophy and the myosin isoform switch demonstrating that Brg1 is essential for the response to cardiac stress (Hang et al. 2010). In comparison to Brd4 KO, depletion of Brg1 shows no basal cardiac phenotype (Hang et al. 2010).

HCM is associated with diastolic dysfunction, arrhythmias, and even sudden cardiac death (Marian and Braunwald 2017), which might be possible explanations for the increased TAC-mediated mortality of Brd4 KO animals. Diastolic dysfunction is manifested by left ventricular stiffening due to thickened ventricular walls with interstitial fibrosis, which leads to decreased left ventricular relaxation reducing the ventricle's ability to fill with blood and contributes to the development of heart failure with preserved ejection fraction (HFpEF) (LeWinter and Meyer 2013; Marian and Braunwald 2017). As Brd4 KO mice show a basal concentric hypertrophy and interstitial fibrosis, the development of a diastolic dysfunction is likely. This could be validated by measuring the left ventricular pressure and -volume via cardiac catheterization (Zhang et al. 2015) in future experiments. Furthermore, cellular disarray that occurs in the damaged heart can disrupt the normal electrical conduction in the heart and lead to arrhythmias, which in turn can cause sudden cardiac death (Farza and Watkins 1999; Marian and Braunwald 2017). Electrocardiography (ECG) could be performed to analyze if Brd4 KO mice show heart rate variability or arrhythmias. The surgical implantation of ECG telemeters is a well-established method for long-term echocardiogram recording in ambulatory mice and can be

used to monitor multiple mice over several weeks (McCauley and Wehrens 2010). Both cardiac catheterization and implantation of ECG telemeters are additional interventions that have to be approved by the authorities and will be conducted thereafter to examine the causes of increased TAC-mediated mortality of Brd4 KO animals in the future.

Consistent with previous observations, mRNA sequencing of Brd4 KO hearts showed that BRD4 controls genes associated with cardiac remodeling. However, in contrast to the reported stress-induced activation, my findings suggest that BRD4 suppresses these genes in the healthy adult murine heart (**Figure 3.31E**). Those opposing functions do not have to be mutually exclusive but rather point towards two distinct roles of *Brd4*, one in the healthy and the other in the stressed heart.

To further examine the effect of cardiomyocyte-specific Brd4 disruption on stress-response, DEGs from the comparison of TAC Brd4 KO and TAC vehicle mice were used for KEGG pathway analysis. The analysis for TAC Brd4 KO specific DEGs revealed an enrichment of genes associated with metabolism, cellular respiration, and various human diseases such as HCM, dilated cardiomyopathy, Parkinson's, Alzheimer's, and Huntington's disease (**Figure 3.33D**), which share features such as mitochondrial dysfunction, oxidative stress, endoplasmic reticulum stress as well as immune response. These findings show that *Brd4* depletion leads to metabolic remodeling, deficient energy metabolism, production of reactive oxygen species, and inflammation, which are known to promote pathologic hypertrophy, fibrosis, and heart failure (Nakamura and Sadoshima 2018).

Interestingly, at our cutoff ($\text{padj} < 0.05$, $\log_2\text{FC} \pm 0.5$) only 34 genes were differentially expressed in Brd4 KO mice after TAC versus Sham and showed no enrichment for KEGG pathways (**Figure 3.33C**). This shows that gene expression of BRD4 KO mice is mostly unaffected by TAC-induced stress and vice versa suggests that BRD4 is essential for the response to such cardiac stress, although basal remodeling is already induced by the *Brd4* disruption itself (**Figure 3.31E**). This is consistent with our experimental results as histologic, morphometric, and echocardiographic analyses showed only slight differences between Brd4 KO mice after Sham or TAC surgery (**3.4.5 - 3.4.7**).

Furthermore, I identified genes that are regulated only upon Brd4 deletion and independent of the surgery and found them associated with mitochondrial membrane organization (**Figure 3.34**), energy metabolism, the response to mechanical stimulus, and cardiac muscle contraction (**Appendix Figure 5.4**) suggesting that BRD4 regulates these processes in cardiomyocytes. Moreover, analysis of genes differentially regulated in Brd4 KO mice in comparison to TAC control showed their involvement in biological processes such as ion transport, membrane repolarization, and muscle contraction (**Figure 3.34**). This is consistent with the observed HCM phenotype, which can be induced by impairments in the sarcomere composition, Ca^{2+} handling, and ATP production (Marian 2002; Marian and Braunwald 2017).

Future studies could compare my transcriptome data to the chromatin occupation of BRD4 in order to determine if the observed expression changes are due to direct regulation by BRD4 or rather secondary effects. Moreover, ATAC (Assay for Transposase-Accessible Chromatin) sequencing (Buenrostro et al. 2015) could be performed to analyze if the overall chromatin structure in Brd4 KO mice is changed.

The here described genetic approach was used to investigate the functions of individual BET members specifically in cardiomyocytes to challenge findings of cardio-protective effects previously described with systemic BET inhibition. However, the comparison of findings from my Brd4 KO experiments to JQ1-mediated BET inhibition is limited. Beside the intended cell-specificity and targeting of one BET member at a time, the general difference between depletion and inhibition as well as the different timepoints of knockout induction and reported BET inhibition need to be considered. Recently Winter and colleagues demonstrated that in contrast to BET inhibition, BET degradation by a small-molecule degrader of BET family proteins (dBET6) impairs the assembly of a transcription elongation complex without affecting CDK9 recruitment. This study proposed BET proteins as master regulators of productive transcription elongation (Winter et al. 2017). The different effects might be due to BET functions apart from chromatin such as competitive interactions with nuclear factors that are lost after degradation but remain with BET inhibitors or by residual chromatin-binding despite inhibition. Furthermore, the here presented Cre-mediated Brd4 knockout was induced three weeks before TAC, whereas BET protein inhibition via JQ1 started one day after TAC in previous studies.

These different timepoints for loss or inhibition of *Brd4* function might lead to distinct effects after PO. As an example, inhibition of the long non-coding RNA cardiac hypertrophy associated epigenetic regulator (*Chaer1*), which is necessary for the development of cardiac hypertrophy, was shown to attenuate cardiac hypertrophy and dysfunction when performed before but not after PO (Wang et al. 2016). To investigate the influence of timing on the effect of *Brd4* deletion, the Cre-mediated recombination could be induced after the onset of PO in future studies and compared to this work.

4.4 Conclusions

To complement existing data on cardiac effects after BET inhibition I have analyzed the survival of JQ1-treated mice after TAC but could not find any significant difference to vehicle treated animals. Indeed, the previously described cardio-protective effects could not be reproduced in this work, possibly due to factors such as gender and genetic background of the examined mice. Therefore, further investigation is needed for clarification.

Next, to explore the potential of targeting BET proteins as treatment of HF and to overcome limitations of previous studies on BET inhibition, I investigated the loss of the first bromodomain

of Brd2 and the complete loss of Brd4 in cardiomyocytes in healthy mice as well as after induction of PO. The deletion of the first bromodomain of *Brd2* did not elicit any substantial phenotype during development, in the adult heart, or after induction of pressure overload leading to the conclusion that the first bromodomain of BRD2 or the full length BRD2 is not essential in murine cardiomyocytes. These findings are relevant in regard to therapeutic BET inhibition, as directed inhibition of the first BET bromodomain in a non-cardiac context most probably would not affect cardiac cells in terms of BRD2 function.

However, a cardiomyocyte-specific knockout of *Brd4* was lethal if induced during early embryonic development but a knockout during adolescence led to the development of a hypertrophic cardiomyopathy (HCM) with the animals surviving for over twelve months. In conclusion, BRD4 is essential during cardiac development and necessary for negative regulation of genes promoting cardiac remodeling and hypertrophy in differentiated cardiomyocytes. Furthermore, Brd4 KO mice showed an increased mortality within the first four weeks after TAC, which is most likely due to diastolic dysfunction, arrhythmias, and sudden cardiac death common for HCM. Nevertheless, surviving Brd4 KO mice showed better heart function than TAC control animals, which might point towards some cardio-protective effect of cardiomyocyte-specific *Brd4* depletion. In addition, cardiac stress had almost no impact on gene expression as only 34 DEGs were detected ($p_{adj} < 0.05$, $\log_2FC \pm 0.5$) for Brd4 KO mice after TAC compared to Sham (**Figure 3.33C**). A likely explanation based on previous reports of BRD4 being integral for the response to hemodynamic stress (Anand et al. 2013; Spiltoir et al. 2013; Haldar and McKinsey 2014) is that our Brd4 KO mice lose the ability to integrate such stress due to the absence of BRD4 from cardiomyocytes. A second, more speculative, explanation might be that a BRD4-independent response to TAC is somehow blunted or inhibited due to Brd4 KO mediated expression changes preceding the surgery such as the induction of HCM.

Based on the findings of this thesis complemented with relevant literature I propose two distinct cardiac functions for BRD4: first, the negative regulation of e.g. pro-hypertrophic genes in the healthy heart and, second, the activation of pro-hypertrophic and other pathologic genes after pressure overload (**Figure 4.1**). BRD4 has recently been proposed as co-repressor in non-cardiac tissues and cells (Conrad et al. 2017; Sakamaki et al. 2017; Lambert et al. 2018) but the underlying mechanisms remain elusive. The dual BRD4 function could be mediated by its interaction with negative transcriptional regulators such as EHMT2 (Sakamaki et al. 2017), NuRD (Lambert et al. 2018), SWI/SNF nucleosome remodelers (Conrad et al. 2017) or with positive transcriptional regulators like P-TEFb (Jang et al. 2005; Yang et al. 2005, p. 200). The functional shift could also be mediated by the switch from the short BRD4 to its long isoform after stress-induction as demonstrated in **3.1.2** hence enabling interaction with either an inactive or active P-TEFb complex (**Figure 4.1**) (Schröder et al. 2012).

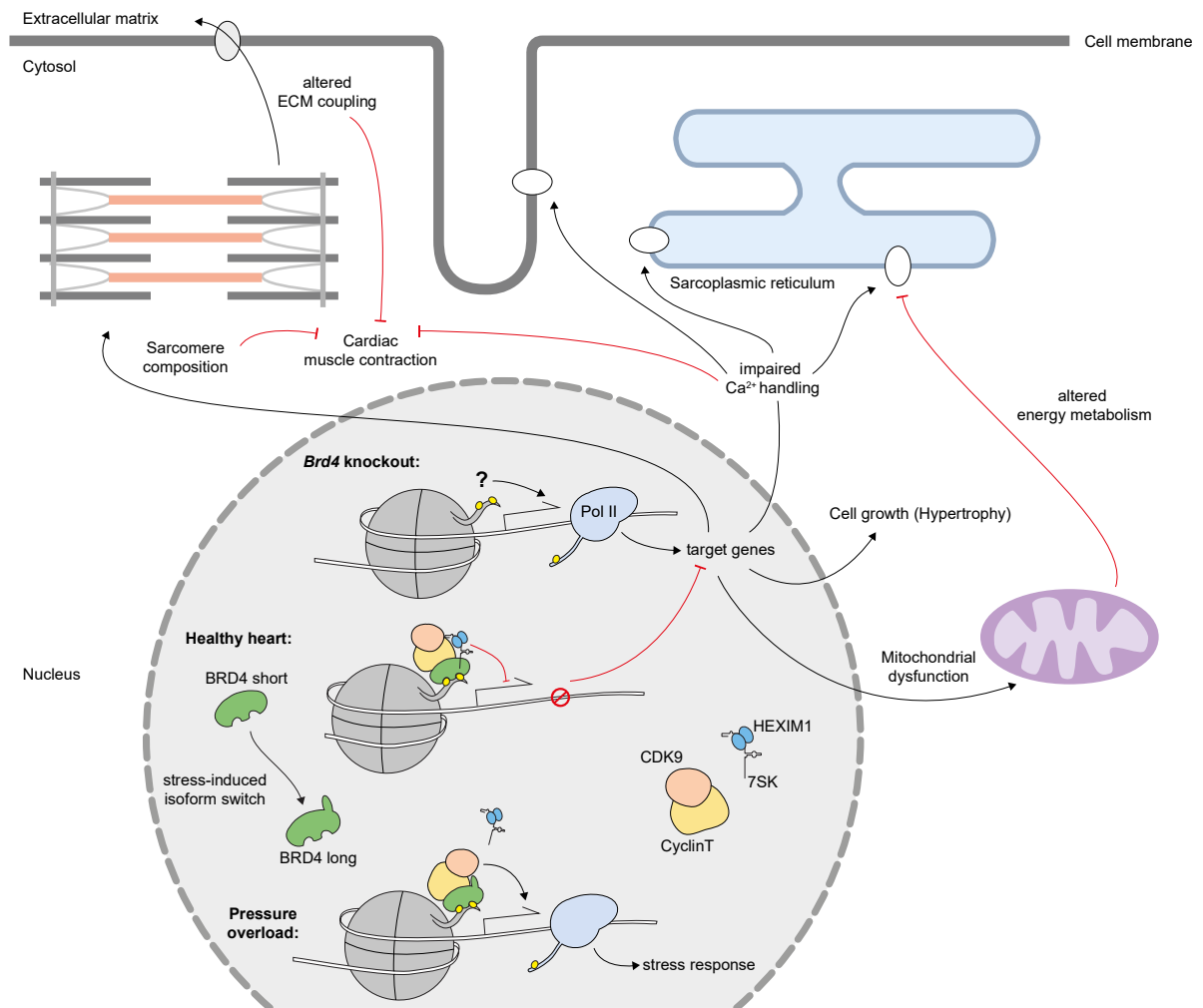


Figure 4.1: A model of BRD4 function in cardiomyocytes including relevant literature.

BRD4 has possibly two distinct functions in cardiomyocytes of the adult murine heart. After pressure overload BRD4 and active P-TEFb (CDK9, CyclinT) induce transcription of the stress response gene program. Findings from this work suggest that in the healthy heart BRD4 co-represses target genes involved in energy metabolism, Ca^{2+} handling, cardiac muscle contraction, ECM coupling, and cell growth as the knockout of *Brd4* leads to their induction. In its absence BRD4 target genes get probably activated by another chromatin reader or a different mechanism. The negative gene regulation might be mediated through chromatin occupation by BRD4 in interaction with e.g. an inactive P-TEFb (HEXIM1-7SK-bound) complex or other negative transcriptional regulators. However, the functional shift from transcriptional repression to activation upon pressure overload could be mediated by a stress-induced isoform switch from short to long BRD4, which prevents the association of the inhibitory HEXIM1-7SK complex to P-TEFb thus promoting the transcription of stress response genes.

Although the underlying mechanisms must be elucidated in future studies, my findings underscore the therapeutic potential of BRD4 for heart failure and depending on the condition might allow two distinct strategies. As the knockout of *Brd4* induced HCM in healthy mice it would be interesting to test if e.g. an AAV-mediated overexpression of the short BRD4 isoform would rescue the phenotype in these mice. If successful, this approach could be tested in an independent HCM model. Furthermore, I concluded that the stress response might be mediated by the long BRD4 isoform. To challenge this hypothesis and to test if an isoform shift could be therapeutically exploited, the long but not the short BRD4 isoform could be silenced in mice that underwent TAC surgery.

5 Appendix

Table 5.1: LV M-Mode – Calculation Definitions

Name	Description	Units	Formula
LV Vol;d	Left ventricle volume diastole	μl	$((7.0 / 2.4 + \text{LVID;d}) * \text{LVID;d}^3)$
LV Vol;s	Left ventricle volume systole	μl	$((7.0 / 2.4 + \text{LVID;s}) * \text{LVID;s}^3)$
%EF	LV ejection fraction	%	$100 * ((\text{LV Vol;d} - \text{LV Vol;s}) / \text{LV Vol;d})$
%FS	LV Fractional Shortening	%	$100 * ((\text{LVID;d} - \text{LVID;s}) / \text{LVID;d})$
LV Mass	LV Mass Uncorrected	mg	$1.053 * ((\text{LVID;d} + \text{PWTh;d} + \text{AWTh;d})^3 - \text{LVID;d}^3)$
LV Mass Cor	LV Mass corrected	mg	$\text{LV Mass} * 0.8$
LV-W/BW	LV weight to bodyweight	mg/g	$\text{LV Mass} / \text{body weight}$

(adapted from Vevo instruction manual)

Table 5.2: ImageJ script - Minimal Fiber diameter

```

1. run("Gaussian Weighted Median", "radius=2");
2. run("Subtract Background...", "rolling=15 sliding");
3. run("Enhance Contrast...", "saturated=0.01 normalize");
4. run("Threshold Regional Gradient", "circularity=0.3 minimum=300 maximum=15000 fill_phase fill_detected method=Fast");
5. run("Adjustable Watershed", "tolerance=5");
6. run("BinaryDilateNoMerge4 ", "iterations=3 white");
7. run("Invert");
8. run("Dilate");
9. run("Invert");
10. run("Fill Holes");
11. run("Analyze Particles...", "size=50-Infinity circularity=0.30-1.00 show=Outlines display exclude add");

```

Table 5.3: ImageJ script – Fibrotic area

```

1. run("RGB Stack");
2. run("Next Slice [>]");
3. run("Next Slice [>]");
4. run("Auto Threshold", "method=Minimum");
5. run("Measure");
6. run("Previous Slice [<]");
7. run("Auto Threshold", "method=MaxEntropy");
8. run("Measure");

```

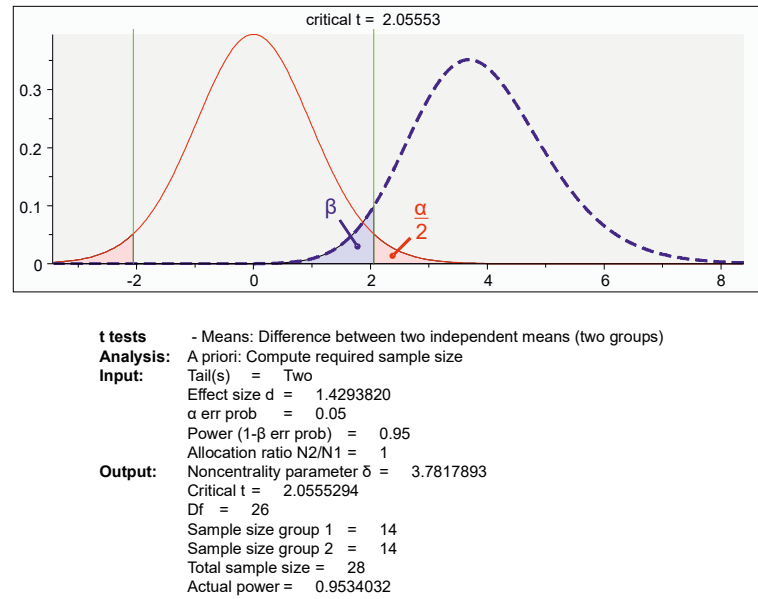


Figure 5.1: Power calculation to determine sample size for animal experiments.

Distribution plot generated with G*Power (v. 3.1.9.2) (Faul et al. 2007) using the depicted parameters for calculation. Effect size was calculated as Cohen's d (Cohen 1988) using previous ejection fraction (%) data from our laboratory: Sham= 50 ± 8 , TAC= 35 ± 12.5

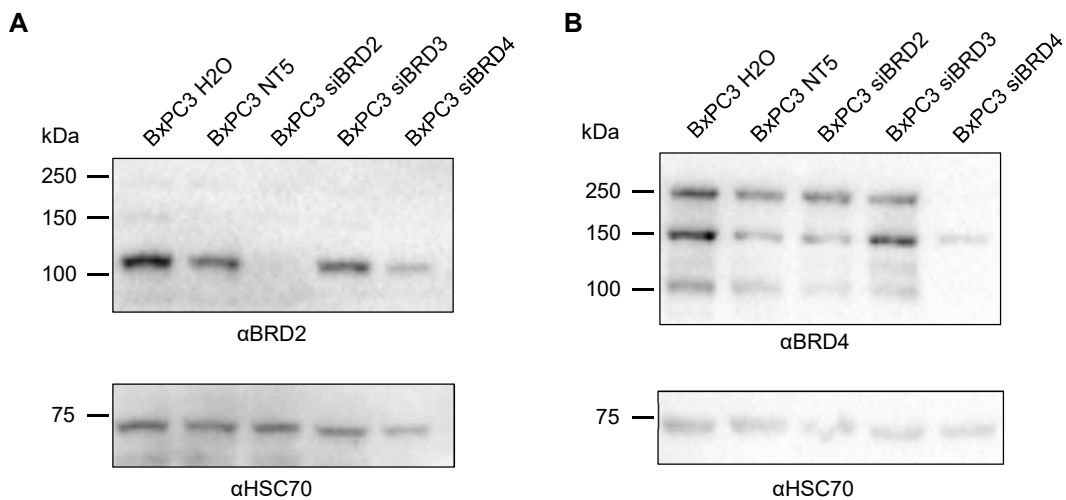


Figure 5.2: Knockdown validation of the BRD2 and BRD4 antibodies used in this thesis.

Protein from wildtype human pancreatic cancer cell line BxPC3 was compared to that of cells after gene silencing of *Brd2*, *Brd3*, or *Brd4* by immunoblotting against BRD2 (**A**) or BRD4 (**B**). Western blot analysis and figures in A-B were performed and kindly provided by Ana Kutschat and Feda Hamdan (Johnsen lab).

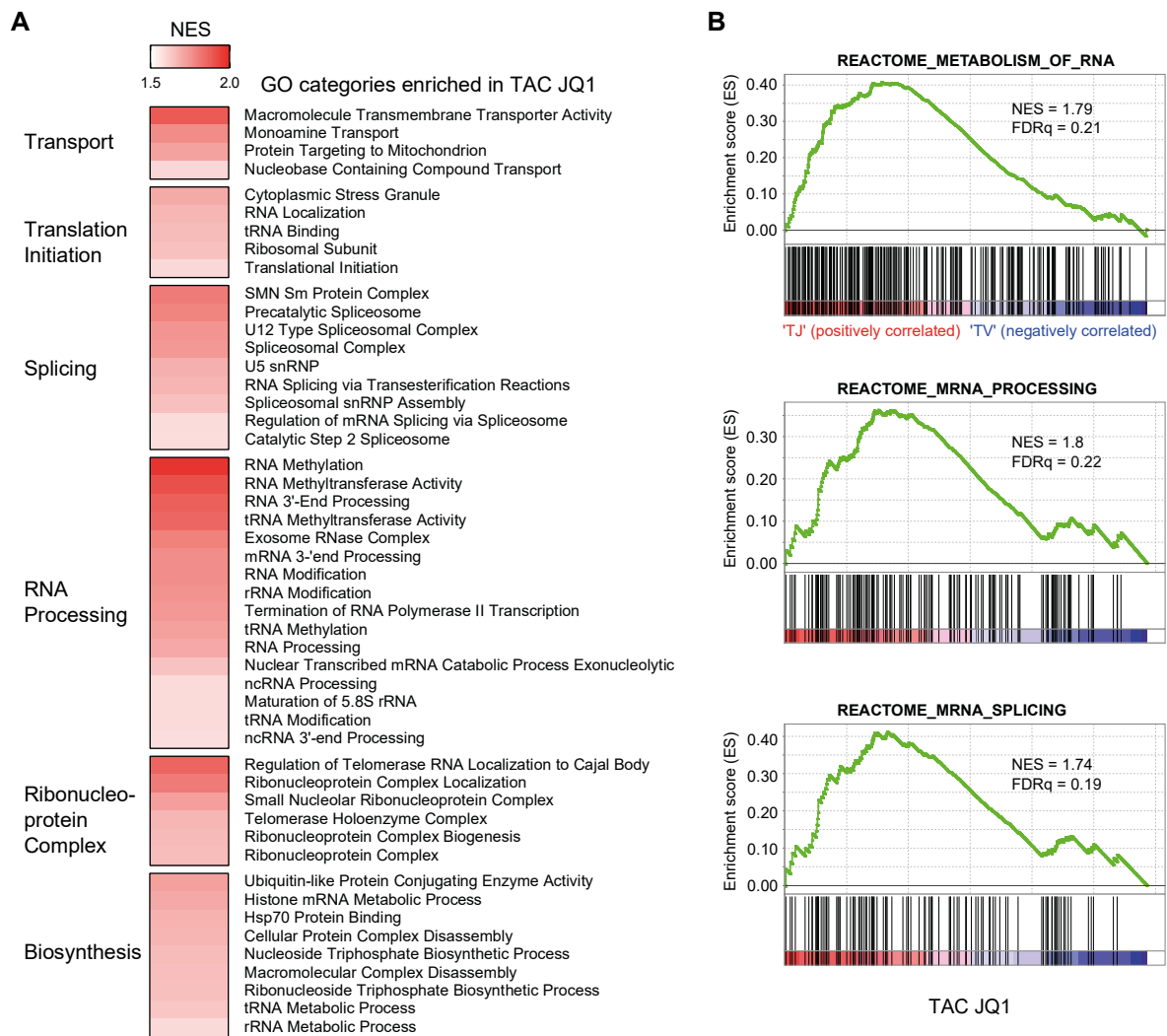


Figure 5.3: Gene set enrichment analysis reveals BET-mediated regulation of RNA processing, translation initiation, biosynthesis, and transport in TAC JQ1 mice.

Gene set enrichment analysis (GSEA, Broad Institute) in TAC vehicle versus TAC JQ1 revealed 49 positively enriched GO gene sets ($\text{padj} < 0.05$, $\text{FDR} < 0.25$). The GO categories were manually clustered into 'Transport', 'Translation initiation', 'Splicing', 'RNA processing', 'Ribonucleoprotein complex', 'Biosynthesis' (A). GSEA for TAC vehicle and TAC JQ1 against exemplary GO gene sets from three of the six GO category clusters from (A). $\text{FWER}q < 0.25$ represents statistically significant enrichment (B).

Table 5.4: Sequence alignment of truncated *Brd2* mRNA

cDNA of the truncated *Brd2* mRNA was sequenced and aligned to the annotated main *Mus musculus* *Brd2* transcript "CCDS28641.1". Original translation start codon (ATG) in exon 2 is highlighted in yellow. The intended premature stop codon (TAA) in exon 5 is underscored. An internal in-frame ATG in exon 5 (green) can act as alternative start codon and lead to the translation of a truncated BRD2 (amino acid sequence provided).

	<exon 2----->exon 3-----
'Brd2 mRNA'	CTGAGCGGCGGGTTCCTGAGGTCAAGATGCTGCAAAAACGTGACTCCCCACAAAGCTCCCTGGGGAAGGGAATGCAGGGTTACTGGGGC
'mutant Brd2 mRNA'	CTGAGCGGCGGGTTCCTGAGGTCAAGATGCTGCAAAAACGTGACTCCCCACAA-----

'Brd2 mRNA'	TGGGCCAGAGGCAGCAGCACCAGGAAAAGGATTGAAAGCCTTCTGCTGTATGAGGGATTGAGAGCCCCACAATGGCTTCTGTAC
'mutant Brd2 mRNA'	-----

'Brd2 mRNA'	CAGCTTTACAACCTGGCCCTGCCAATCCACCACCCCTGAGGTGTCCAATCCAAAAAGCCAGGACGGGTAACAAACCAACTGCAGTACC
'mutant Brd2 mRNA'	-----
	-----><
'Brd2 mRNA'	TGCACAAGGTAGTGATGAAGGCTCTGTGGAAGCATCAGTTGCATGGCCATCCGGCAGCCTGTGGACGCTGTGAAGCTGGGTTGCCGG
'mutant Brd2 mRNA'	-----

'Brd2 mRNA'	exon 4----- ATTATCACAAAATTATAAAACAGCCTATGGACATGGGTACTATCAAGAGGAGACTTGAAACAATTACTACTGGCTGCCTCAGAATGTA
'mutant Brd2 mRNA'	-----
	----->exon 5-----
'Brd2 mRNA'	TGCAGGATTTTAATACTATGTTTACCAACTGTTACATTATAACAAGCCACCGATGATATTGTCTAATGGCACAGACACTGGAAAAGA <M><A><Q><T><L><E><K><
'mutant Brd2 mRNA'	-----CCACCGATGATATTGTCTAATGGCACAGACACTGGAAAAGA

'Brd2 mRNA'	TCTTCTACAGAAAGTAGCATCCATGCCACAAGAGGAGCAAGAGCTTGTGGTGACCATCCCTAAAAACAGCCATAAGAAGGGGGCCAAGT I><F><L><Q><K><V><A><S><M><P><Q><E><E><Q><E><L><V><V><T><I><P><K><N><S><H><K><K><G><A><K><
'mutant Brd2 mRNA'	TCTTCTACAGAAAGTAGCATCCATGCCACAAGAGGAGCAAGAGCTTGTGGTGACCATCCCTAAAAACAGCCATAAGAAGGGGGCCAAGT
	----->exon 6-----
'Brd2 mRNA'	TAGCAGCACTCCAGGGCAGTATTACAGTGCCCATCAGGTGCCTGTCTCTTCTGTGTCGCATACAGCCCTGTATACACCACCACCTG L><A><A><L><Q><G><S><I><T><S><A><H><Q><V><P><A><V><S><S><V><S><H><T><A><L><Y><T><P><P><P><
'mutant Brd2 mRNA'	TAGCAGCACTCCAGGGCAGTATTACAGTGCCCATCAGGTGCCTGTCTCTTCTGTGTCGCATACAGCCCTGTATACACCACCACCTG

'Brd2 mRNA'	AAATACCTACCCTGTCTCAACATTCCCCACCCATCAGTCATCTTCTCTCTCTTCTTAAAGTCCCTGCATTCTGTGGACCCCACTCC E><I><P><T><T><V><L><N><I><P><H><P><S><V><I><S><S><P><L><L><K><S><L><H><S><A><G><P><P><L><
'mutant Brd2 mRNA'	AAATACCTACCCTGTCTCAACATTCCCCACCCATCAGTCATCTTCTCTCTCTTCTTAAAGTCCCTGCATTCTGTGGACCCCACTCC
	----->exon 7-----
'Brd2 mRNA'	TTGCTGTATCAGCAGCGCCTCCAGCTCAGCCCTTGCCAAGAAAAAGGCGTTAAACGGAAAGCGGATACTACCACCCCTACACCCACAG L><A><V><S><A><A><P><P><A><Q><P><L><A><K><K><K><G><V><K><R><K><A><D><T><T><T><P><T><P><T><
'mutant Brd2 mRNA'	TTGCTGTATCAGCAGCGCCTCCAGCTCAGCCCTTGCCAAGAAAAAGGCGTTAAACGGAAAGCGGATACTACCACCCCTACACCCACAG

'Brd2 mRNA'	CCATCTGGCTCCTGGTTCCTCCAGCTAGTCTCTCTGGGAGTCTTGAGCCAAAGGCAGCAAGGCTCCCTCTATGCGCAGAGAGAGTGGCC A><I><L><A><P><G><S><P><A><S><P><P><G><S><L><E><P><K><A><A><R><L><P><P><M><R><R><E><S><G><
'mutant Brd2 mRNA'	CCATCTGGCTCCTGGTTCCTCCAGCTAGTCTCTCTGGGAGTCTTGAGCCAAAGGCAGCAAGGCTCCCTCTATGCGCAGAGAGAGTGGCC

'Brd2 mRNA'	GCCCAATCAAACCCACGAAAAGACTTGCTGACTCGCAACAGCAACACCAGAGCTCTAAGAAAGGGAAGCTGTCAGAGCAGTTAAAGC R><P><I><K><P><P><R><K><D><L><P><D><S><Q><Q><Q><H><Q><S><S><K><K><G><K><L><S><E><Q><L><K><
'mutant Brd2 mRNA'	GCCCAATCAAACCCACGAAAAGACTTGCTGACTCGCAACAGCAACACCAGAGCTCTAAGAAAGGGAAGCTGTCAGAGCAGTTAAAGC

```

-----
'Brd2 mRNA'      ACTGCAACGGCATCCTGAAGAACTGCTCTCAAGAAGCACGCTGCCTACGCCTGGCCCTTCTATAAGCCAGTGGACGCTTCTGCTCTTG
H><C><N><G><I><L><K><E><L><L><S><K><K><H><A><A><Y><A><W><P><F><Y><K><P><V><D><A><S><A><L><
'mutant Brd2 mRNA'  ACTGCAACGGCATCCTGAAGAACTGCTCTCAAGAAGCACGCTGCCTACGCCTGGCCCTTCTATAAGCCAGTGGACGCTTCTGCTCTTG

----->exon 8-----
'Brd2 mRNA'      GCCTTCATGATTACCATGACATCATTAAACACCCCATGGACCTCAGCACTGTCAAGCGGAAGATGGAGAACCCTGACTACCGGGATGCAC
G><L><H><D><Y><H><D><I><I><K><H><P><M><D><L><S><T><V><K><R><K><M><E><N><R><D><Y><R><D><A><
'mutant Brd2 mRNA'  GCCTTCATGATTACCATGACATCATTAAACACCCCATGGACCTCAGCACTGTCAAGCGGAAGATGGAGAACCCTGACTACCGGGATGCAC

-----
'Brd2 mRNA'      AGGAGTTTGTCTGCTGATGTACGGCTTATGTTCTCCAAGTGTATAAGTACAATCCTCCAGACCACGATGTTGTGGCTATGGCACGAAAGT
Q><E><F><A><A><D><V><R><L><M><F><S><N><C><Y><K><Y><N><P><P><D><H><D><V><V><A><M><A><R><K><
'mutant Brd2 mRNA'  AGGAGTTTGTCTGCTGATGTACGGCTTATGTTCTCCAAGTGTATAAGTACAATCCTCCAGACCACGATGTTGTGGCTATGGCACGAAAGT

----->exon 9-----
'Brd2 mRNA'      TGCAGGATGTGTTTGAGTTTCGCTATGCCAAGATGCCAGATGAGCCACTGGAACCCAGGACCTCTACCAGTCTCTACTGCCTTGCCCTCTG
L><Q><D><V><F><E><F><R><Y><A><K><M><P><D><E><P><L><E><P><G><P><L><P><V><S><T><A><L><P><P><
'mutant Brd2 mRNA'  TGCAGGATGTGTTTGAGTTTCGCTATGCCAAGATGCCAGATGAGCCACTGGAACCCAGGACCTCTACCAGTCTCTACTGCCTTGCCCTCTG

-----
'Brd2 mRNA'      GGTTGACCAATCCTCTTCCAGAGTCTCCAGTGGAGAAAGTAGCAGTGGAGTTCCTCTGAGGAAGAGGAGGAGGAGGAAGAAGATGAGG
G><L><T><K><S><S><S><E><S><S><S><E><E><S><S><S><E><S><S><S><E><E><E><E><E><E><E><E><D><E><
'mutant Brd2 mRNA'  GGTTGACCAATCCTCTTCCAGAGTCTCCAGTGGAGAAAGTAGCAGTGGAGTTCCTCTGAGGAAGAGGAGGAGGAGGAAGAAGATGAGG

----->exon 10-----
'Brd2 mRNA'      ACGAGGAGGAGAGTGAAAGCTCAGACTCTGAGGAGGAAAGGCTCATCGCCTAGCAGAGCTGCAGGAGCAGCTTCGGGCAGTTCATGAAC
D><E><E><E><S><E><S><D><S><E><E><E><R><A><H><R><L><A><E><L><Q><E><Q><L><R><A><V><H><E><
'mutant Brd2 mRNA'  ACGAGGAGGAGAGTGAAAGCTCAGACTCTGAGGAGGAAAGGCTCATCGCCTAGCAGAGCTGCAGGAGCAGCTTCGGGCAGTTCATGAAC

-----
'Brd2 mRNA'      AACTGGCTGCCCTGTCCAGGGCCCAATATCTAAGCCCAAGCGGAAGAGAGAGAAAAAGGAAAAAAGAAGAACGGAAGGCAGAGAAAC
Q><L><A><A><L><S><Q><G><P><I><S><K><P><K><R><K><R><E><K><K><E><K><K><K><R><K><A><E><K><
'mutant Brd2 mRNA'  AACTGGCTGCCCTGTCCAGGGCCCAATATCTAAGCCCAAGCGGAAGAGAGAGAAAAAGGAAAAAAGAAGAACGGAAGGCAGAGAAAC

-----
'Brd2 mRNA'      ATCGTGGCCGAATTGGGATCGATGAAGATGATAAAGGGCCCTAGGGCACCTCGCCACCTCAGCCCAAGAAATCTAAGAAAGCAGGTGGTG
H><R><G><R><I><G><I><D><E><D><D><K><G><P><R><A><P><R><P><P><Q><P><K><K><S><K><K><A><G><G><
'mutant Brd2 mRNA'  ATCGTGGCCGAATTGGGATCGATGAAGATGATAAAGGGCCCTAGGGCACCTCGCCACCTCAGCCCAAGAAATCTAAGAAAGCAGGTGGTG

----->exon 11-----
'Brd2 mRNA'      GGGGTAGCAATGCTACTACACTCAGCCATCTGGCTTGGGACTTCCGGAGGAAGTAGCAACAAGCTACCTAAAAAGTCTCAAAGACAG
G><G><S><N><A><T><T><L><S><H><P><G><F><G><T><S><G><G><S><S><N><K><L><P><K><K><S><Q><K><T><
'mutant Brd2 mRNA'  GGGGTAGCAATGCTACTACACTCAGCCATCTGGCTTGGGACTTCCGGAGGAAGTAGCAACAAGCTACCTAAAAAGTCTCAAAGACAG

-----
'Brd2 mRNA'      CTCCACCTGTCCTTCCACTGGCTATGATTCTGAGGAGGAGGAAGAAAGCAGGCCCATGAGTTATGATGAGAAGAGACAGTTAAGCCTGG
A><P><P><V><L><P><T><G><Y><D><S><E><E><E><E><E><S><R><P><M><S><Y><D><E><K><R><Q><L><S><L><
'mutant Brd2 mRNA'  CTCCACCTGTCCTTCCACTGGCTATGATTCTGAGGAGGAGGAAGAAAGCAGGCCCATGAGTTATGATGAGAAGAGACAGTTAAGCCTGG

-----
'Brd2 mRNA'      ATATCAATAAGTTACCTGGGAAAAGCTGGGTCGAGTAGTACATATCATCAAGCCAGGGAACCTCTCTACGTGATTCAAATCCAGAAG
D><I><N><K><L><P><G><E><K><L><G><R><V><V><H><I><I><Q><A><R><E><P><S><L><R><D><S><N><P><E><
'mutant Brd2 mRNA'  ATATCAATAAGTTACCTGGGAAAAGCTGGGTCGAGTAGTACATATCATCAAGCCAGGGAACCTCTCTACGTGATTCAAATCCAGAAG

-----
'Brd2 mRNA'      AAATTGAGATTGATTTTGAACACTCAAGCCGTCACACTTAGAGAGCTTGAGCGATATGTTTATCTGCCTTCGAAAGAAACCCCGGA
E><I><E><I><D><F><E><T><L><K><P><S><T><L><R><E><L><E><R><Y><V><L><S><C><L><R><K><K><P><R><
'mutant Brd2 mRNA'  AAATTGAGATTGATTTTGAACACTCAAGCCGTCACACTTAGAGAGCTTGAGCGATATGTTTATCTGCCTTCGAAAGAAACCCCGGA

----->exon 12-----
'Brd2 mRNA'      AGCCCTACACTATTAGGAAACCTGTGGGAAAAACAAGGAGGAAGTGGCTTTGGAGAAGAGCGGGAGCTAGAGAAGCGGTTGCAGGATG
K><P><Y><T><I><R><K><P><V><G><K><T><K><E><E><L><A><L><E><K><K><R><E><L><E><K><R><L><Q><D><
'mutant Brd2 mRNA'  AGCCCTACACTATTAGGAAACCTGTGGGAAAAACAAGGAGGAAGTGGCTTTGGAGAAGAGCGGGAGCTAGAGAAGCGGTTGCAGGATG

----->exon 13-----
'Brd2 mRNA'      TCAGTGGACAGCTCAACTCCACAAAAAGCCTCCCAAGAAAGCGAGTGAGAAGACAGAGTCATCTGCACAGCAAGTGGCAGTGTCCCGTC
V><S><G><Q><L><N><S><T><K><K><P><P><K><K><A><S><E><K><T><E><S><S><A><Q><Q><V><A><V><S><R><
'mutant Brd2 mRNA'  TCAGTGGACAGCTCAACTCCACAAAAAGCCTCCCAAGAAAGCGAGTGAGAAGACAGAGTCATCTGCACAGCAAGTGGCAGTGTCCCGTC

```


Biological processes regulated by Brd4 KO specific DEGs

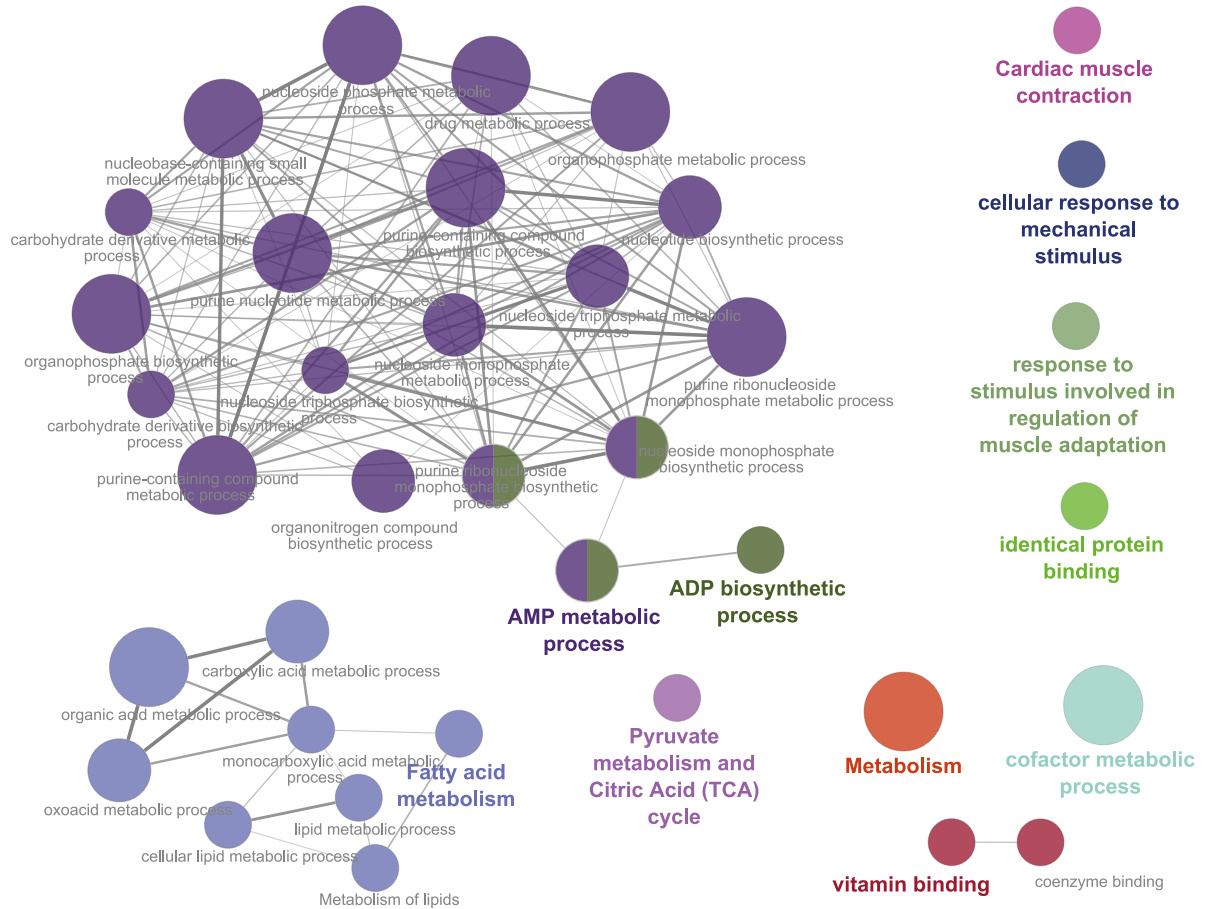


Figure 5.4: Brd4 KO-specific DEGs regulate metabolic processes, cellular response to stimuli and cardiac muscle contraction.

ClueGO pathway analysis of 742 Brd4 KO specific DEGs from (Figure 3.34B) ($\text{padj} < 0.05$, $\log_2\text{FC} \pm 0.5$) showed GO terms enriched for energy metabolism, response to stimulus, and cardiac muscle contraction ($\text{padj} < 0.05$, $\text{Kappa} = 0.4$). Circle size represents padj .

6 Bibliography

- Agah R, Frenkel PA, French BA, Michael LH, Overbeek PA, Schneider MD (1997): Gene recombination in postmitotic cells. Targeted expression of Cre recombinase provokes cardiac-restricted, site-specific rearrangement in adult ventricular muscle in vivo. *Journal of Clinical Investigation* 100, 169–179
- Ambros V (2004): The functions of animal microRNAs. *Nature* 431, 350–355
- An L, Hu X, Zhang S, Hu X, Song Z, Naz A, Zi Z, Wu J, Li C, Zou Y, et al. (2017): UVRAG Deficiency Exacerbates Doxorubicin-Induced Cardiotoxicity. *Scientific Reports* 7, 43251
- Anand P, Brown JD, Lin CY, Qi J, Zhang R, Artero PC, Alaiti MA, Bullard J, Alazem K, Margulies KB, et al. (2013): BET bromodomains mediate transcriptional pause release in heart failure. *Cell* 154, 569–582
- Andrews S (2010): FastQC A Quality Control tool for High Throughput Sequence Data. <http://www.bioinformatics.babraham.ac.uk/projects/fastqc/>(version 0.11.5).
- Azevedo PS, Polegato BF, Minicucci MF, Paiva SAR, Zornoff LAM (2016): Cardiac Remodeling: Concepts, Clinical Impact, Pathophysiological Mechanisms and Pharmacologic Treatment. *Arq Bras Cardiol* 106, 62–69
- Babicki S, Arndt D, Marcu A, Liang Y, Grant JR, Maciejewski A, Wishart DS (2016): Heatmapper: web-enabled heat mapping for all. *Nucleic Acids Res* 44, W147–153
- Backs J, Olson EN (2006): Control of Cardiac Growth by Histone Acetylation/Deacetylation. *Circulation Research* 98, 15–24
- Backs J, Backs T, Neef S, Kreusser MM, Lehmann LH, Patrick DM, Grueter CE, Qi X, Richardson JA, Hill JA, et al. (2009): The δ isoform of CaM kinase II is required for pathological cardiac hypertrophy and remodeling after pressure overload. *Proc Natl Acad Sci U S A* 106, 2342–2347
- Banerjee C, Archin N, Michaels D, Belkina AC, Denis GV, Bradner J, Sebastiani P, Margolis DM, Montano M (2012): BET bromodomain inhibition as a novel strategy for reactivation of HIV-1. *J Leukoc Biol* 92, 1147–1154
- Bao Y, Wu X, Chen J, Hu X, Zeng F, Cheng J, Jin H, Lin X, Chen L-F (2017): Brd4 modulates the innate immune response through Mnk2–eIF4E pathway-dependent translational control of I κ B α . *PNAS* 201700109
- Barnabei MS, Palpant NJ, Metzger JM (2010): Influence of genetic background on ex vivo and in vivo cardiac function in several commonly used inbred mouse strains. *Physiol Genomics* 42A, 103–113
- Barrow JJ, Balsa E, Verdeguer F, Tavares CDJ, Soustek MS, Hollingsworth LR, Jedrychowski M, Vogel R, Paulo JA, Smeitink J, et al. (2016): Bromodomain Inhibitors Correct Bioenergetic Deficiency Caused by Mitochondrial Disease Complex I Mutations. *Mol Cell* 64, 163–175
- Bell O, Tiwari VK, Thomä NH, Schübeler D (2011): Determinants and dynamics of genome accessibility. *Nature Reviews Genetics* 12, 554–564

- Benjamin EJ, Virani SS, Callaway CW, Chamberlain AM, Chang AR, Cheng S, Chiuve SE, Cushman M, Delling FN, Deo R, et al. (2018): Heart Disease and Stroke Statistics—2018 Update: A Report From the American Heart Association. *Circulation*
- van Berlo JH, Maillet M, Molkentin JD (2013): Signaling effectors underlying pathologic growth and remodeling of the heart. *J Clin Invest* 123, 37–45
- Bersell K, Choudhury S, Mollova M, Polizzotti BD, Ganapathy B, Walsh S, Wadugu B, Arab S, Kuhn B (2013): Moderate and high amounts of tamoxifen in MHC-MerCreMer mice induce a DNA damage response, leading to heart failure and death. *Disease Models & Mechanisms* 6, 1459–1469
- Bindea G, Mlecnik B, Hackl H, Charoentong P, Tosolini M, Kirilovsky A, Fridman W-H, Pagès F, Trajanoski Z, Galon J (2009): ClueGO: a Cytoscape plug-in to decipher functionally grouped gene ontology and pathway annotation networks. *Bioinformatics* 25, 1091–1093
- Blakey CA, Litt MD: Epigenetic gene expression—an introduction; in: *Epigenetic Gene Expression and Regulation*; Elsevier 2015a, 1–19
- Blakey CA, Litt MD: Histone modifications—models and mechanisms; in: *Epigenetic Gene Expression and Regulation*; Elsevier 2015b, 21–42
- Bueno OF, De Windt LJ, Tymitz KM, Witt SA, Kimball TR, Klevitsky R, Hewett TE, Jones SP, Lefer DJ, Peng C-F, et al. (2000): The MEK1–ERK1/2 signaling pathway promotes compensated cardiac hypertrophy in transgenic mice. *EMBO J* 19, 6341–6350
- Buenrostro J, Wu B, Chang H, Greenleaf W (2015): ATAC-seq: A Method for Assaying Chromatin Accessibility Genome-Wide. *Curr Protoc Mol Biol* 109, 21.29.1-21.29.9
- Burchfield JS, Xie M, Hill JA (2013): Pathological ventricular remodeling: mechanisms: part 1 of 2. *Circulation* 128, 388–400
- Catalanotto C, Cogoni C, Zardo G (2016): MicroRNA in Control of Gene Expression: An Overview of Nuclear Functions. *Int J Mol Sci* 17
- Cheung K, Lu G, Sharma R, Vincek A, Zhang R, Plotnikov AN, Zhang F, Zhang Q, Ju Y, Hu Y, et al. (2017a): BET N-terminal bromodomain inhibition selectively blocks Th17 cell differentiation and ameliorates colitis in mice. *Proc Natl Acad Sci U S A* 114, 2952–2957
- Cheung KL, Zhang F, Jaganathan A, Sharma R, Zhang Q, Konuma T, Shen T, Lee J-Y, Ren C, Chen C-H, et al. (2017b): Distinct Roles of Brd2 and Brd4 in Potentiating the Transcriptional Program for Th17 Cell Differentiation. *Molecular Cell* 65, 1068-1080.e5
- Cohen J: *Statistical power analysis for the behavioral sciences*. 2nd ed; L. Erlbaum Associates, Hillsdale, N.J 1988
- Conrad RJ, Fozouni P, Thomas S, Sy H, Zhang Q, Zhou M-M, Ott M (2017): The Short Isoform of BRD4 Promotes HIV-1 Latency by Engaging Repressive SWI/SNF Chromatin-Remodeling Complexes. *Molecular Cell* 67, 1001-1012.e6
- Davis J, Maillet M, Miano JM, Molkentin JD (2012): Lost in Transgenesis: A Users guide for Genetically Manipulating the Mouse in Cardiac Research. *Circ Res* 111, 761–777

- deAlmeida AC, van Oort RJ, Wehrens XHT (2010): Transverse Aortic Constriction in Mice. *J Vis Exp*
- Delmore JE, Issa GC, Lemieux ME, Rahl PB, Shi J, Jacobs HM, Kastiris E, Gilpatrick T, Paranal RM, Qi J, et al. (2011): BET bromodomain inhibition as a therapeutic strategy to target c-Myc. *Cell* 146, 904–917
- Dey A, Nishiyama A, Karpova T, McNally J, Ozato K (2009): Brd4 Marks Select Genes on Mitotic Chromatin and Directs Postmitotic Transcription. *Mol Biol Cell* 20, 4899–4909
- Dickstein K, Cohen-Solal A, Filippatos G, McMurray JJV, Ponikowski P, Poole-Wilson PA, Strömberg A, Veldhuisen V, J D, Atar D, et al. (2008): ESC Guidelines for the diagnosis and treatment of acute and chronic heart failure 2008 The Task Force for the Diagnosis and Treatment of Acute and Chronic Heart Failure 2008 of the European Society of Cardiology. Developed in collaboration with the Heart Failure Association of the ESC (HFA) and endorsed by the European Society of Intensive Care Medicine (ESICM). *Eur Heart J* 29, 2388–2442
- Dobin A, Davis CA, Schlesinger F, Drenkow J, Zaleski C, Jha S, Batut P, Chaisson M, Gingeras TR (2013): STAR: ultrafast universal RNA-seq aligner. *Bioinformatics* 29, 15–21
- Donner DG, Kiriazis H, Du X-J, Marwick TH, McMullen JR (2018): Improving the quality of preclinical research echocardiography: observations, training, and guidelines for measurement. *American Journal of Physiology-Heart and Circulatory Physiology* 315, H58–H70
- Duan Q, McMahon S, Anand P, Shah H, Thomas S, Salunga HT, Huang Y, Zhang R, Sahadevan A, Lemieux ME, et al. (2017): BET bromodomain inhibition suppresses innate inflammatory and profibrotic transcriptional networks in heart failure. *Science Translational Medicine* 9, eaah5084
- Durinck S, Spellman PT, Birney E, Huber W (2009): Mapping Identifiers for the Integration of Genomic Datasets with the R/Bioconductor package biomaRt. *Nat Protoc* 4, 1184–1191
- Duygu B, Poels EM, Costa Martins PA da (2013): Genetics and epigenetics of arrhythmia and heart failure. *Frontiers in Genetics* 4
- Fabian MR, Sonenberg N, Filipowicz W (2010): Regulation of mRNA Translation and Stability by microRNAs. *Annual Review of Biochemistry* 79, 351–379
- Farza H, Watkins H (1999): Animal models of familial hypertrophic cardiomyopathy. *Molecular Medicine Today* 5, 544–545
- Fatkin D, Graham RM (2002): Molecular Mechanisms of Inherited Cardiomyopathies. *Physiological Reviews* 82, 945–980
- Faul F, Erdfelder E, Lang A-G, Buchner A (2007): G*Power 3: A flexible statistical power analysis program for the social, behavioral, and biomedical sciences. *Behavior Research Methods* 39, 175–191
- Filippakopoulos P, Qi J, Picaud S, Shen Y, Smith WB, Fedorov O, Morse EM, Keates T, Hickman TT, Felletar I, et al. (2010): Selective inhibition of BET bromodomains. *Nature* 468, 1067–1073

- Filippakopoulos P, Picaud S, Mangos M, Keates T, Lambert J-P, Barsyte-Lovejoy D, Felletar I, Volkmer R, Müller S, Pawson T, et al. (2012): Histone Recognition and Large-Scale Structural Analysis of the Human Bromodomain Family. *Cell* 149, 214–231
- Fu L, Tian M, Li X, Li J, Huang J, Ouyang L, Zhang Y, Liu B (2015): Inhibition of BET bromodomains as a therapeutic strategy for cancer drug discovery. *Oncotarget* 6, 5501–5516
- Gacias M, Gerona-Navarro G, Plotnikov AN, Zhang G, Zeng L, Kaur J, Moy G, Rusinova E, Rodriguez Y, Matikainen B, et al. (2014): Selective Chemical Modulation of Gene Transcription Favors Oligodendrocyte Lineage Progression. *Chem Biol* 21, 841–854
- Gamsjaeger R, Webb SR, Lamonica JM, Billin A, Blobel GA, Mackay JP (2011): Structural Basis and Specificity of Acetylated Transcription Factor GATA1 Recognition by BET Family Bromodomain Protein Brd3 ν . *Mol Cell Biol* 31, 2632–2640
- Garcia-Menendez L, Karamanlidis G, Kolwicz S, Tian R (2013): Substrain specific response to cardiac pressure overload in C57BL/6 mice. *Am J Physiol Heart Circ Physiol* 305, H397–H402
- Gilham D, Wasiak S, Tsujikawa LM, Halliday C, Norek K, Patel RG, Kulikowski E, Johansson J, Sweeney M, Wong NCW (2016): RVX-208, a BET-inhibitor for treating atherosclerotic cardiovascular disease, raises ApoA-I/HDL and represses pathways that contribute to cardiovascular disease. *Atherosclerosis* 247, 48–57
- Gillette TG, Hill JA (2015): Readers, writers and erasers: Chromatin as the Whiteboard of Heart Disease. *Circ Res* 116, 1245–1253
- Gilsbach R, Preissl S, Grüning BA, Schnick T, Burger L, Benes V, Würch A, Bönisch U, Günther S, Backofen R, et al. (2014): Dynamic DNA methylation orchestrates cardiomyocyte development, maturation and disease. *Nature Communications* 5, 5288
- Gyuris A, Donovan DJ, Seymour KA, Lovasco LA, Smilowitz NR, Halperin ALP, Klysik JE, Freiman RN (2009): The chromatin-targeting protein Brd2 is required for neural tube closure and embryogenesis. *Biochimica et Biophysica Acta (BBA) - Gene Regulatory Mechanisms* 1789, 413–421
- Haldar SM, McKinsey TA (2014): BET-ting on chromatin-based therapeutics for heart failure. *Journal of Molecular and Cellular Cardiology* 74, 98–102
- Hang CT, Yang J, Han P, Cheng H-L, Shang C, Ashley E, Zhou B, Chang C-P (2010): Chromatin regulation by Brg1 underlies heart muscle development and disease. *Nature* 466, 62–67
- Harrison A, Shanahan H: An Overview of Gene Regulation; in: *Approaches in Integrative Bioinformatics*; ed. by Chen M, Hofestädt R; Springer Berlin Heidelberg, Berlin, Heidelberg 2014, 21–69
- Heberle H, Meirelles GV, da Silva FR, Telles GP, Minghim R (2015): InteractiVenn: a web-based tool for the analysis of sets through Venn diagrams. *BMC Bioinformatics* 16, 169
- Heidenreich PA, Trogon JG, Khavjou OA, Butler J, Dracup K, Ezekowitz MD, Finkelstein EA, Hong Y, Johnston SC, Khara A, et al. (2011): Forecasting the Future of Cardiovascular Disease in the United States: A Policy Statement From the American Heart Association. *Circulation* 123, 933–944

- Heidenreich PA, Albert NM, Allen LA, Bluemke DA, Butler J, Fonarow GC, Ikonomidis JS, Khavjou O, Konstam MA, Maddox TM, et al. (2013): Forecasting the Impact of Heart Failure in the United States: A Policy Statement From the American Heart Association. *Circulation: Heart Failure* 6, 606–619
- Helin K, Dhanak D (2013): Chromatin proteins and modifications as drug targets. *Nature* 502, 480–488
- Higashi AY, Ikawa T, Muramatsu M, Economides AN, Niwa A, Okuda T, Murphy AJ, Rojas J, Heike T, Nakahata T, et al. (2009): Direct Hematological Toxicity and Illegitimate Chromosomal Recombination Caused by the Systemic Activation of CreERT2. *The Journal of Immunology* 182, 5633–5640
- Hill JA, Olson EN (2008): Cardiac Plasticity. *New England Journal of Medicine* 358, 1370–1380
- Hogg S, Newbold A, Vervoort SJ, Cluse LA, Martin BP, Gregory GP, Lefebure M, Vidacs E, Tothill RW, Bradner JE, et al. (2016): BET-inhibition induces apoptosis in aggressive B-cell lymphoma via epigenetic regulation of BCL-2 family members. *Mol Cancer Ther* molcanther.0924.2015
- Holoch D, Moazed D (2015): RNA-mediated epigenetic regulation of gene expression. *Nature Reviews Genetics* 16, 71–84
- Hougen K, Aronsen JM, Stokke MK, Enger U, Nygård S, Andersson KB, Christensen G, Sejersted OM, Sjaastad I (2010): Cre-loxP DNA recombination is possible with only minimal unspecific transcriptional changes and without cardiomyopathy in Tg(α MHC-MerCreMer) mice. *American Journal of Physiology-Heart and Circulatory Physiology* 299, H1671–H1678
- Houzelstein D, Bullock SL, Lynch DE, Grigorieva EF, Wilson VA, Beddington RSP (2002): Growth and Early Postimplantation Defects in Mice Deficient for the Bromodomain-Containing Protein Brd4. *Molecular and Cellular Biology* 22, 3794–3802
- Hu P, Zhang D, Swenson L, Chakrabarti G, Abel ED, Litwin SE (2003): Minimally invasive aortic banding in mice: effects of altered cardiomyocyte insulin signaling during pressure overload. *American Journal of Physiology-Heart and Circulatory Physiology* 285, H1261–H1269
- Hussong M, Kaehler C, Kerick M, Grimm C, Franz A, Timmermann B, Welzel F, Isensee J, Hucho T, Krobisch S, Schweiger MR (2017): The bromodomain protein BRD4 regulates splicing during heat shock. *Nucleic Acids Res* 45, 382–394
- Isensee J, Witt H, Pregla R, Hetzer R, Regitz-Zagrosek V, Ruiz Noppinger P (2008): Sexually dimorphic gene expression in the heart of mice and men. *J Mol Med* 86, 61–74
- Jang MK, Mochizuki K, Zhou M, Jeong H-S, Brady JN, Ozato K (2005): The Bromodomain Protein Brd4 Is a Positive Regulatory Component of P-TEFb and Stimulates RNA Polymerase II-Dependent Transcription. *Molecular Cell* 19, 523–534
- Jenuwein T (2001): Translating the Histone Code. *Science* 293, 1074–1080
- Jiang YW, Veschambre P, Erdjument-Bromage H, Tempst P, Conaway JW, Conaway RC, Kornberg RD (1998): Mammalian mediator of transcriptional regulation and its possible role as an end-point of signal transduction pathways. *Proceedings of the National Academy of Sciences* 95, 8538–8543

- Kanno T, Kanno Y, Siegel RM, Jang MK, Lenardo MJ, Ozato K (2004): Selective Recognition of Acetylated Histones by Bromodomain Proteins Visualized in Living Cells. *Molecular Cell* 13, 33–43
- Kapahnke M, Banning A, Tikkanen R (2016): Random Splicing of Several Exons Caused by a Single Base Change in the Target Exon of CRISPR/Cas9 Mediated Gene Knockout. *Cells* 5
- Kauffmann A, Gentleman R, Huber W (2009): arrayQualityMetrics—a bioconductor package for quality assessment of microarray data. *Bioinformatics* 25, 415–416
- Keung AJ, Joung JK, Khalil AS, Collins JJ (2015): Chromatin regulation at the frontier of synthetic biology. *Nature Reviews Genetics* 16, 159–171
- Khalil CA (2014): The emerging role of epigenetics in cardiovascular disease. *Therapeutic Advances in Chronic Disease* 2040622314529325
- Lambert J-P, Picaud S, Fujisawa T, Hou H, Savitsky P, Uusküla-Reimand L, Gupta GD, Abdouni H, Lin Z-Y, Tucholska M, et al. (2018): Interactome Rewiring Following Pharmacological Targeting of BET Bromodomains. *Molecular Cell*
- Lamonica JM, Deng W, Kadauke S, Campbell AE, Gamsjaeger R, Wang H, Cheng Y, Billin AN, Hardison RC, Mackay JP, Blobel GA (2011): Bromodomain protein Brd3 associates with acetylated GATA1 to promote its chromatin occupancy at erythroid target genes. *Proceedings of the National Academy of Sciences* 108, E159–E168
- Lee J-E, Park Y-K, Park S, Jang Y, Waring N, Dey A, Ozato K, Lai B, Peng W, Ge K (2017): Brd4 binds to active enhancers to control cell identity gene induction in adipogenesis and myogenesis. *Nature Communications* 8, 2217
- LeRoy G, Rickards B, Flint SJ (2008): The Double Bromodomain Proteins Brd2 and Brd3 Couple Histone Acetylation to Transcription. *Molecular Cell* 30, 51–60
- LeWinter MM, Meyer M (2013): Mechanisms of Diastolic Dysfunction in HFpEF: If It's Not One Thing It's Another. *Circ Heart Fail* 6, 1112–1115
- Lexow J, Poggioli T, Sarathchandra P, Santini MP, Rosenthal N (2013): Cardiac fibrosis in mice expressing an inducible myocardial-specific Cre driver. *Dis Model Mech* 6, 1470–1476
- Liao Y, Smyth GK, Shi W (2014): featureCounts: an efficient general purpose program for assigning sequence reads to genomic features. *Bioinformatics* 30, 923–930
- Lin X, Huang X, Uziel T, Hessler P, Albert DH, Roberts-Rapp LA, McDaniel KF, Kati WM, Shen Y (2017): HEXIM1 as a Robust Pharmacodynamic Marker for Monitoring Target Engagement of BET Family Bromodomain Inhibitors in Tumors and Surrogate Tissues. *Mol Cancer Ther* 16, 388–396
- Lindsey ML, Kassiri Z, Virag JAI, de Castro Brás LE, Scherrer-Crosbie M (2018): Guidelines for measuring cardiac physiology in mice. *American Journal of Physiology-Heart and Circulatory Physiology* 314, H733–H752
- Love MI, Huber W, Anders S (2014): Moderated estimation of fold change and dispersion for RNA-seq data with DESeq2. *Genome Biology* 15

- Mahmoud SA, Poizat C (2013): Epigenetics and Chromatin Remodeling in Adult Cardiomyopathy: Epigenetic Modifications in Adult Cardiomyopathy. *The Journal of Pathology* 231, 147–157
- Marian AJ (2002): Modifier genes for hypertrophic cardiomyopathy. *Curr Opin Cardiol* 17, 242–252
- Marian AJ, Roberts R (1998): Familial hypertrophic cardiomyopathy: a paradigm of the cardiac hypertrophic response to injury. *Ann Med* 30 Suppl 1, 24–32
- Marian AJ, Braunwald E (2017): Hypertrophic Cardiomyopathy: Genetics, Pathogenesis, Clinical Manifestations, Diagnosis, and Therapy. *Circulation Research* 121, 749–770
- McCauley MD, Wehrens XH. (2010): Ambulatory ECG Recording in Mice. *J Vis Exp*
- McKinsey TA, Olson EN (2005): Toward transcriptional therapies for the failing heart: chemical screens to modulate genes. *J Clin Invest* 115, 538–546
- Merino D, Gil A, Gómez J, Ruiz L, Llano M, García R, Hurlé MA, Nistal JF (2018): Experimental modelling of cardiac pressure overload hypertrophy: Modified technique for precise, reproducible, safe and easy aortic arch banding-debanding in mice. *Scientific Reports* 8, 3167
- Mohamed BA, Asif AR, Schnelle M, Qasim M, Khadjeh S, Lbik D, Schott P, Hasenfuss G, Toischer K (2016): Proteomic analysis of short-term preload-induced eccentric cardiac hypertrophy. *Journal of Translational Medicine* 14
- Molkentin JD, Lu J-R, Antos CL, Markham B, Richardson J, Robbins J, Grant SR, Olson EN (1998): A Calcineurin-Dependent Transcriptional Pathway for Cardiac Hypertrophy. *Cell* 93, 215–228
- Mootha VK, Lindgren CM, Eriksson K-F, Subramanian A, Sihag S, Lehar J, Puigserver P, Carlsson E, Ridderstråle M, Laurila E, et al. (2003): PGC-1 α -responsive genes involved in oxidative phosphorylation are coordinately downregulated in human diabetes. *Nature Genetics* 34, 267–273
- Mou H, Smith JL, Peng L, Yin H, Moore J, Zhang X-O, Song C-Q, Sheel A, Wu Q, Ozata DM, et al. (2017): CRISPR/Cas9-mediated genome editing induces exon skipping by alternative splicing or exon deletion. *Genome Biol* 18
- Nakamura M, Sadoshima J (2018): Mechanisms of physiological and pathological cardiac hypertrophy. *Nature Reviews Cardiology* 15, 387–407
- Nakamura Y, Umehara T, Nakano K, Jang MK, Shirouzu M, Morita S, Uda-Tochio H, Hamana H, Terada T, Adachi N, et al. (2007): Crystal Structure of the Human BRD2 Bromodomain INSIGHTS INTO DIMERIZATION AND RECOGNITION OF ACETYLATED HISTONE H4. *J Biol Chem* 282, 4193–4201
- Nandi SS, Mishra PK (2015): Harnessing fetal and adult genetic reprogramming for therapy of heart disease. 6
- Newton AC, Antal CE, Steinberg SF (2016): Protein kinase C mechanisms that contribute to cardiac remodelling. *Clin Sci (Lond)* 130, 1499–1510
- Pérez-Salvia M, Esteller M (2017): Bromodomain inhibitors and cancer therapy: From structures to applications. *Epigenetics* 12, 323–339

- Picaud S, Wells C, Felletar I, Brotherton D, Martin S, Savitsky P, Diez-Dacal B, Philpott M, Bountra C, Lingard H, et al. (2013): RVX-208, an inhibitor of BET transcriptional regulators with selectivity for the second bromodomain. *Proc Natl Acad Sci U S A* 110, 19754–19759
- Pistner A, Belmonte S, Coulthard T, Blaxall BC (2010): Murine Echocardiography and Ultrasound Imaging. *J Vis Exp*
- Ritchie ME, Phipson B, Wu D, Hu Y, Law CW, Shi W, Smyth GK (2015): limma powers differential expression analyses for RNA-sequencing and microarray studies. *Nucleic Acids Res* 43, e47
- Rockman HA, Ross RS, Harris AN, Knowlton KU, Steinhilber ME, Field LJ, Ross J, Chien KR (1991): Segregation of atrial-specific and inducible expression of an atrial natriuretic factor transgene in an in vivo murine model of cardiac hypertrophy. *Proc Natl Acad Sci U S A* 88, 8277–8281
- Rogers FJ (2013): Aortic Stenosis: New Thoughts on a Cardiac Disease of Older People. *J Am Osteopath Assoc* 113, 820–828
- ROSE BA, FORCE T, WANG Y (2010): Mitogen-Activated Protein Kinase Signaling in the Heart: Angels Versus Demons in a Heart-Breaking Tale. *Physiol Rev* 90
- Roth DM, Swaney JS, Dalton ND, Gilpin EA, Ross J (2002): Impact of anesthesia on cardiac function during echocardiography in mice. *American Journal of Physiology-Heart and Circulatory Physiology* 282, H2134–H2140
- Rueden CT, Schindelin J, Hiner MC, DeZonia BE, Walter AE, Arena ET, Eliceiri KW (2017): ImageJ2: ImageJ for the next generation of scientific image data. *BMC Bioinformatics* 18, 529
- Sakamaki J-I, Wilkinson S, Hahn M, Tasdemir N, O'Prey J, Clark W, Hedley A, Nixon C, Long JS, New M, et al. (2017): Bromodomain Protein BRD4 Is a Transcriptional Repressor of Autophagy and Lysosomal Function. *Mol Cell* 66, 517-532.e9
- Schindelin J, Arganda-Carreras I, Frise E, Kaynig V, Longair M, Pietzsch T, Preibisch S, Rueden C, Saalfeld S, Schmid B, et al. (2012): Fiji: an open-source platform for biological-image analysis. *Nature Methods* 9, 676–682
- Schröder S, Cho S, Zeng L, Zhang Q, Kaehlcke K, Mak L, Lau J, Bisgrove D, Schnölzer M, Verdin E, et al. (2012): Two-pronged Binding with Bromodomain-containing Protein 4 Liberates Positive Transcription Elongation Factor b from Inactive Ribonucleoprotein Complexes. *Journal of Biological Chemistry* 287, 1090–1099
- Shang E, Nickerson HD, Wen D, Wang X, Wolgemuth DJ (2007): The first bromodomain of Brdt, a testis-specific member of the BET sub-family of double-bromodomain-containing proteins, is essential for male germ cell differentiation. *Development* 134, 3507–3515
- Shang E, Wang X, Wen D, Greenberg DA, Wolgemuth DJ (2009): The Double Bromodomain-containing Gene Brd2 Is Essential for Embryonic Development in Mouse. *Dev Dyn* 238, 908–917
- Sharpe JJ, Cooper TA (2017): Unexpected consequences: exon skipping caused by CRISPR-generated mutations. *Genome Biol* 18

- Shi J, Wang Y, Zeng L, Wu Y, Deng J, Zhang Q, Lin Y, Li J, Kang T, Tao M, et al. (2014): Disrupting the Interaction of BRD4 with Di-acetylated Twist Suppresses Tumorigenesis in Basal-like Breast Cancer. *Cancer Cell* 25, 210–225
- Shu S, Lin CY, He HH, Witwicki RM, Tabassum DP, Roberts JM, Janiszewska M, Jin Huh S, Liang Y, Ryan J, et al. (2016): Response and resistance to BET bromodomain inhibitors in triple-negative breast cancer. *Nature* 529, 413–417
- Simon MM, Greenaway S, White JK, Fuchs H, Gailus-Durner V, Wells S, Sorg T, Wong K, Bedu E, Cartwright EJ, et al. (2013): A comparative phenotypic and genomic analysis of C57BL/6J and C57BL/6N mouse strains. *Genome Biology* 14, R82
- Sohal DS, Nghiem M, Crackower MA, Witt SA, Kimball TR, Tymitz KM, Penninger JM, Molkentin JD (2001): Temporally Regulated and Tissue-Specific Gene Manipulations in the Adult and Embryonic Heart Using a Tamoxifen-Inducible Cre Protein. *Circulation Research* 89, 20–25
- Spiltoir JI, Stratton MS, Cavasin MA, Demos-Davies K, Reid BG, Qi J, Bradner JE, McKinsey TA (2013): BET Acetyl-Lysine Binding Proteins Control Pathological Cardiac Hypertrophy. *J Mol Cell Cardiol* 63, 175–179
- Spitz F, Furlong EEM (2012): Transcription factors: from enhancer binding to developmental control. *Nature Reviews Genetics* 13, 613–626
- Subramanian A, Tamayo P, Mootha VK, Mukherjee S, Ebert BL, Gillette MA, Paulovich A, Pomeroy SL, Golub TR, Lander ES, Mesirov JP (2005): Gene set enrichment analysis: A knowledge-based approach for interpreting genome-wide expression profiles. *PNAS* 102, 15545–15550
- Suzuki HI, Young RA, Sharp PA (2017): Super-Enhancer-Mediated RNA Processing Revealed by Integrative MicroRNA Network Analysis. *Cell* 168, 1000-1014.e15
- Toischer K, Rokita AG, Unsold B, Zhu W, Kararigas G, Sossalla S, Reuter SP, Becker A, Teucher N, Seidler T, et al. (2010): Differential Cardiac Remodeling in Preload Versus Afterload. *Circulation* 122, 993–1003
- Toischer K, Zhu W, Hünlich M, Mohamed BA, Khadjeh S, Reuter SP, Schäfer K, Ramanujam D, Engelhardt S, Field LJ, Hasenfuss G (2017): Cardiomyocyte proliferation prevents failure in pressure overload but not volume overload. *J Clin Invest* 127, 4285–4296
- Tonna S, El-Osta A, Cooper ME, Tikellis C (2010): Metabolic memory and diabetic nephropathy: potential role for epigenetic mechanisms. *Nature Reviews Nephrology* 6, 332–341
- Tsujikawa L, Kulikowski E, Calosing C, Wasiak S, Gilham D, Halliday C, Johansson JO, Sweeney M, Wong NC (2018): Apabetalone (RVX-208) Lowers Major Adverse Cardiovascular Events (MACE) in Diabetes Mellitus Patients with CVD by Attenuating Monocyte Adhesion to Endothelial Cells. *Diabetes* 67, 1136-P
- Umehara T, Nakamura Y, Jang MK, Nakano K, Tanaka A, Ozato K, Padmanabhan B, Yokoyama S (2010): Structural Basis for Acetylated Histone H4 Recognition by the Human BRD2 Bromodomain. *J Biol Chem* 285, 7610–7618
- WANG F, LIU H, BLANTON WP, BELKINA A, LEBRASSEUR NK, DENIS GV (2009): Brd2 disruption in mice causes severe obesity without Type 2 diabetes. *Biochem J* 425, 71–83

- Wang X, Lu Z, Gomez A, Hon GC, Yue Y, Han D, Fu Y, Parisien M, Dai Q, Jia G, et al. (2014): N6-methyladenosine-dependent regulation of messenger RNA stability. *Nature* 505, 117–120
- Wang X, Zhao BS, Roundtree IA, Lu Z, Han D, Ma H, Weng X, Chen K, Shi H, He C (2015): N6-methyladenosine Modulates Messenger RNA Translation Efficiency. *Cell* 161, 1388–1399
- Wang Z, Zhang X-J, Ji Y-X, Zhang P, Deng K-Q, Gong J, Ren S, Wang X, Chen I, Wang H, et al. (2016): A Long Non-Coding RNA Defines an Epigenetic Checkpoint in Cardiac Hypertrophy. *Nat Med* 22, 1131–1139
- WHO (2018): Global Health Estimates 2016: Disease burden by Cause, Age, Sex, by Country and by Region, 2000-2016. Geneva, World Health Organization 2018
- Winter GE, Mayer A, Buckley DL, Erb MA, Roderick JE, Vittori S, Reyes JM, di Iulio J, Souza A, Ott CJ, et al. (2017): BET Bromodomain Proteins Function as Master Transcription Elongation Factors Independent of CDK9 Recruitment. *Molecular Cell* 67, 5-18.e19
- Wu S-Y, Lee A-Y, Lai H-T, Zhang H, Chiang C-M (2013): Phospho Switch Triggers Brd4 Chromatin Binding and Activator Recruitment for Gene-Specific Targeting. *Mol Cell* 49, 843–857
- Yang SH, Bergo MO, Farber E, Qiao X, Fong LG, Young SG (2009): Caution! Analyze transcripts from conditional knockout alleles. *Transgenic Res* 18, 483–489
- Yang Z, Yik JHN, Chen R, He N, Jang MK, Ozato K, Zhou Q (2005): Recruitment of P-TEFb for Stimulation of Transcriptional Elongation by the Bromodomain Protein Brd4. *Molecular Cell* 19, 535–545
- Yeh TC, O'Connor G, Petteruti P, Dulak A, Hattersley M, Barrett JC, Chen H (2017): Identification of CCR2 and CD180 as Robust Pharmacodynamic Tumor and Blood Biomarkers for Clinical Use with BRD4/BET Inhibitors. *Clin Cancer Res* 23, 1025–1035
- Zhang B, Kirov S, Snoddy J (2005): WebGestalt: an integrated system for exploring gene sets in various biological contexts. *Nucleic Acids Res* 33, W741-748
- Zhang B, Davis JP, Ziolo MT (2015): Cardiac Catheterization in Mice to Measure the Pressure Volume Relationship: Investigating the Bowditch Effect. *J Vis Exp*
- Zhang L, Malik S, Pang J, Wang H, Park KM, Yule DI, Blaxall BC, Smrcka AV (2013): Phospholipase C ϵ Hydrolyzes Perinuclear Phosphatidylinositol 4-Phosphate to Regulate Cardiac Hypertrophy. *Cell* 153, 216–227
- Zhang T (2003): The deltaC Isoform of CaMKII Is Activated in Cardiac Hypertrophy and Induces Dilated Cardiomyopathy and Heart Failure. *Circulation Research* 92, 912–919
- Zhao R, Nakamura T, Fu Y, Lazar Z, Spector DL (2011): Gene bookmarking accelerates the kinetics of post-mitotic transcriptional re-activation. *Nat Cell Biol* 13, 1295–1304
- Zhao W, Zhao T, Chen Y, Zhao F, Gu Q, Williams RW, Bhattacharya SK, Lu L, Sun Y (2015): A Murine Hypertrophic Cardiomyopathy Model: The DBA/2J Strain. *PLOS ONE* 10, e0133132

Karve TM, Cheema AK. <https://www.hindawi.com/journals/jaa/2011/207691/>; retrieved 10/28/2018

MacDonald JW. <http://bioconductor.org/packages/mogene10sttranscriptcluster.db/>; retrieved 09/21/2018

Acknowledgements

There are many people I want to thank for helping me putting this work together. First, I want to thank Karl for giving me the opportunity to work in his laboratory with all the freedom and confidence needed to work creatively and autonomously.

I would also like to thank my thesis committee members André Fischer, Steven Johnsen, and Roland Dosch, who actively supported my project with their knowledge, helpful scientific criticism and the friendly atmosphere in our annual meetings.

Additionally, my warm thanks go to Sigrid Hoyer-Fender and Bernd Wollnik who agreed to join my extended examination board.

Sara, thank you for starting my scientific career, telling me about the open PhD position and for helping me out, especially with pathway analysis.

I want to thank the entire Toischer-Schnelle-Seidler-Lab for the support and atmosphere at work. Sabrina and Alessya, without your endless effort this thesis wouldn't have been possible. Joanna, thanks for the echoes. Belal, thank you for your advice and nice talks. Eric thank you for all the help, fun, and for our caffeine addiction, "wubba lubba dub dub!"

Also, I am grateful for collaborations and fruitful discussions with a bunch of people from the Fischer Lab: Eva thanks for establishing the conditional mice and all the advice given. Henning, Hendrik and Christian thank you for the collaboration and guaranteed laughter.

Furthermore, I would like to thank the Johnson Lab: Fedra, thanks for the input and for teaching me what to do with endless tables of expression data. Ana, thanks for your antibody validation.

I want to express my gratitude to the whole SFB1002 Service Unit consisting of Sarah, Roland, and Marcel for the excellent job with all the surgeries and echoes.

Many thanks to Gabriela, Orr and Kaamini from the TAL for excellent service and support.

Not to forget I am thankful to all the mice that spend their lives in terms of giving me the knowledge and data for this thesis and the caretakers who took care of them in all the years.

I want to thank my parents, brothers and friends for loving and supporting me as I come.

My final thanks go to you, Ricarda, for our wonderful kids who remind me of the important things in life, for your support during all the years of my studies and for your patience, especially towards the end of this work (I know it was challenging for you). I am looking forward for all the adventures to come, now that I have almost finished my PhD.

Curriculum Vitae

Personal information

Name	Dawid Lbik
Date of birth	25 th of October 1987
Place of birth	Lublin, Poland

Education

2014 – 2019	Ph.D. Thesis at University Medical Center Göttingen. Title of thesis: <i>From Chromatin Readers To Heart Failure: BET Protein Family Members In Cardiac Remodeling</i>
2011 – 2013	M.Sc. Developmental Biology at Georg-August University Göttingen Title of master thesis: <i>Potential use of penetratin fusion proteins as trans-membrane and trans-synaptic tracers</i>
2007 – 2011	B.Sc. Biology at Georg-August University Göttingen Title of bachelor thesis: <i>The role of PATJ in the establishment of epithelial polarity in Drosophila melanogaster</i>
2000 – 2007	Max-Planck-Gymnasium Delmenhorst

Honorary Office

2016 - 2017	PhD Student Representative GAUSS - Göttingen
-------------	---

Working experience

11/2013 – 08/2014	Research Assistant at Göttingen Center for Molecular Biosciences (GZMB), Dept. of Developmental Biology, Göttingen Tasks: gene expression analysis, fluorescence microscopy, image processing
02/2010 – 03/2013	Student Assistant at GZMB, Dept. of Developmental Biology, Göttingen Tasks: generation of transgenic insects, spider breeding, supervision of the Cell- and Developmental Biology practical course
03/2009 – 08/2009	Student Assistant at MPI for biophysical chemistry, Göttingen Tasks: annotation of gene- and protein- sequences

Publications

Peer-reviewed publications

- 2016
Mohamed BA, Schnelle M, Khadjeh S, **Lbik D**, Herwig M, Linke WA, Hasenfuss G, Toischer K (2016a). Molecular and structural transition mechanisms in long-term volume overload: Chronic volume overload. *European Journal of Heart Failure* 18, 362–371
- Mohamed BA, Asif AR, Schnelle M, Qasim M, Khadjeh S, **Lbik D**, Schott P, Hasenfuss G, Toischer K (2016b). Proteomic analysis of short-term preload-induced eccentric cardiac hypertrophy. *Journal of Translational Medicine* 14Test

Selected poster presentations

- 2018
German Centre for Cardiovascular Research (DZHK) Retreat, Königsstein
“The absence of Brd4 from cardiomyocytes leads to a basal concentric hypertrophy and increased mortality after pressure overload” Nominated
- 2017
American Heart Association Scientific Sessions 2017, Anaheim CA
“The Absence of the Chromatin Reader Brd2 Decreases Heart Function and Increases Mortality After Pressure Overload”
- 2016
German Cardiac Society (DGK) annual Congress, Mannheim
“Maximal resolution of the heart transcriptome with cell type specific profiling”

Teaching activities

- 2017
Master thesis supervision Robin Hindmarsch
- 2016
Master thesis supervision Vanessa Kernke
Diploma thesis supervision Maximilian Hofmann
Supervision of Mila Höhne (Lab rotation 18.05. – 10.07.2016)
Supervision of Robin Hindmarsch (Lab rotation 15.03. – 19.05.2016)